University of Alberta

Influences of Grain boundaries an Surface Nanocrystallization on stainless steel on *Psedomonas Aeruginosa* Biofilm's adherence

by

Bin Yu

A thesis submitted to the Faculty of Graduate Studies and Research
in partial fulfillment of the requirements for the degree of

Master of Science

Department of Biomedical engineering

Spring 2011
Edmonton, Alberta

ABSTRACT

A common complication associated with medical implants is the infectious bio-film, which can cause chronic infection that is difficult to control. Grain boundaries (GBs) in materials of medical implants are often preferential locations for bacteria to congregate, which could be attributed to higher affinity of grain boundaries for bacterial bio-films. In this study, the molecular interaction of the *Pseudomonas aeruginosa* receptor binding domain, a self-folding domain of 17 amino acid residues derived for the PilA structural protein, which can represents properties of *Pseudomonas aerginosa* biofilm, with microcrystalline stainless steel surfaces was examined with atomic force microscopy (AFM) both at grain boundaries and within grains. Adherence of *Pseudomonas aeruginosa* biofilm to nanocrystallized stainless steel surface was also determined using AFM. Results indicate that adherence of biofilm' adherence at grain boundaries of microcrystalline surface is 2-fold higher than that of inside grains. Nanocrytalline surface is more resistant to biofilm than the microcrystalline one due to the formation of a strong oxidation film after annealing and thermal oxidation process. Surface nanocrystallization for enhanced corrosion resistance of Ag-incorporated 304 stainless steel surface was also studied. It is demontstrated that nanocrystallization of the antibacterial agent-incorporated stainless steel surface also provides an effective approach to control the corrosion problem resulting from the typical galvanic effect of multiphase alloys.

ACKNOWLEDGEMENTS

I would like to appreciate the people who have helped me during my M.Sc study at the university of Alberta.

Sincere appreciation is given to my supervisor, Dr. D.Y. Li, and co-supervisor Dr. Randy Irvin, for their constant support, advice and guidance throughout the course of my graduated program. They are excellent models for me of how a researcher who keep seeking scientific truth without tiredness. I will always remember and treasure what they give me in my future career.

I also would like to thanks my colleagues, Elisabeth Davis, Carmen Giltner and Adam Lesuik, for their help during my research. Discussions with them gave me a new perspective on thinking.

CONTENTS

4   Surface nanocrystallization of stainless steel for reduced biofilm's adherence

5 Quantitative evaluation about the influence of grain size of nanograined stainless steel on the surface activity and bacterial binding

6 Surface nanocrystallization of silver incorporated 304 stainless steel for

reduced *Pseudomonas aeruginosa* biofilm formation and enhanced corrosion resistance

LIST OF FIGURES

List of tables

Chapter 1

INTRODUCTION AND LITERATURE REVIEW

1.1 biofilm and its related medical issues

Development of indwelling medical devices or medical implants makes great contributions to modern medicine. However, a common complication associated with medical implants is infectious bio-films, which can cause chronic infection that is difficult to control, since bacteria within a biofilm are very resistant to antibiotics and the human body immune system [1]. More than 60% infections are believed to involve biofilms. Human infections may result from the use of any of indwelling medical devices. Organisms such as Gram-positive and Gram-negative bacteria and yeast are commonly found as pure cultures. Biofilms may also affect the device operation or its integrity. The exact mechanisms involved in biofilm associated infections are still poorly understood, though infection due to bacterial biofilms on medical implants have long been recognized as a serious problem and considerable investigations have been conducted.

A bacterial biofilm is a community defined as microorganisms attached to a surface or interface enclosed in an exopolysaccharide matrix of microbial and host origin to produce a spatially organized three-dimensional structure [2,3]. Fig 1.1

shows a *P. aeruginosa* biofilm which is a commonly observed biofilm in medicine [1].
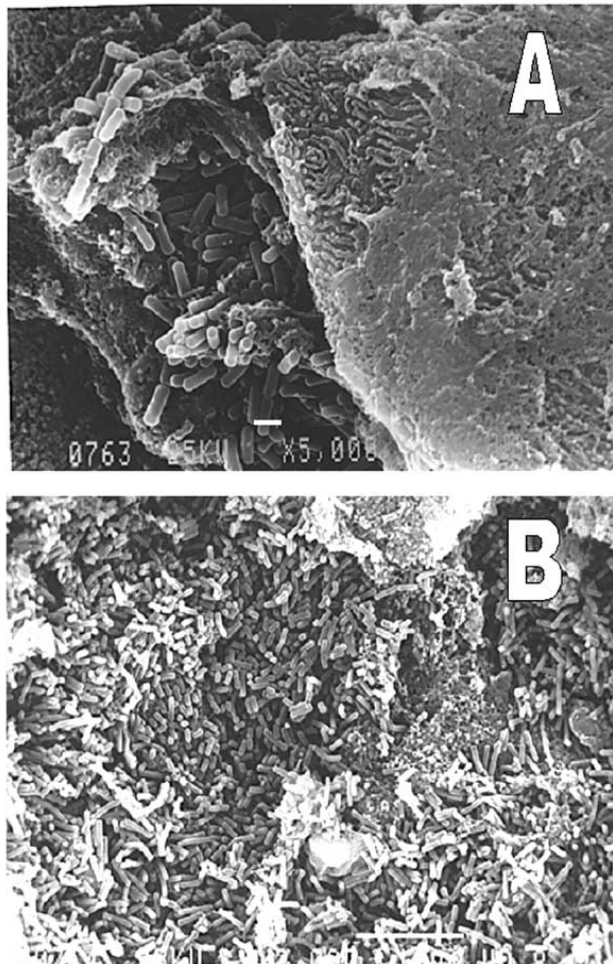
Fig 1.1 *P. aeruginosa* biofilm binding on a substrate *[1]*

This definition emphasizes the complexity of microbial composition and structure and also implies the infections associated with implants, such as catheters and orthopaedic plates. A number of infections where bacteria form large aggregates on tissue surfaces have also been considered as biofilms, including *Pseudomonas aeruginosa,* which often results in infections in cysitic fibrosis(CF)lungs or microbial plaques on heart valves[4,5]. Although biofilms are generally perceived as a complex consortium of microorganisms attached to a surface or interface. These microbial

structures have been identified as biofilms based on phenotypic characteristics and their physiological properties. A definition that includes the different phenotypic aspects between biofilm and planktonic bacteria may more accurately describe the important features without specifically defining all the physical properties that may vary with the biofilm structure.

The ability to adhere to materials and to form biofilm are important bacteria virulence factors in foreign-body-associated infection, due to colonization of a surface and forming multilayered cell clusters, which are embedded in an amorphous extracellular material that is tightly associated with the prosthetic device. Infection in the vicinity of an implant surface probably initates through the inoculation of the implant with only a few bacteria, generally these bacteria are introduced through the surgical procedures and originate from the patients' skin or mucous membranes [6]. The colonizing bacteria together with the extracellular material, which is mainly composed of cell wall polymers, are refered to as a biofilm. The presence of large adherent biofilms, including multilayered *Staphylococcal* cell clusters on explanted intravascular catheter has been demonstrated by scanning electron microscope [7,8].

Microbial biofilms are inevitably associated with man's failure to control them without effective approaches to battle with bacterial biofilms. This is particularly notable with current unsatisfied status of dealing with biofilms on medical implants—the only effective treatment to date is the surgical removal of the implant.

Considerable research interest in the biofilm stems from our inability to control or eradicate them using antibiotics. Indeed, bacteria within biofilms are reported to be

some 10-10000 times less susceptible, towards a wide variety of differently acting antibiotics, than the equivalent planktonic cells[9]. There are some factors that make biofilms resistant to antibiotics as depicted below.

a) **Resistance due to Extracellular Polymeric Matrix and Physico-chemical gradients**

Resistance to antibiotics and biocides can be mediated through reaction-diffusion limitation [10,11,12]. However, this is sufficient only to explain the inability of some chemically reactive molecules and those molecules that possess strong positive charges for penetrating the glycocalyx or extracellular matrix that surrounds a biofilm. Similarly, enzyme-mediated reaction-diffusion limitation takes account of only those molecules that provide a substrate for specific enzymes such as β-lactamases[13,14]. Regardless, for long-term resistance to agent result in either case, the reaction capacity of the biofilm for the agent must be sufficient to deplete the bulk treatment phase [15,16]. Alternative explanations of the resistance to antibiotics are related to the generation of close proximity of cells, nutrient gradients, and thereby a plethora of phenotypes that includes unsusceptible ones [17,18]. Since the least susceptible phenotype might be different for each treatment agent in terms of antibiotics, yet still be represented within the community, this explanation takes some account of their diverse physical, chemical and biochemical properties. Such phenotypes, however, depend upon the physical-chemical environment in which the cells grow. This will change as susceptible community members succumb to the treatment and no longer

consume nutrients. Thus, slow-growing unsusceptible cells may increase their rate of growth and become susceptible. Neither diffusion limitation nor physiological gradients can therefore account for the long-term survival of biofilm communities during chronic exposure to inimical agents [19]. Rather, such mechanisms only delay killing of a subset of cells. A structure of bacteria cells which can protect bacteria from disinfectants is shown in Figure 1.2.
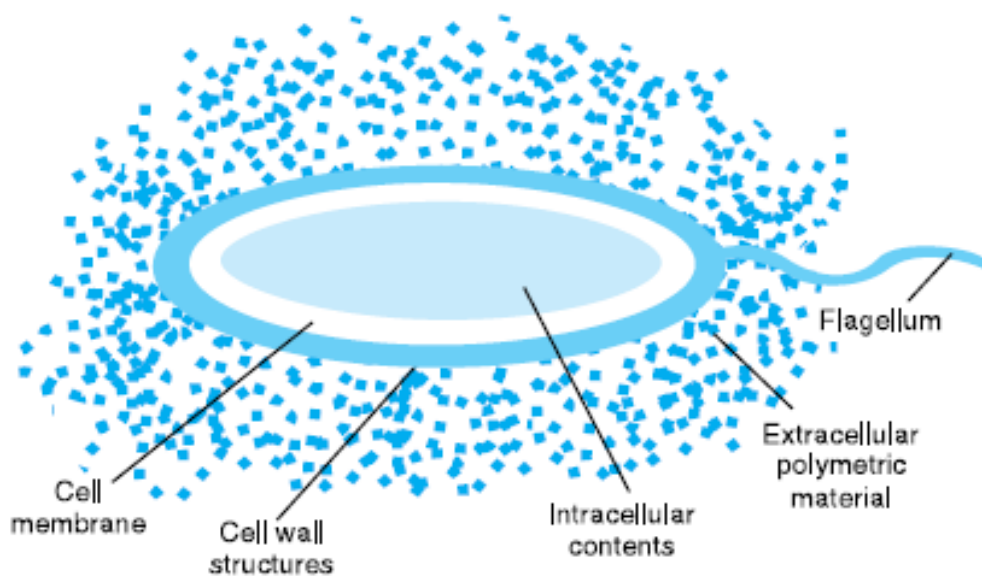
Fig 1.2 bacteria cells with extracellular polymers which stick to surfaces, concentrate nutrients, and protect bacteria from disinfectants. [1]
(This diagram does not include pili.)

b)Adoption/selection of Resistance Phenotypes

It has been suggested that the long-term survival of biofilm communities might be related to the adopting or clonal expansion of more resistant phenotypes during the delayed action of the treatment agents. Such phenotypes might be related to the growth rate of a biofilm, the so-called "biofilm phenotype", to non-specific responses

towards localized high cell densities or to the proximity of the treatment agents might also induce the expression of efflux pumps and possibly select for efflux mutants.

Biofilm formation is a continual dynamic sequence of events, which has been divided into distinct developmental stages. Biofilm development and maturation are generally described with different developmental stages including the emigration of cells from the biofilm to generate new planktonic cells that allows for the development of additional biofilms at different locations. The initial stage is the bacterial growth as planktonic cells, which are then transported to a surface or interface. The bacteria then become associated with a conditioned surface and form a monolayer. The bacteria are attached to the surface in a reversible manner, so that they can easily detach and move along the surface. This surface-associated motility has been visualized by O'toole and Kolter using time-lapse phase-contrast microscopy of *P.aeruginosa biofilms*[20].

Biofilm formation may lead to different structures, which result form different processes and have different bacterial properties. When planktonic bacteria become associated with a surface, they adhere and begin to form microcolonies .Once attached, the bacteria divide and produce EPS, which helps to cement the biofilm matrix together to create a characteristic three-dimensional structure. The biofilm then expands until the rates of growth and attachment are equal to those of   death and detachment, thus becoming the mature biofilm. The genetic requirements for biofilm formation are known for *P.aeruginosa* and *E.coli*. Many aspects of biofilm formation and detachment are still unclear and identified by a question mark [21].

Different stages of biofilm formation have been described for Gram-negative species such as *P.aeruginosa, Pseudomonas fluorescens*, and *E.coli*. However, the biofilm forming processes for Gram-positive bacteria are less known [21]. This has attracted particular interest, as the majority of implant related infections are associated with Gram-positive strains, predominantly the coagulase negative *Staphylococcus epidermidis*. Some of these genetic requirements, in addition to other factors that influence biofilm formation, such as environmental and physical conditions, have been identified for a limited number of bacterial species [22]. As a example, a biofilm structure and formation is shown in pictures below in figure1.3
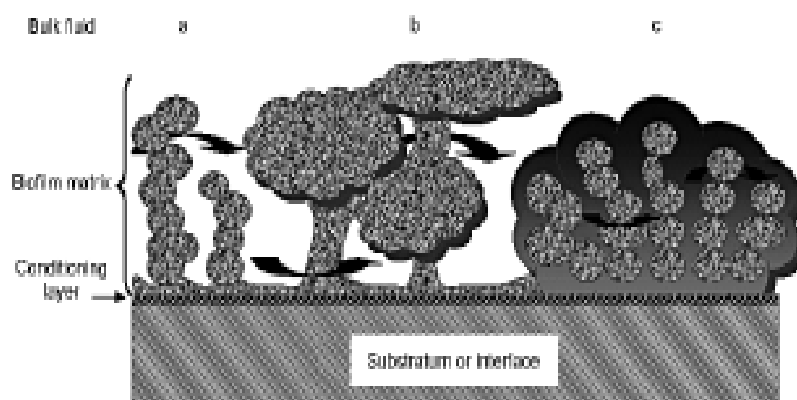
Fig.1.3 Formation process of bacterial biofilm on substrate [1]**.**

Bacterial adhesion to surfaces is the first step in the formation of a biofilm and has been studied extensively over the past decades in implants applications, such as biofilms on biomaterials implanted in the human body [23]. Bacteria adhere to a surface and make an extracellular polymeric matrix in which they embed.   Biofilms can be made of one or many species of bacteria.   Growing in association with one

another, bacteria are able to sense density. They coordinate behavior with quorum sensing, or cell-to-cell communication, and exchange nutrients and wastes through channels. Functionally, they play a role in bioremediation of hazardous wastes, filtration of water, disease, and virulence.

Some indwelling medical devices are particularly favorable for the development of biofilms [24]. Some examples are depict below in Figure 1.4 a and b.
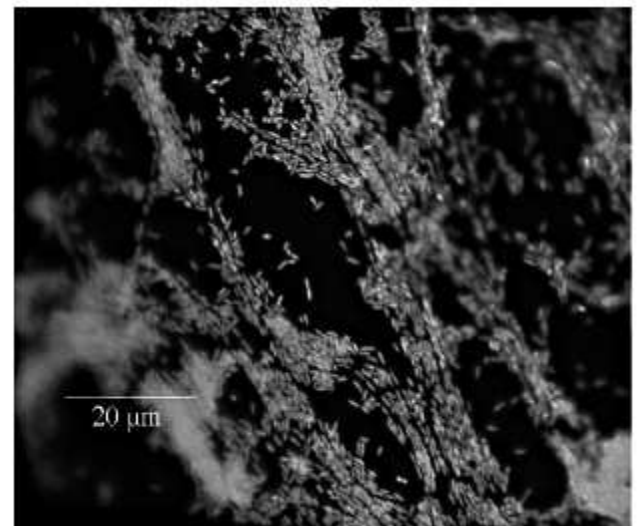
a)   b)

Figure1.4 (a) cranioplasty plates, (b) bacterial biofilm formation[1]

Biofilm formation on medical implants may also influence the operation or integrity of the device. Problems might include the destruction of tissues surrounding prosthestic heart valves, resulting in leakage, material destruction, obstruction of urinary catheters, or loosening of artificial hip and knee prostheses [25]. It is also reported that a number of patients with culture-positive hip implants also had joint loosening [26].

1.2 Biofilm's past, present, and future

Biofilm's past

The effect of a surface on the bacterial population was noted since one century ago [27]. Over the last decades our knowledge of microbial biofilms was increased dramatically, as shown by the increase in the numbers of publications on the subject. There are also numerous books and many conferences devoted to biofilms, particularly their visualization, problems that they may cause, and the measures needed to control biofilms. Looking back over the way our knowledge was accumulated in passed years, a few notable steps are highlighted.

First, the recognition of 'surface-associated microbial activity and colonization', or 'biofilm formation', as a phenomenon that occurs in both natural and man-made environments has attached increasing interest in both medical and non-medical fields. In reality, not all surface-associated bacteria have been, or still are generally thought of as biofilms. For example in dentistry, the term 'dental plaque' is used to define a consortium of organisms forming a biofilm.

Events leading to biofilm formation

By the early 1990s scientists were well on the way to understanding the importance of biofilms, the mechanisms for their formation and their role in microbial

survival. The importance of surfaces as sites associated with increased microbial activity was recognized with efforts to elucidate the principles of adhesion. The important steps in biofilm formation were considered as:

(1) Surface conditioning[28] and the mechanisms responsible for the bacterial adhesion, which is dependent on both the physiological status of the microorganism[29] and on the nature of the substratum.

(2) Physical and electrochemical properties and relative hydrophobicity of the surface as important factors in the biofilm formation process[30], in addition to the receptor interactions in binding to living surfaces. For example, rougher surfaces were preferentially colonized, providing niches protected from being affected by shear stress, turbulent flow and biocide activity[31].

(3) Adherence to surfaces in natural and industrial environments-the role of extracellular polysaccharide substances (EPSs), or the glycocalyx, secreted by the cells is considered to play an important role in secondary colonization by different species[32]. These high molecular weight EPS molecules are believed not to act directly as adhesions rather other factors, possibly low molecular weight polysaccharides, shown to be produced in trace amounts, mediated the initial colonization process, followed by higher molecular weight EPS production as response to later events.

(4)   Resistance to biocide treatments was shown to be increased in bacteria attached to surfaces[33] and the glycocalyx roles as a barrier affording various constituents of the biofilm partial protection from antibacterial agents and toxic substrates upon which a biofilm forms. It is still unclear whether this is a phenotypic response of the microbial population to surface growth that plays a role in increasing the resistance of biofilm to antibotics.

(5)   Significant progress occurred in 1994, when Nichols suggested that the resistance to antimicrobial compounds may not be solely due to the physical impedance of the antimicrobial agent, but that there may be other factors such as absorption or catalytic destruction of the agent by microbes at the biofilm surface [34].

Biofilm's present

A number of new strategies have been developed by researchers to overcome the problems encountered in biofilm control in vitro. Although many of these are still under investigation and are being tested in clinical application, they provide the key to future strategies   for biofilms control. These include:

(1) Novel combinations of chemical and physical techniques to control biofilms, such

as ultrasound or electrical enhancement of antibiotics.[35]

(2)   Novel antibiotic derivatives with increased antibacterial capability [36].

(3)   Novel anti-adhesive compounds that prevent or inhibit bacterial binding to either tissue surfaces or implants, such as soluble receptor analogues[37], antibodies that block adhesion, and compounds that prevent bacterial adhesion.

(4)   Use of probiotic bacteria and fungi to prevent or remove microbial contamination. For example, the use of bacteria to prevent yeast contamination of artificial voice boxes is a good example. Such techniques are of great interest in terms of being cost effective and having a low impact on the environment[38]. Fig 1.5 shows the artificial throat equipped with 3 Groningen button voice prostheses:
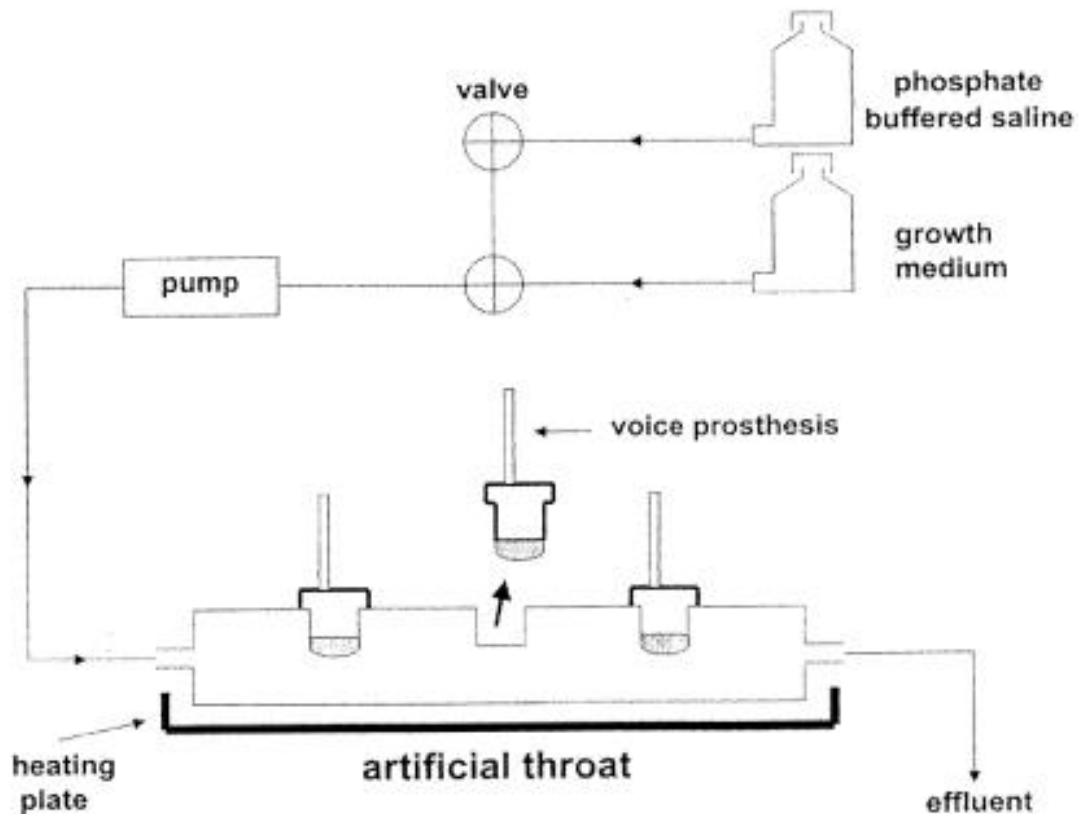
Fig 1.5 Using of probiotic bacteria and fungi to prevent or remove microbial contamination[1]

The first report of biofilm recalcitrance to aggressive antibiotic therapy was coincident to the realization that implanted medical devices represented a significant risk of infection with skin microorganisms, such as *Staphylococci, Enterococci, diphtheroids* and others, In such situations, a common scenario emerged whereby bacteria was treated with success, but that bacteria recurred soon after treatment was finished. Analysis of the isolated organisms showed that these bacteria given above were sensitive to the agents. In many cases the same organisms are subsequently isolated from the implanted device, either when this is removed or at post-modern[39-42]. It has been apparent that the growth of otherwise non-pathogenic

bacteria on the surfaces of implanted plastics and othe biomaterials leads to a population of microorganisms that are almost completely intractable with conventional antibiotic treatments. The situation today is that many hospital doctors and clinicians believe that antibiotic therapy without concomitant surgical intervention is of little use[43].

Antibiotic Regimes

In spite of the poor prognosis associated with the use of antibiotics to treat device-associated infections, there are a number of cases in which such treatment is an available option. For example, in dealing with the prosthetic vascular graft infections, the combined systemic administration of vancomycin, aminoglycoside and a broad-spectrum cephalosporin is often considered to be appropriate in the absence of a specific susceptibility profile. After re-surgery, 4 to 6 weeks of parenteral administration followed by 6months of oral administration are often advocated, but some authors have recommended lifelong administration of oral antibiotics in high-risk situations. Similarly, in the context of infections of prosthetic heart valves, treatment is commonly recommended over a 6-week period, previously determined to be the most appropriate agent. Consequently, it is important that the aetiology of prosthetic valve endocarditis is not cured by premature treatment. Indolent endocarditis, which mandated early surgical intervention, does not require immediate antimicrobial therapy. Antibiotics should be withheld briefly pending the isolation and characterization of the causative organism.

In the treatment of infections associated with prosthetic joints, antibiotic therapy without surgical intervention is not considered to be an option. In one study of 25 patients, none had a satisfactory functional outcome after and average of 1.3years follow up[44]; another study found that only 3 out of 13 prostheses were retained after a mean of 37.6 months among patients treated with antimicrobial suppression[45]. Accordingly, prevention of device-associated infections is significantly more successful than a cure.

Current approaches for prevention of device associated infections

When considering antimicrobial prophylaxis, it is important first to define the degrees of intimacy with which the various devices interact with the body. Bayston(1995) has categorized devices as follows :

Category 1 Devices are totally implanted in the tissues of the body and intended to remain in place for the life of the patient. Examples include large joint replacements, prosthetic heart valves, joint replacement,(hip, knee, shoulder, elbow replacement. ligaments, bone cement, synovial fluid replacements); trauma and osteosynthesis internal and external fixation including bone screws, plates ,and nails. According to different situations of patient, the shape or size of implants can be flexible, such as spinal implants, hydrocephalus shunts.

Category 2 Devices are partially implanted, and are intended to remain in situ for long-time periods (e.g. central venous catheters, external ventricular drains, implants for orthopaedics.

Category 3 Device are not true implants, such as urinary catheters and voice prostheses. Since devices in categories 1 and 2 are situated in normally sterile tissues and body compartments, the risk of infection is greater during and immediately after implantation and will normally comprise of single species. Since devices category 3 are essentially open to the environment, challenge from successions of microorganisms throughout the period of implantation will occur. Accordingly, strategies for the successful prophylaxis and treatment of category 3 devices will differ from that of categories 1 and 2.

Antibacterial prophylaxis

When considering category 1 implants, such as large joint replacements, once an implanted medical device becomes infected, the treatment is extremely problematic and rarely successful. When infection is detected, therapy with powerful antibiotics (e.g. aminoglycosides) is frequently attempted, although the inherent toxicity of these drugs makes therapy difficult. For example, the notorious resistance of biofilm infections makes therapy based on planktonic MICs of little use. Whereas a conventional broth MIC gives a value of 1 mgl^{-1}, the minimum biofilm eradication concentration (MBEC) may need to exceed 100 $mgml^{-1}$ where the agent may be toxic at levels above 50mgl^{-1}[46][47]. Symptoms may be reduced for the duration of the

antibiotic administration, only to relapse after cessation of treatment. In most cases, removal and replacement of the prosthesis are usually required to eradicate the infection, with associated patient trauma and increased cost[48]. So every effort should be made to prevent the initial colonization of the implant using well controlled surgical clean procedures, air clean technology and with irrigated antimicrobial agents.

Prophylactic intravenous antibiotic administration has become the accepted practice for procedures involving the implantation of prosthetic devices of categories 1 and 2, and is widely endorsed by most authorities. This practice is effective for large joint replacement. The general strategy is to administer an intravenous antibiotic, just before the initial skin infection[49].

Antimicrobial polymer and surface coatings

The performance of urethral catheter coated with silver has been ambiguous. It has been reported that a silver-coated indwelling device failed to its demonstrate efficacy in preventing urinary tract infection, and vascular catheters impregnated with silver sulphadiazine and chlorhexidine completely lost their antibacterial activity after 10 days of use[50]. The evidence that these catheters resist bacterial colonization is therefore suspect[51]. Such catheters are challenged with microorganisms throughout their implantation; indwelling medical devices, on the other hand, are only at risk from microorganisms during and immediately after implantation. Therefore there will only be a minimal opportunity for early colonizers to deplete the antibacterial agents,

and the subsequent diffusion and loss of the agents will be inconsequential. It is conceivable, therefore, that impregnation with the correct antibiotics may prove efficacious. It seems likely that, in clinical situations, the efficacy of surface-coated devices may be compromised by antibiotic-resistant bacteria, together with the barrier effect of conditioning films that rapidly coat the biomaterials in vivo.

Biofilms in future

The future of bacteriophage therapy

The development of phage therapies with the possibility of treating chronic *P.aeruginosa* biofilm infections, by the application of phage carrying and encoding hydrolytic enzymes to destroy the alginate supporting the biofilm, offer a major therapeutic benefit. The use of phage technology may expand with an increase in our understanding of the structural properties and the stability of phages. This could lead to the design of suitable delivery and targeting strategies and co-administration of phage with existing drugs using novel delivery vehicles. In the future, we may see increased delivery of phage in combination with other agents designed to reduce the severity of the symptoms of cystic fibrosis and bacterial colonization, such as antibiotics, DNAse or antimicrobial peptides [52].

Quorum-sensing in biofilm-related infections

There are a large number of gram-negative bacteria involved in biofilm formation and infections that may also be controlled by autoinduction and Quorum-sensing

systems. Gram-positive bacteria and fungi also produce cell communication and quorum-sensing signals, however, they are different to those found in Gram negative bacteria. How these chemical signals affect virulence expression and which genes they regulate are not fully understood. It is clear, therefore, that substantial research is required in this area to determine the role of quorum-sensing in biofilm growth, cell-cell and species-species interaction and virulence. In the future, we may be able to develop approaches to confuse or alter this signaling to our benefit[53]. This kind of approach would allow us not only to destroy or prevent the development of unwanted biofilms, but also perhaps to promote the development of health-promoting biofilms such as probiotic organisms.

1.3 Preferential formation of bacterial biofilm at grain boundaries

Stainless steel is widely used in the food sector and commonly in hospitals for medical devices[54] to which *Pseudomonas aeruginosa* often adhere, causing serious infection in cystic fibrosis, intensive care burn and immunocompromised patients [55]. The binding of the bacterium to an abiotic or a cellular substrate is considered to be the first stage of colonization for both biofilm formation [56] and initiation of an infection[57]. *P. aeruginosa* biofilms contribute to morbidity of patients having medical implants including catheters[58], prosthetics[59] and stainless steel implants[60]. *P. aeruginosa* readily binds to stainless steel to form highly recalcitrant, organized communities known as biofilms[61]. A *P. aeruginosa* biofilm on stainless steel surfaces can serve as a significant hospital reservoir for infection of susceptible

patients that include the immunocompromised and burn patients[62]. It is interesting to notice that recent observations illustrate that bacteria prefer to stay at grain boundaries of stainless steel. As shown in Figure 1.6, there are more bacteria binding at grain boundaries of stainless steel surface than within grains.
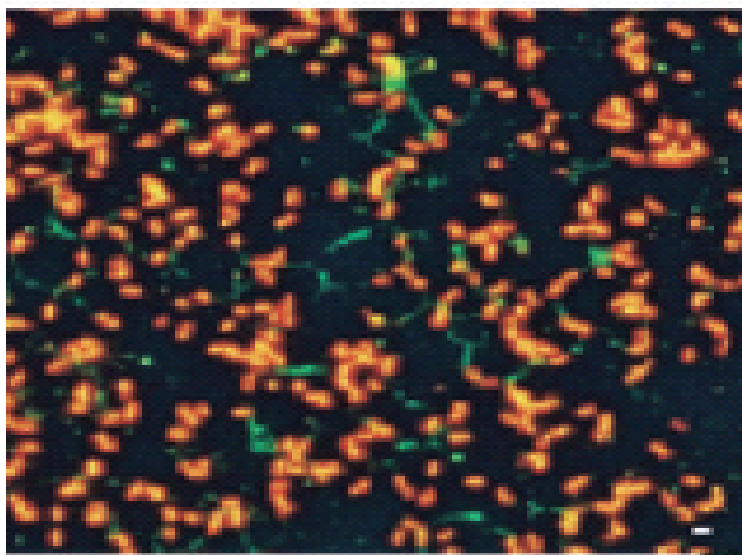
Figure1.6. *P.aeruginosa* bacteria formation on stainless steel surface, particularly at grain boundaries [83]**.**

1.4 Nanocrystalline metallic materials

Nanocrystalline metals and alloys with average grain sizes typically smaller than 100nm, have attracted a lot of interest for their improved mechanical, physical and chemical properties [63]. Relative to their coarse-grained counterpart (microcrystalline grains), nanocrystalline materials contain a higher fraction of grain-boundary volume, which plays a significant role in the altered physical properties of these materials [64]. Nanotechnology is widely used in industries and has been found increasing research in medicine areas, such as drug delivery using

nano-powder conducted by magnetic field [65]. It has been reported that nanocrystallization affects the early stages of biofilm formation on metal surface [66]. Therefore nanocrystallization of metallic material surface could be an approach to control biofilm formation on medical implants.

Several techniques have been developed to achieve surface nanocrystallization such as mechanical attrition [67-68], sliding wear, punching and sandblasting [69] etc. The formation of nanocrystalline surface results from intense cold work applied to a metallic surface. The introduced high-density dislocation cells are turned to nano-sized grains by subsequent recovery heat treatment that rearranges the dislocation cells and sharpens the diffuse dislocation cell boundaries [67]. Similarly, the synthesis of bulk nanocrystalline materials by severe plastic deformation such as in equal channel pressing can be achieved by introducing high-density dislocations. The recovery treatment applied to the deformed material leads to the formation of a nanocrystalline structure materials[68].

In this work, sandblasting and annealing were applied to nanocrystallize the surface of stainless steel.

1.5 Nanocrystallization for passivation of passive steels

High-density dislocation cells can be produced in the surface layer of a material, and with low-temperature recovery treatments, these dislocation cells can be rearranged and become nanosized grains with sharp grain boundaries.[129] Although it would be expected that electron activity may be increased as the grain boundary

density increases in nano-grained steel[130,131], this is not the case as already documented for passive steels.[131] Specifically, in nanograined stainless steel, the high-density grain boundaries promote chromium diffusion, accelerating the reaction with oxygen to form a more protective film (Cr_2O_3), thus making the steel surface more stable and resistant to corrosion.[131,132] Although the effect of surface nanocrystallization on the surface stability or inertness of stainless steel had been documented, now the surface nanocrystallization affected the biofiom's adherence and bacterial binding were unclear before this study.

1.6 Surface free energy and electron work function (EWF)

It is known that the adhesion of biofilm and associated bacterial binding in general are affected by the surface free energy of a material.[134,135] The free energy, which is largely governed by the surface electronic behavior that may be characterized by the electron work function (EWF). EWF is the minimum energy (eV) required to move an electron from inside a material to just outside its surface in a vacuum[136,137]. Thus, EWF should be a strong predictor of the biofilm-forming propensity of the surface.

1.7 Antibacterial behavior of Ag

In this study, Ag was used to further enhance the stainless steel's resistance to biofilm development or bacterial binding by incorporating Ag into the stainless steel's surface before nano-crystallization. Ag is an antibacterial agent, whose antibacterial activity has long been known and Ag has found a variety of applications because its toxicity to human cells is considerably lower than to bacteria. The most widely uses are prophylactic treatment of burns and water disinfection. Ionic silver (Ag^+) is considered to be effective against a broad range of micro-organisms. Silver has been described as being 'oligodynamic' because of its ability to exert a bactericidal effect at minute concentrations. A large number of healthcare products contain silver, such as silver-coated catheters, municipal water systems and wound dressings, etc.

The anti-bacterial activity of silver is dependent on the release of Ag^+ ions. Silver is fairly unreactive. Unlike most other metals, Ag does not react with oxygen in the air. However silver will lose its shiny white appearance over time.

The mechanism responsible for the antimicrobial capability of silver ions is closely related to their interaction with thiol (sulfhydryl) groups [138][139] although other target sites are also possible [140]. Amino acids, such as cysteine, and other compounds containing thiol groups, such as sodium thioglycolate, neutralized the activity of silver against bacteria [141]. In contrast, disulfide bond-containing amino acids, non-sulfur-containing amino acids, and sulfur-containing compounds, such as cystathione, cysteic acid, L-methionine, taurine, sodium bisulfate, and sodium thiosulfate, are all unable to neutralize the activity of silver ions. These findings imply

that the interaction of silver ions with thiol groups in enzymes and proteins plays an essential role in its antimicrobial action, although other cellular components, like hydrogen bonding, may also be involved [142]. Silver ions may cause the release of K^+ ions from bacteria. Thus, the bacterial plasma or cytoplasmic membrane, which is associated with many important enzymes, is an important target site for silver ions [143][144].

In addition to their effects on bacterial enzymes, silver ions cause marked inhibition of bacterial growth and are deposited in the vacuole and cell wall as granules [145]. They inhibit cell division and damage the cell envelope and contents of bacteria [146]. Under the influence of Ag, bacterial cells may increase in size, and the cytoplasmic membrane, cytoplasmic contents, and outer cell layers all exhibit structural abnormalities. Silver ions can interact with nucleic acids [147]; they interact preferentially with the bases in DNA rather than with the phosphate groups, although the significance of this in terms of their lethal action is unclear [148]

The silver ion can be generated by electrolyzing the silver metal or dissolving the silver compounds. It is known that the electrically generated silver ion appeared to be superior to the silver compounds in antimicrobial activity [149][150]. However, in most of the studies on the mechanism for action of silver used silver ions produced from silver compounds like silver nitrate or silver sulfadiazine, and thus there has been limited research on the electrically generated silver ion. Recently, a laundry machine that emits electrically generated silver ions was developed for hygiene,

namely, in order to prevent easily transmissible bacterial and fungal skin infections from being transmitted by contaminated laundry. In particular, it could be beneficial to hospitals and homes in which immunocompromised people (the elderly, children, and medical patients) or pets may dwell.

With the development of modern medical science, biomaterials play an important role in replacing human organs, tissues and modifying their functions. Among them, metallic biomaterials such as stainless steel, titanium and its alloy have been widely used in dental orthopaedic and cardiovascular surgery. However, infection, which is usually caused by adherence and colonization of bacteria on biomaterials, makes patients develop serious complication. Silver is well known for its antibacterial and biomedical properties. Some related researches have been reported, indicating an effective treatment to reduce bacterial infection by incorporating silver in the biomaterials. For instance, incorporating Ag in the surface layer of biomaterials by ion implantation and directly coating of Ag on their surface are attractive approaches.

Physical vapor deposition （PVD）

Ultra thin layers of silver coating only a few microns thick, can be coated on surface of a biomaterial by sputter vapor deposition. Such a silver coating on medical devices may lead to anti-microbial capability. The PVD silver coating process could be realized at ambient temperatures and thus does not affect other properties of medical devices. The thin Ag layers do not change surface geometry of the medical products that are coated.

Ion implantation

Ion implantation is a process in which ions are accelerated towards a target at energies high enough to eject them into the target's surface layer. Depending on the application, the acceleration energies can be ranged from a few keV to MeV.

1.8 Objective of This Study

Although many efforts have been made to prevent implant infection, the adherence of bacteria biofilm to implant materials more or less exists, which is the first step of biofilm-related infection and has not been effectively controlled. It is thus crucial to find effective approaches to minimize the affinity of biomaterials for biofilms.

The objective of the present study is to investigate the adherence of *P. aeruginosa* bacterial biofilm to stainless steel, since this type of material is widely used for medical implants. The effect of surface structure, mainly grain boundary and its density, on biofilm's adherence to stainless steel was investigated. We observed that grain boundaries of stainless steel attracted more bacteria. In order to determine the adhesion of biofilm at grain boundaries and within gains, atomic Force Microscope (AFM) was employed. A peptide which has its properties similar to those of *P.aeruginosa* was used as a biofilm substitute and coated on a AFM silicon nitride

tip. The adhesive force between the peptide coated AFM tip and a stainless steel surface can be measured . Hence, the adhesive forces between the peptide and stainless steel surface both at grain boundaries and within grains were evaluated using AFM. When the grain boundary density is sufficiently high (nanocrystallized surface), the surface adhesion behavior could be very different. In this study, nanocrystalline stainless steel surfaces were fabricated and investigated to determine how high density grain boundaries influence the adhesion of bacteria to nanocrystalline stainless steel surface. Furthermore, how the thermal oxidation influenced the abilities of stainless steel in both microcrystalline and nanocrystalline states to reduce the biofilm adherence was also investigated.

In order to further suppress bacterial binding an anti-bacteria agent (Ag) was incorporated into the steel surface. Since it was previously repoted that incorporation of Ag in stainless steel resulted in decreased resistance to corrosion, the emphasis of the present study was put on how the surface nanocrystallization influenced the corrosion behavior of Ag-containing stainless steel surfaces and the effectiveness of the combination of surface nanocrystallization and incorporation of Ag in suppressing bacterial development on stainless steel surface.

Chapter 2

ATOMIC FORCE MICROSCOPE SYSTEM

2.1 Introduction

The atomic force microscope (AFM)

In this study, the biofilm's adherence to a metallic surface was determined using the atomic force microscope (AFM). As the most important instrument for the present research, AFM is briefly described in this chapter. The atomic force microscope (AFM) is a high-resolution microscope, with demonstrated resolution of fractions of a nanometer, more than 1000 times better than the optical diffraction limit. The precursor to the AFM, the scanning tunneling microscope, was developed by Gerd Binnig and Heinrich Rohrer in the early 1980s, a development that earned them the Nobel Prize for Physics of 1986. Binnig, Quate and Gerber invented the first AFM in 1986[72]. The AFM is one of the foremost tools for imaging, measuring and manipulating matter at the nanoscale. The term' microscope' in the nanme is actually a misnomer because it implies looking, while in fact the information is gathered by "feeling" the surface with a mechanical probe. Piezoelectric elements that facilitate tiny but accurate and precise movements on (electronic) command are what facilitates the very precise scanning. Since its invention in 1986, atomic force microscope (AFM) has become the most widely used form of scanning probe microscope (SPM) with applications in surface, materials, and biological sciences.

The AFM consists of several major components: scanning probe microscope (SPM) (AFM or LFM), controller, computer, display and control monitors (Fig 2.1).
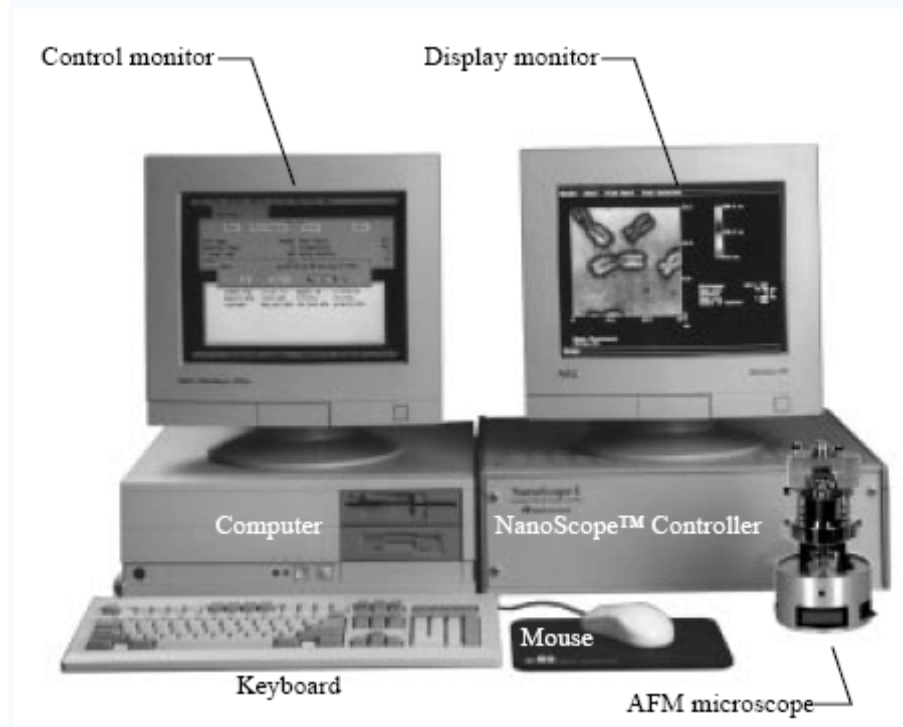
Fig 2.1 Contact AFM system hardware

The heart of the system is either the AFM or LFM (Lateral force microscopy) scanning probe microscope as shown in Fig 2.2a and 2.2b
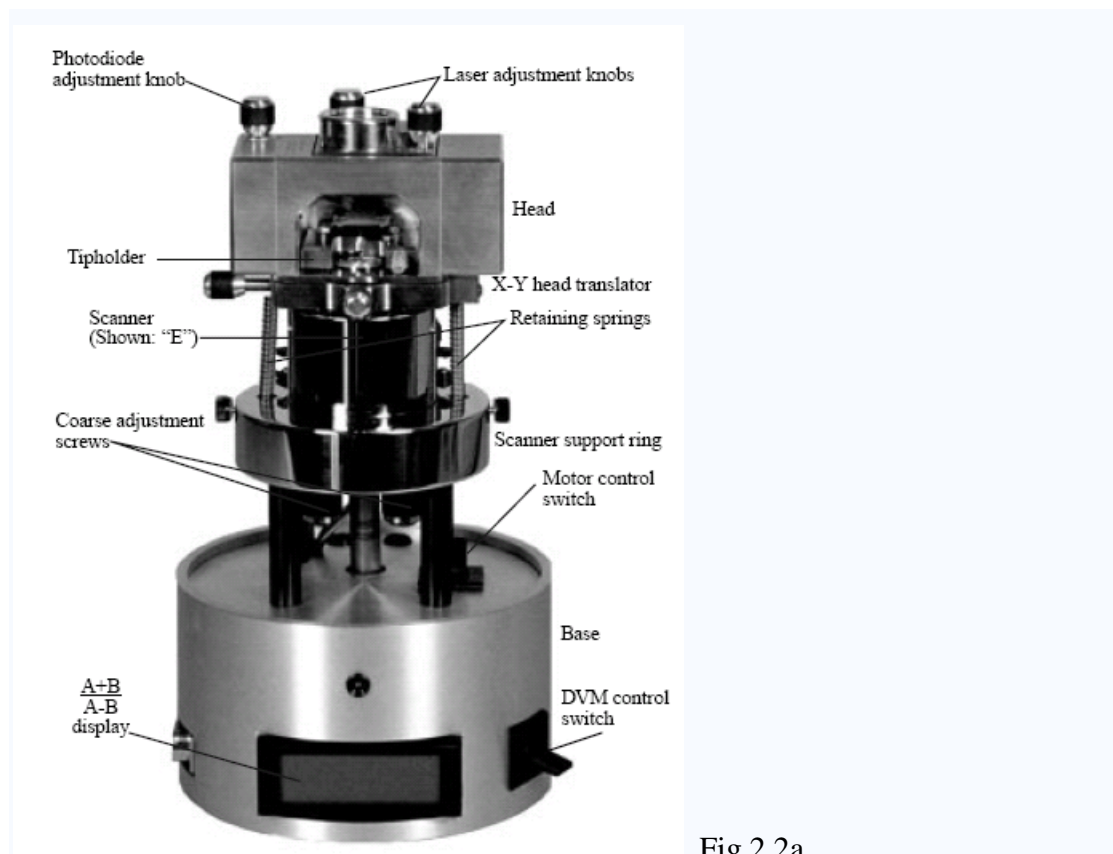
Fig 2.2a
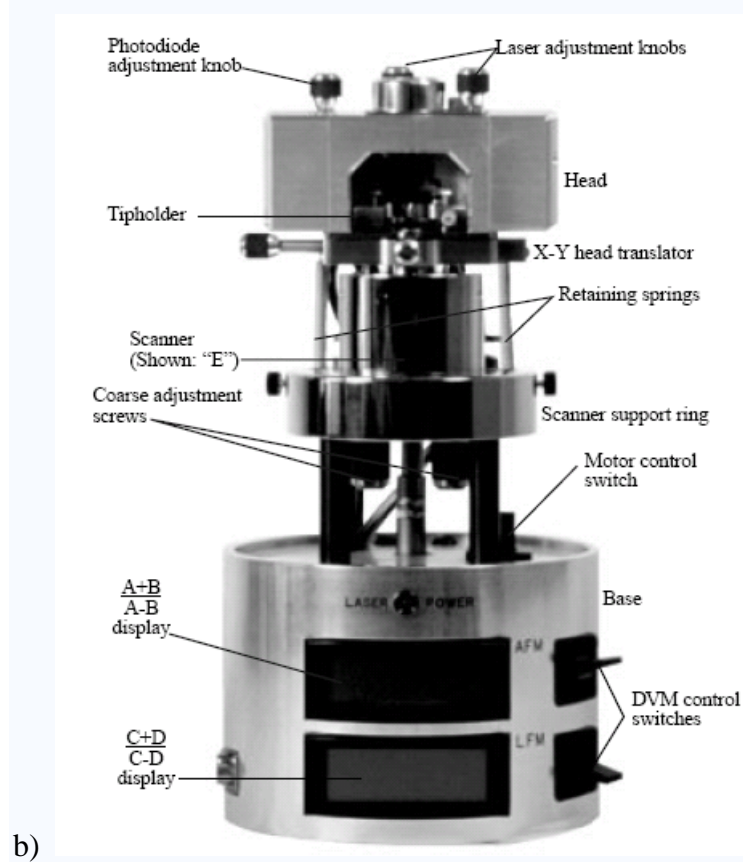
b)

Figure 2.3 shows an AFM head with various adjustment Knobs. The head and attached X-Y stage are kinematically mated to the scanner via three contact points. A pair of retaining springs hold down the head, allowing it to be raised and lowered using adjustment screws threaded through the scanner body.
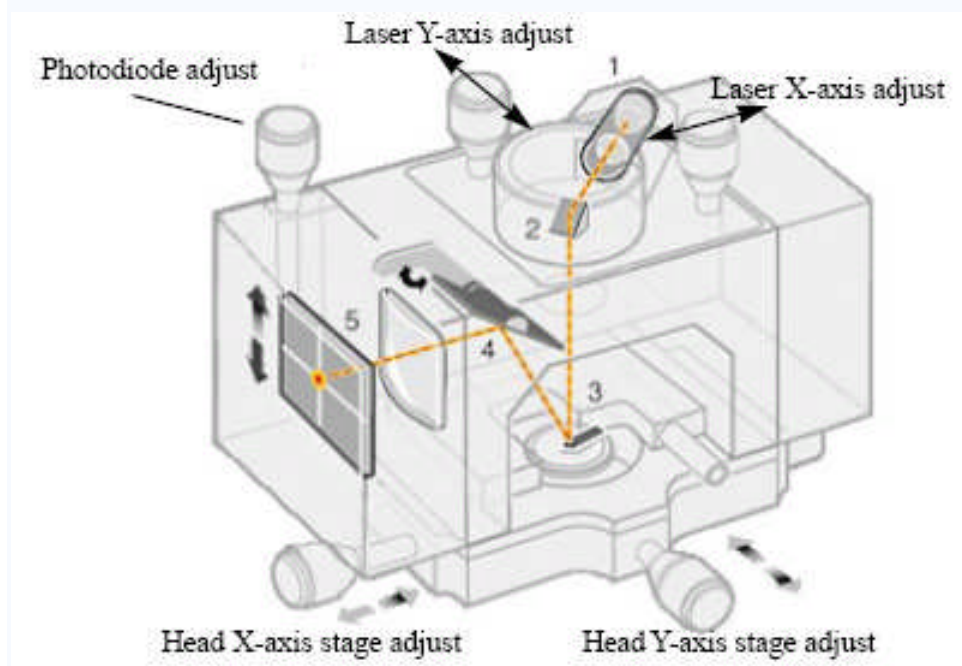
Figure 2.3 . AFM head and major components: lazer(1); mirror(2); cantilever (3); tilt mirror (4); photodector (5)

Another important part of AFM (SPM) is the Scanner. The maximum scan size and resolution of images depend upon the choice of scanner. Figure 2.4 illustrates several types of scanners. Smaller scanners tend to be more noise-free at acoustic frequencies because of their compact size and rigidity. Larger scanner offer wider scans, while requiring extra noise dampening precautions at samller scan sizes of high

resolution. The scan size and the vertical range of scanners are ranging from 0.4um * 0.4 um to 200um * 200um and from 0.4um to 8.0um, respectively.

Fig 2.4. Various scanners available with the AFM.

The AFM system maintains the tip at the end of the cantilever which is hold inside the SPM head in contact with the sample surface (Fig 2.5a,b). Most SPM work is done using cantilevered probes. These consist of a flexible cantilever extending from a rigid substrate, to which a tip has been attached. In the contact mode, the cantilever's flexibility acts as a nanometric spring, allowing the tip to measure surface forces. Most contact AFMs are performed with silicon nitride tips. These tips exhibit excellent flexibility, making them easier to use and more "forgiving" than stiffer crystal silicon cantilevers.
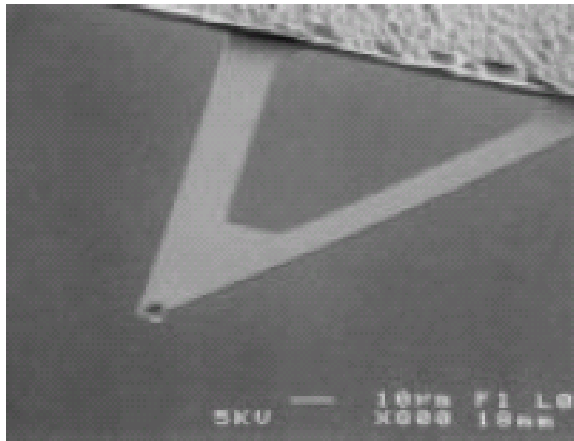
a)
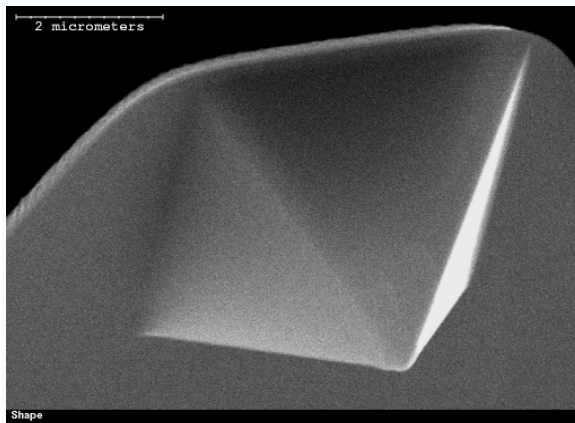
b)

Fig 2.5. AFM cantilever (a)and silicon nitride tip at the of the cantilever(b)

Since the sample is scanned under the tip, features on the sample surface deflect

the cantilever, which in turn changes the position of the laser spot on a photodiode.

This position change is read by feedback loop, from which the variation in the height

is recorded, thus providing the information on surface roughness or geometrical

features.

An AFM system is comprised of two main components; the scanner and the AFM

detection system. The scanner houses the piezoelectric element. The piezo element

physically moves the sample in the X, Y and Z direction. The detection system consists of a laser which generates a spot of light that is reflected off of a microfabricated cantilever onto a mirror and finally into a photodetector (Fig 2.6). The position of the spot is determined by circuitry which generates a voltage form the difference between the photodiode segments (A-B). the circuit outputs a voltage ranging from +10v to -10v depending on the position of the spot on the two photodiodes.
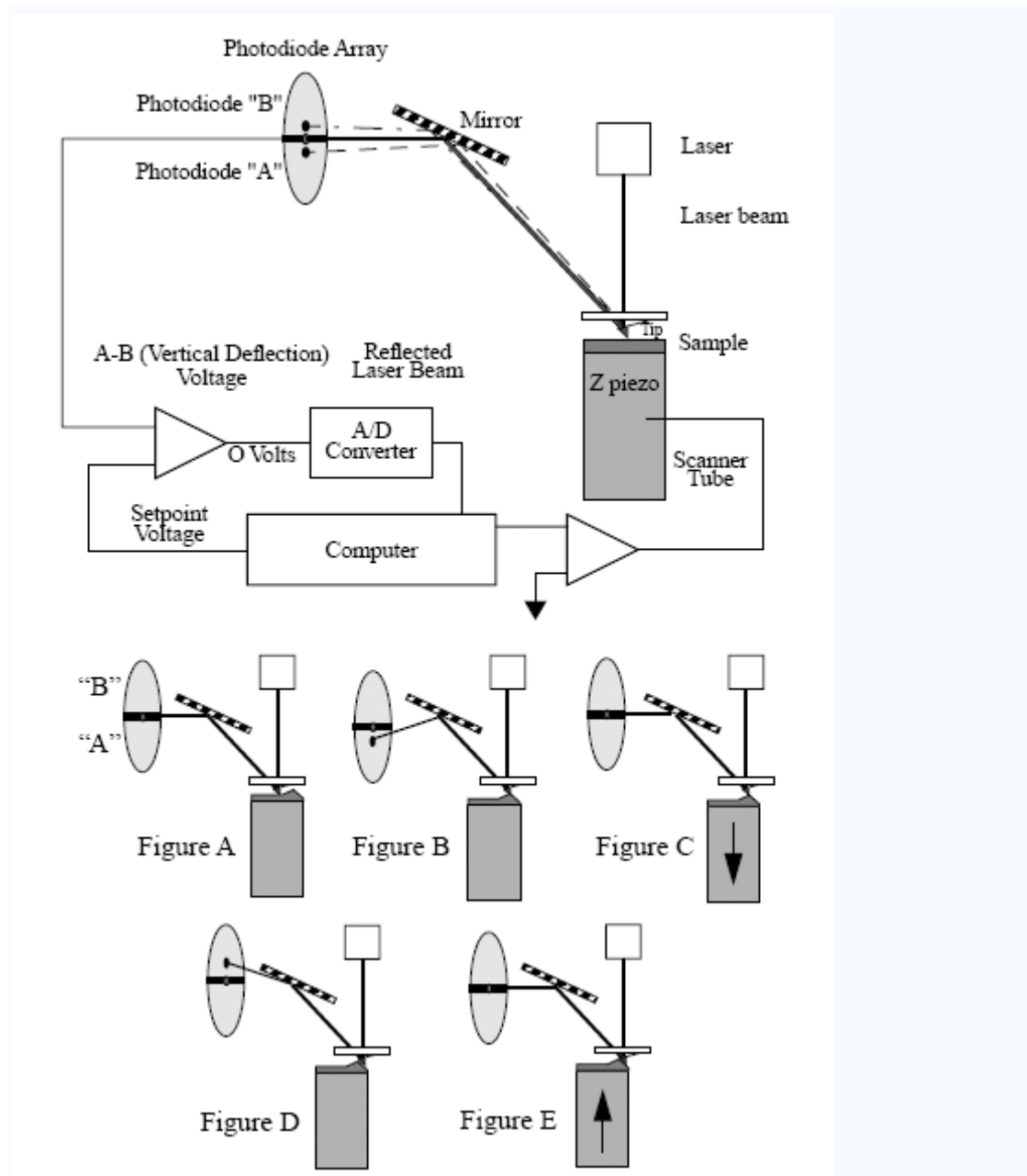
Figure 2.6   The mechanism of contact AFM

A. A flat portion of the sample surface is scanned beneath the tip left-to-right, maintaining the laser beam at the center of the photodiode array.

B. As the tip encounters a raised feature, the cantilever is pushed up, deflecting the laser beam upward onto the "A" portion of the array. With the "A" photodiode

receiving and increased portion of the laser light, its voltage increases while portion "B's" decreases (A>B)

C. The vertical deflection (A-B) voltage differential is sensed by the feedback electronics, causing a dropped voltage to the Z piezo crystal--- the piezo retracts. As the Z piezo retracts, the cantilever recenters the laser beam onto the photodiode array (A=B)

D. As the tip encounters a decline in the sample topology, the tip drops. This directs more of the beam onto the "B" portion of the photodiode array. With the "B" photodiode receiving an increased portion of the laser light, its voltage increases while portion "A's" decreases (A<B).

E. Again, the vertical deflection (A-B) voltage differential is sensed by the feedback electronics, increasing voltage to the Z piezo crystal---- the piezo extends. As the Z piezo extends, the tip is pushed down until the laser beam recenters on the photodiode array (A=B).

To produce quality images, the AFM must be capable of controlling the tip-sample interaction with great precision. This is accomplished with the use of an electronic feed back loop, which safeguards the tip and sample by keeping forces between them at a user-specified setpoint level. Although signal processing varies according to the image mode used, the feedback loop performs essentially the same

36

function. AFM feedback system had relied upon optical method to monitor the rise and fall of a sharp tip (due to the flexible cantilever) over sample surface. This offered good sensitivity by reflecting a laser beam off the end of the tip and into a photodetector to obtain an "optical lever: capable of detecting even the smallest movements.

The image can be obtained in several ways, such as the contact mode, tapping mode and non-contact mode [73]. The contact mode is the most common one. In this mode, the tip and sample remain in contact as the scanning proceeds. Tapping mode is another most common mode used in AFM. When operated in air or other gases, the cantilever is oscillated at a resonant frequency and positioned above the surface. More recently, there has been much interest in phase imaging. Non-contact mode is another one which may be employed when imaging by AFM. The cantilever must be oscillated above the surface at such a distance that we are no longer in the repulsive regime of the inter-molecular force curve. In addition, if the scanner moves the sample perpendicular the long axis of the cantilever, friction between the tip and sample causes the cantilever to twist. Through signal separation, the AFM can distinguish the resultant left-and-right motion from the up-and-down motion the reflected laser beam. Therefore, it can measure tip-sample friction while imaging the sample topography.

For instance, Figure 2.7 illustrates images of a nano-crystalline 304stainless steel surface. The surface morphology can be readily revealed.
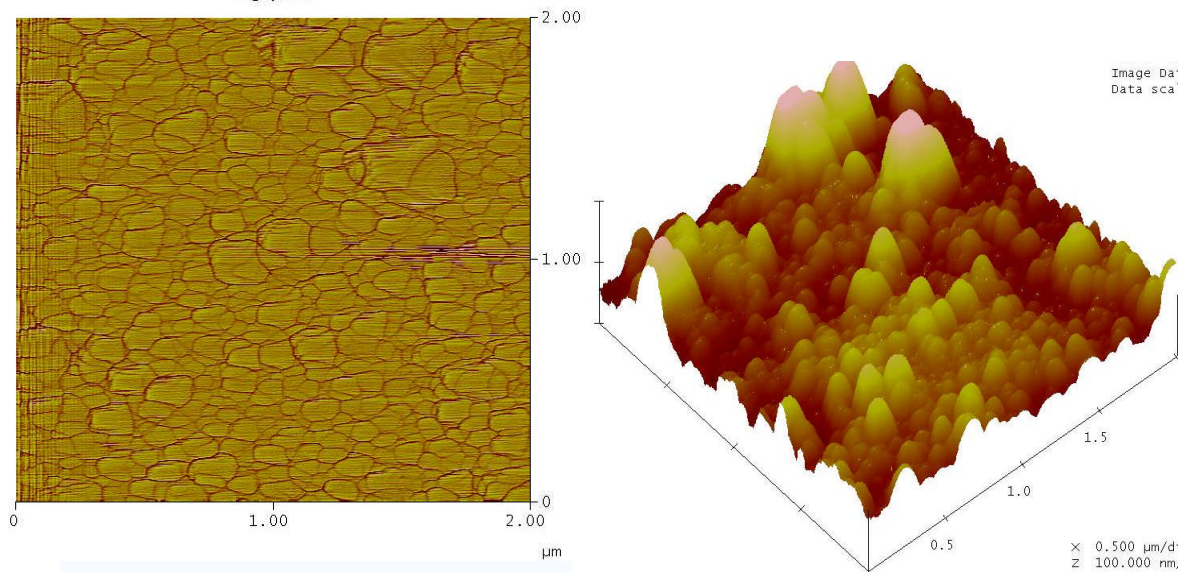
Fig 2.7 Images of nano-crystalline surface taken by the AFM

2.2   Adhesive force measurement using AFM

A force plot is used to measure tip-sample interactions. A force plot is an observation of tip-sample interaction which yields information regarding the sample and/or tip. Adhesive forces are reflected by the deflection of the cantilever when it is approaching to sample surface and lifting off (Fig 2.8).
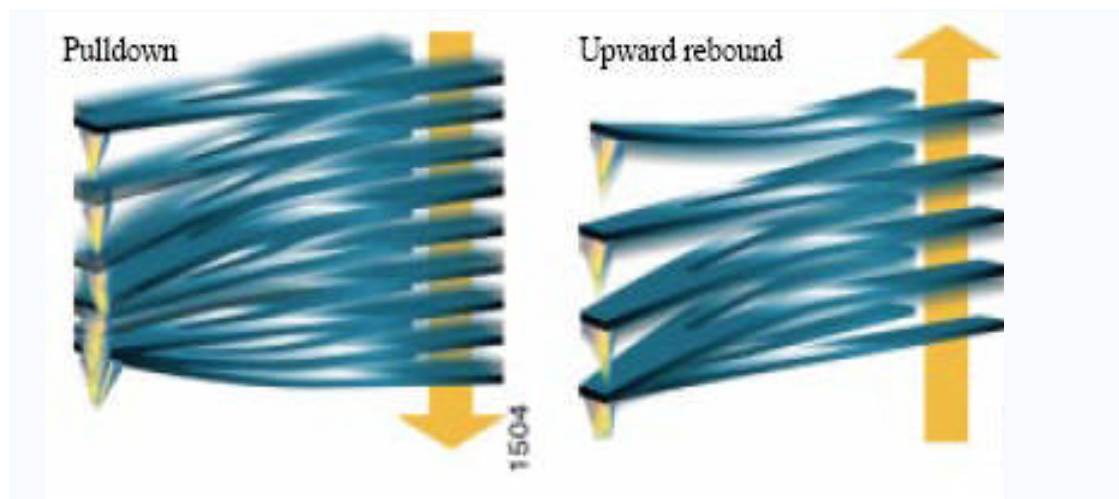
Fig 2.8 As the tip approaches the surface, it is frequently pulled down by attractive forces (left). As the tip lifts off, it sticks to the sample until pulled away, resulting in a sharp rebound (right)

A contact AFM force plot using a silicon nitride tip determines the interaction of tip with a sample surface. For the pliant property (and lower spring constant) of silicon nitride probes, they are sensitive to attractive and repulsive forces. A force plot in contact AFM is illustrated in Fig 2.9

2 position - 0.10 µm/div
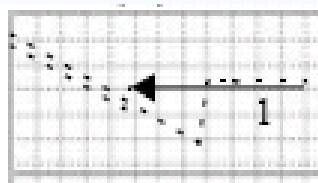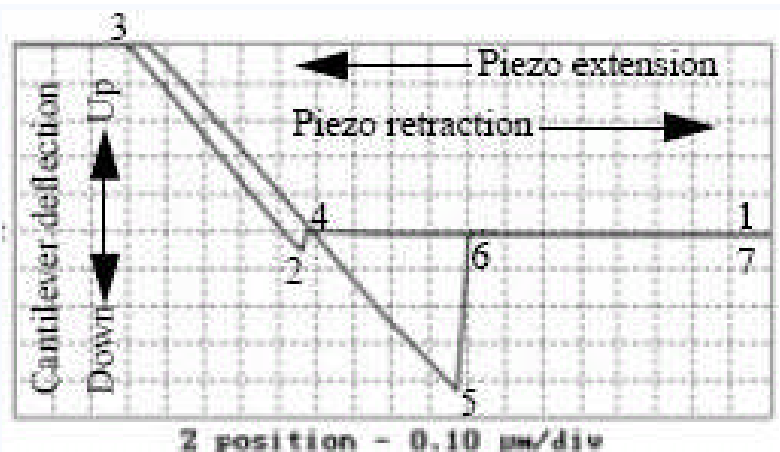
Piezo extends; tip descends. No contact with surface yet.
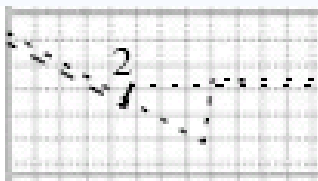
Tip is pulled down by an attractive force near the surface
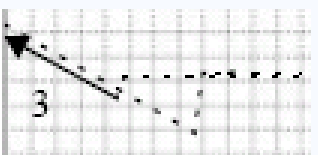
As tip is pressed into the surface, the cantilever bends upward
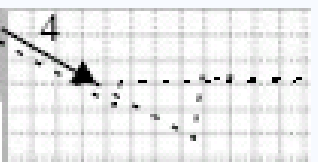
Piezo retracts; tip ascends. Cantilever relaxes downward until the tip force is in equilibrium with the surface forces.
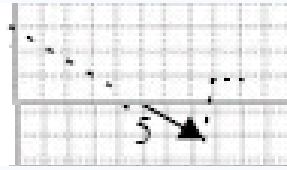
Piezo continues retraction; tip ascends further. Cantilever bends downward as surface attraction holds onto the tip.
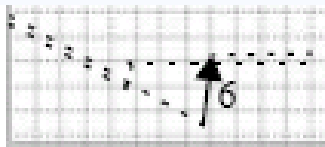
As tip continues its ascent, tip finally breaks free of surface attraction. Cantilever rebounds sharply upward.
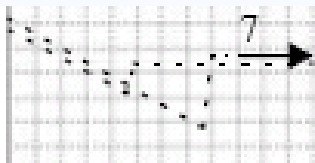
As piezo continues retracting, tip continues its ascent. No further contact with surface this cycle.

Fig 2.9   A representative force curve

In addition to dedicated force measurement, the force plot may be used to enhance routine topographic imaging. Force plot is frequently used to adjust , calculate ,and minimize contact force between the cantilever and sample. Force plot may also be used diagnose SPM performance and determine sensitivity of the cantilever deflection voltage versus voltage applied to the piezo as shown in (Fig

2.10). Figure 2.10 illustrates images of cantilever shape changes corresponding to various stages of deflection which can help us better understanding a force plotting process.
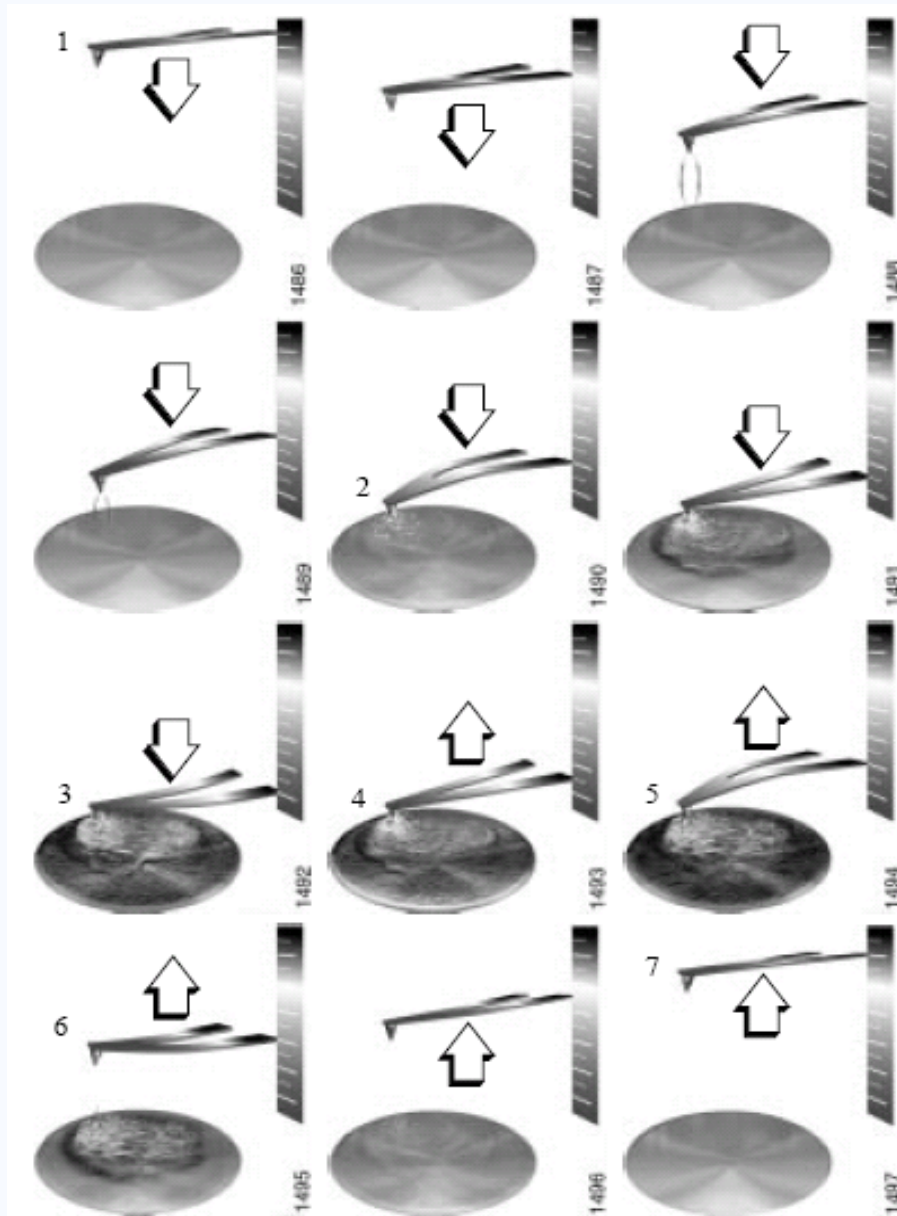
Fig 2.10 Tip-sample interaction during force ploting

In scanning probe microscopy, the setpoint refers to how much tip-sample force is maintained. In contact AFM, setpoint is determined by the amount of cantilever flexion. As the setpoint increases, the cantilever flexes more and tip-sample force increases. The setpoint can be adjusted so that it lies between the flat segment of the force curve which corresponds to the zero deflection point, and the tip of the retraction scan where the cantilever pulls off the sample surface Vcsmin. (The contact force is at its minimum when Vcsmin is on the centerline of the deflection-signal axis.)

The force curve (Figure 2.11) clearly shows the relationship between the setpoint and the deflection of the cantilever. Because the setpoint defines the value of the deflection signal maintained by the feedback loop, the force curve can be used to calculate the adhesive force of the tip in the sample if the spring constant, k, of the cantilever is known. The contact force is defined by the equation:

$$\mathbf{F = k(\triangle Z)}$$

$\triangle Z$ is the Z distance from the control point to Vcsmin in nanometers. An example of how to calculate the contact force from the force plot graph is shown in Fig 2.11
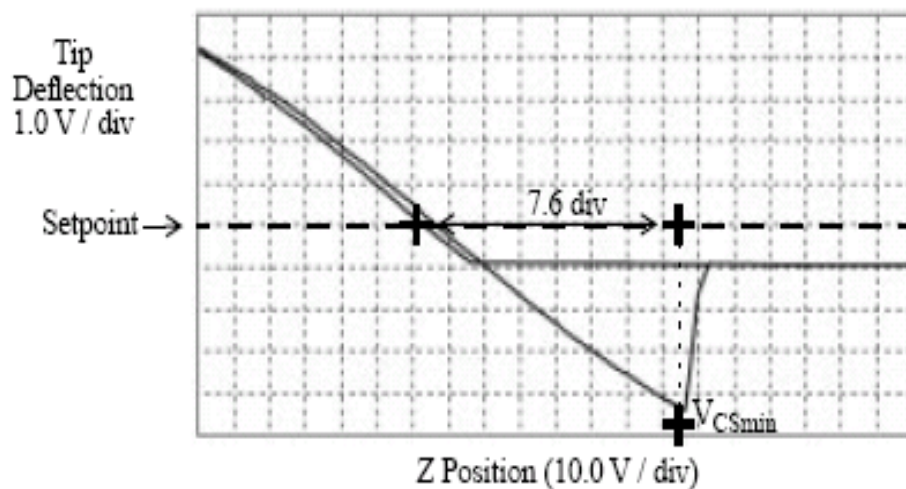
Fig 2.11 computing contact force

Recalling that contact force F is equal to k($\triangle$Z), we can calculate the contact force from the sample plot above . Let us assume, for example , that the spring constant of the cantilever is k=0.06N/m and that Z piezo sensitivity= 2 nm/v. The plot in Fig. 2.11 may be measured at the point where the retract portion of the curve intersects the setpoint to tip pull-off. The distance is then times the Z piezo sensitivity to obtain $\triangle$Z. In this example: we have

$\triangle$Z =7.6div x 10.0V/div x 2nm/V= 152nm

Therefore, the contact force is calculated as :

F= 0.06n/m * 152nm = 9.12nN

2.3 Biological applications of AFM

One of the advantages of AFM is that it can also image the non-conducting surfaces, which leads to a variety of applications for biological systems, such as analyzing the crystals of amino acids and organic monolayers. Applications of AFM in the biosciences include: DNA and RNA analysis [74]; Protein-nucleic acid complexes; Chromosomes; Cellular membranes; Proteins and peptides[75]; Molecular crystals; Polymers and biomaterials; Ligand-receptor binding. Bio-samples have been investigated on lysine-coated glass and mica substrate, and in buffer solution. By using phase imaging technique one can distinguish the different components of the cell membranes.

Little sample preparation is required for bioimaging with the AFM [76]. In most cases it is as simple as spotting a few microliters of solution on mica or glass. Contaminations that cover surface features have to be avoided or removed. First the substrate-adsorbate should be rinsed with a large excess of buffer. The following

procedures are dialysis, centrifugation and homogenization. In order to get good contrast and to reduce mechanical damage of the soft biological materials, the samples can be stabilized by adding covalent cross-linking agents or certain cations that are able to link the constituents of the sample to each other or to the substrate. Cooling can also stiffen the sample. Nevertheless, all these methods have significant influence on the properties of biomolecules. The sharper tip (15-20nm in diagram) now is available commercially, which significantly facilitates the application of AFM in characterization of biological systems. One area of significant progress is the imaging of nucleic acids [77]. The ability to generate nanometer-resolved images of unmodified nucleic acids has broad biological applications. Chromosome mapping (Fig 2.12, transcription, translation and small molecule-DNA interactions such as intercalating mutagens, provide exciting topics for high-resolution studies. A highly reproducible AFM image of DNA was obtained in 1995[78]. Four major advances that have enabled clear resolution of nucleic acids are: Control of the local imaging environment including sample modification; TappingMode scanning techniques. (Tapping mode is used to obtain high resolution topographic imaging of sample surfaces that are easily damaged. In *tapping mode* the AFM cantilever is driven to oscillate up and down at near its resonance frequency by a small piezoelectric element mounted in the AFM tip holder. The piezo motion causes the cantilever to oscillate with a high amplitude (typically greater than 20nm) when the tip is not in contact with the surface. The oscillating tip is then moved toward the surface until it begins to lightly touch, or tap the surface.); Improved AFM probes (such as standard silicon

nitride probes modified by electron beam deposition and Oxide Sharpened NanoProbes) and Compatible substrates (such as salinized mica and carbon coated mica).
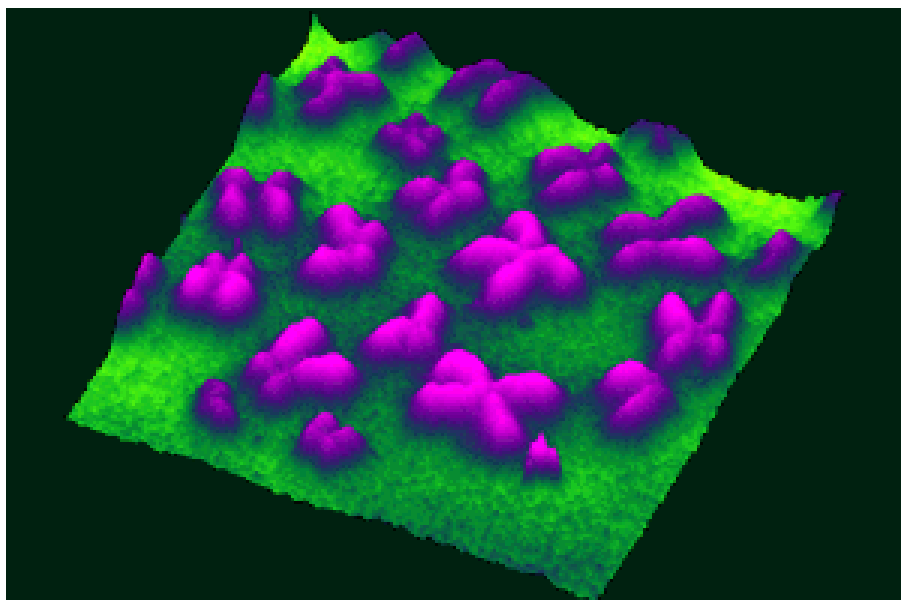
Fig 2.12   Human chromosomes taken by AFM[78]

Cell biologists have applied the AFM's unique capabilities to study the dynamic behavior of living and fixed cells such as red and white blood cells, bacteria, platelets, cardiac myocytes, living renal epithelial cells, and glial cells. For example, plasma membrane has been imaged [79]. The dynamic membrane invagination process was observed in the presence of calcium and when calcium levels were reduced the process was prevented. 30nm lipidic pore formation could also be resolved during calcium reduction. AFM imaging of cells usually achieves a resolution of only 20-50 nm, not sufficient for resolving membrane proteins but still suitable for imaging other

47

surface features, such as rearrangements of plasma membrane or movement of submembrane filament bundles. The requirement for the imaging buffer is not restrictive, as long as the buffer does not severely affect the integrity of the cells.

There has been recent success in imaging individual proteins (Fig 2.13) and other small molecules with the AFM such as collogen [80]. Smaller molecules that do not have a high affinity for common AFM substrates have been successfully imaged by employing selective affinity binding procedures [80]. For instance, low affinity that IgG molecules have for mica is overcome by cloning a metal-chelating peptide into the carboxy terminus sequence of the IgG's heavy chain. The recombinant sequence is transformed into cells that expressed the complementary light chain. The purified IgG containing the metal-chelating peptide is shown to bind to nickel-treated mica. Covalent binding of biological structures to derivatized glass substrates has also enabled high resolution imaging of some samples that are not stable on untreated glass substrates. New approaches in AFM have made higher resolution imaging of a variety of small molecules possible.
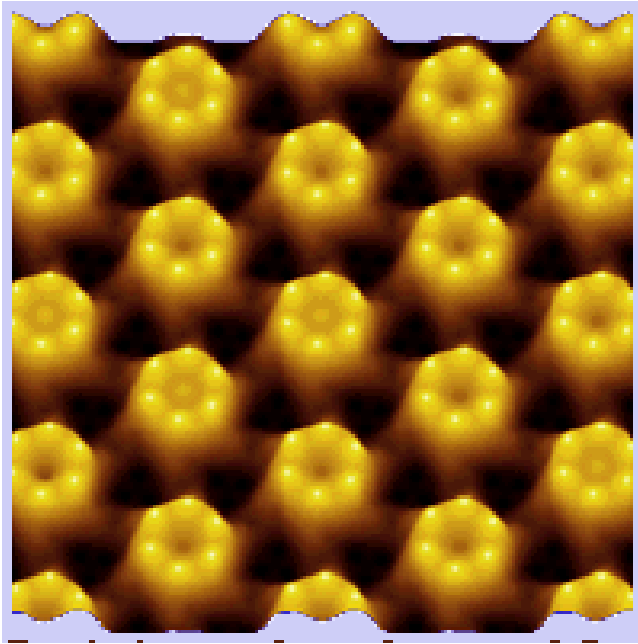
Fig 2.13 A protein surface layer taken by AFM

The recent innovation, such as Digital Instruments BioScope system, which combines the high resolution of AFM with the ease of use and familiarity of inverted optical microscopes, has further enhanced AFM for biological imaging.

Countless biological processes - DNA replication, protein synthesis, drug interaction, and many others - are largely governed by intermolecular forces. AFM has the ability to measure forces in the nanonewton range. This makes it possible to quantify the molecular interaction in biological systems such as a variety of important ligand-receptor interactions. Another application of AFM force measurements is to image or quantify electrical surface charge. The dynamics of many biological systems depends on the electrical properties of the sample surface. In addition to measuring binding forces and electrostatic forces, the AFM can also probe the micromechanical properties of biological samples. Specifically, the AFM can be used to determine

elasticity and, the viscosity of samples ranging from live cells and membranes to bone and cartilage.

In summary, AFM has the following functions:

·Characterization of morphology, texture and roughness of surfaces.

·Measurement of surface adhesive force

·Measurement of the frictional force at the nanometer scale.

·Evaluation of mechanical properties such as hardness and elasticity, of soft substances.

Chapter 3

Adherence of *Pseudomonas aeruginosa* Biofilm to Stainless Steel and Its Enhancement at Grain Boundaries

3.1 Introduction

Surface adhesion is known to be important to the formation of bacterial biofilms on medical implants, a leading cause of medical implant failure [81]. Grain boundaries (GBs) in materials of medical implants have been noticed to be preferential locations for bacteria to stay, e.g., congregation of *P. aeruginosa* at grain boundaries of stainless steel [82], implying that the GBs have higher affinity for bacterial biofilms which protect bacteria from antibody attack. It is therefore essential to investigate the difference in the interaction with a bacterial biofilm between the GB and a grain in order to effectively control the formation of bacterial biofilms through surface engineering of implants. This requires a quantitative means to determine the interaction between a biofilm and a specific surface area.

Biologically relevant interactions generally occur in aqueous salt environments

where all components are fully hydrated. While the affinity of biological interactions varies substantially, apparent affinity constants generally range from nmolar to millimolar (most physiologically regulated interactions have an affinity constant in the micromolar range) for univalent interactions (with multi-valent interactions allowing for much higher apparent affinity constants due to avidity). The pilin receptor binding domain (RBD) interacts with stainless steel surfaces with a very high apparent affinity, where a monomeric synthetic peptide has an apparent K_i (the concentration of the peptide that inhibits 50% of the binding of the pilus ligand (which displays 3 independent receptor binding domains, under conditions where the pilus ligand does not saturate the stainless steel surface) of 0.2 nM, a reflection of an apparent affinity constant that is higher than is observed for most biological interactions (the highest affinity biological interaction that has been document is that of biotin with avidin where half saturation of binding would be observed in the pM range). The interaction of proteins and their ligands is generally highly specific and dependent upon a range of specific molecular interactions and spatial complementarily. However, the affinity and stability of the interaction is largely determined by what are termed hydrophobic interactions. In thermodynamic terms, most of the energetic contribution to receptor-ligand interactions arises from the exclusion of bulk solvent (water) from the interaction site as the change in entropy does not positively contribute to the occurrence of the molecular interaction, and the energetic contribution of the direct molecular interactions does not generally negate the entropic energy term but rather confers the specificity of the interaction. Tightly

bound water or solvation or hydration waters are not freely exchangeable with bulk solvent water and do not contribute to receptor-ligand binding energetics and are readily observed in protein crystallographic studies of protein-ligand complex interfacial regions. Thus the very high affinity of the pilin RBD for stainless steel is highly unusual due to the domain's high flexibility in both the cognate protein and as the synthetic peptide which increases the entropic penalty for the interaction, and due to the rather small potential interaction area of the monomeric peptide with the steel. This suggests that a hydrophobic effect does not account for the affinity of the interaction of the peptide with the steel surface or a conditioning film found on that surface. We thus pursued a methodological approach that reduces the potential of interaction of the peptide with a conditioning film and constrains the hydrophobic effect. Stainless steel was polished, etched, solvent washed to remove organics, washed with H_2O (deionized, then filtered to remove ions, organics and particles immediately before use), and air dried. Thus bulk water has been removed, limiting available H_2O to what can experimentally be defined as solvation water or bound water. Thus RBD interactions determined by force mapping represent a system where there is minimal potential for a "conditioning film" and no bulk water to drive or stabilize a molecular interaction between the RBD and the steel surface.

P. aeruginosa type IV pili mediate high affinity binding to stainless steel surfaces (a common material for medical implants) via what is termed the receptor binding domain, a semi-conserved sequence located at the C-terminus of the *P. aeruginosa* PilA structural protein [83]. Fig 3.1A illustrates full-length pilin sequences of *P*

aeruginosa strains PAK PAO KB7 and K122-4. Boxed area represents disulphide loop

region of residures 128-144 of the PAK sequence. The disulphide loop region contains

and epithetical cell bonding domain and displays a conserved antigenic epitope

despite extensive sequence variation. Fig 3.1B. shows Structural overlay of *P.*

aeruginosa strains PAK (red) and K122-4 (blue) structured monomeric pilins.

Disulphide loop region is highlighted by boxed area.

A
```
          ************************ **:*,:*:: : .:: . *** *. :. . :              .         .. .
PAK    FTLIELMIVVAIIGILAAIAIPQYQNYVARSEGASALASVNPLKTTVEEALSRGWS-VKSGTGTED--ATKKEVPLGVAA
PAO    FTLIELMIVVAIIGILAAIAIPQYQNYVARSEGASALATINPLKTTVEESLSRGIAGSKIKIGTTA--STATETYVGVEP
KB7    FTLIELMIVVAIIGILAAIAIPAYQDYTSRSQVSRVMAEAGSLKTAVEACLQDGRTAVGTAAGQCDPGATGSSLLTGASQ
K122-4 FTLIELMIVVAIIGILAAIAIPAYQDYTARAQLSEAMTLASGLKTKVSDIFSQDGSCPANTAATAG---IEKDTDINGKY

          ::      :     .        . . .      .. : :*. .: *|* : * : *: *|
PAK    DANKLGTIALKPDP-ADGTADITLTFTMG-GAGPKNKGKIITLTRTAADG---LW|CTSDQDEQFIPKGCSR|------
PAO    DANKLGVIAVAIE--DSGAGDITFTFQTG-TSSPKNATKVITLNRT-ADG---VW|ACKSTQDPMFTPKGCDN|------
KB7    TSQTLPTNTGVPQVLDPLTTQTTIIVTFGNGASAAISGQTLTWTRD-VNG---GW|SCATTVDAKFRPNGCTD|------
K122-4 VAKVTTGGTAAAS----GGCTIVATMKAS-DVATPLRGKTLTLTLGNADKGSYTW|CTSNADNKYLPKTCQ|TATTTTP
```

B

Fig 3.1   Sequence and structure of *P. aeruginosa* pilins[83]

It has been previously demonstrated that a synthetic receptor binding domain derived from the PAK pilin, peptide PAK(128-144)ox, inhibits heterologous *Pseudomonas* biofilm formation on steel and that the synthetic receptor binding domain derived from strain PAO pili, PAO(128-144)ox, inhibits PAK pili and PAK bacterial cell binding to stainless steel while PAO(128-144)ox_Scrambled [83] (a peptide of identical composition with an oxidized disulfide bridge but scrambled amino acid sequence) does not inhibit pilus or bacterial cell binding to steel. Therefore some of the peptides have same binding properties of *Pseudomonas* biofilm to stainless steel surface. All synthetic peptides used in this study were synthesized by solid phase. All peptides are N-α-acetylated with a free carboxyl. Peptides with a formed disulfide bridge between cysteine 129 and 142 are identified by an ox. E-coil PAK(128-144)ox was expressed recombinantly form a pRLD-E plasmid where the PAK(128-144)ox DNA sequence was spliced inframe with the E-coil utilizing synthetic oligonucleotides and expressed in *E. coli* strain BL-21. The expressed peptide was purified by metal affinity chromatography, the purity and formation of the disulfide bridge was confirmed by mass-spectroscopy and N-terminal protein sequencing [83]. The binding of the synthetic receptor binding domains to steel is of high affinity, with PAK(128-144)ox displaying an apparent Ki of 0.2 nM for inhibition of purified pili binding to steel while the affinity of PAO(128-144)ox is considerably higher than that of the PAK binding domain [81]. The previous experiments were performed in solution and thus determining whether the receptor binding domain interacted directly

with the steel surface or with a conditioning film that might have formed on the steel surface could not be determined. In order to further investigate the peptide-steel interaction, in this study a direct force measurement was carried out by utilizing atomic force microscopy (AFM) in a "dry" (normal building relative humidity, 30-40 %RH) air environment.

3.2. Specimen preparation

Preparation of peptide derivatized AFM tip

The Au-coated AFM tips were uniformly coated with Au and displayed no apparent structural anomalies when examined by SEM (Fig. 3.2).
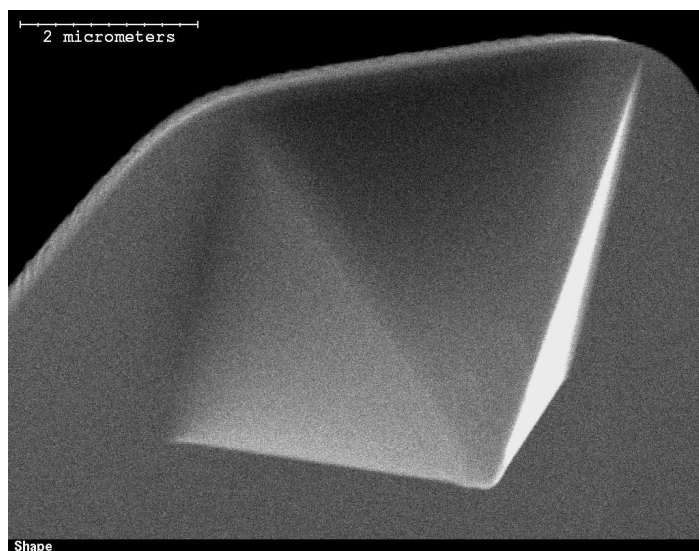
Fig 3.2. AFM tip that has been coated with 20 nm of gold

As the synthetic receptor binding domain is small (roughly rectangular in nature

with dimensions of ~15.7 Å by ~17.5 Å), coupling the peptide directly to an AFM tip could compromise the interaction of the peptide with a steel surface area on a nano/micro scale. As it is a nano/micro scale interaction, the adhesion of receptor binding domain to a grain boundary could be influenced by the properties of the grain boundary. An approach was utilized to indirectly derivatize AFM tips with the peptide presented on a coiled-coil structure such that the peptide would be maintained ~41 Å way from the AFM tip surface and thus allowed the receptor binding domain have a higher degree of freedom to interact with the metal surface. A *de novo* designed heterodimeric coiled-coil system was utilized for this application [84,85] , which consisted of a 35 residue K-coil that was coupled to the AFM tip and served to capture a 35 residue E-coil [86] with the receptor binding domain (PAK(128-144)ox) fused to the C-terminus of the E-coil peptide. The affinity of the coiled-coil interaction is 60 pM [87] and the resulting coiled-coil is an extraordinarily stable structure that is only partially dissociated in solvent at an ambient temperature of 80^0 C [88]. The construction of the derivatized AFM tip is illustrated in Figure 3.3.
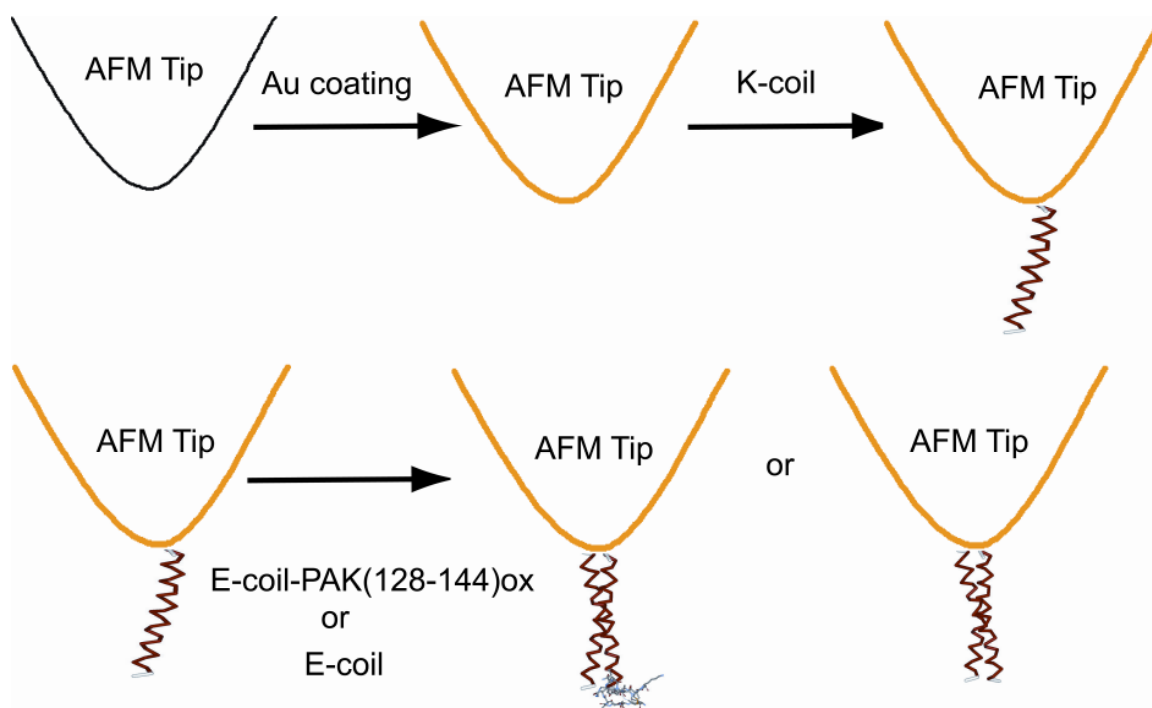
Fig 3.3. Schematic diagram of the derivatization of a standard AFM tip with a coiled-coil displayed PAK(128-144)ox pilin receptor binding domain.

A standard AFM silicon nitride tip was coated with 20 nm of Au by sputtering and the Au-coated tip was then immersed in 25 μM K-coil peptide synthesized with an additional N-terminal cysteine residue in PBS pH 7.2 for 40 min at room temperature such that the K-coil was coupled to the Au coating through the free sulfhydryl of the cysteine residue. The derivatized AFM tip was then washed with distilled H_2O and then immersed in 5 mM cysteine in PBS pH 7.2 for 40 minutes at room temperature, washed with distilled H_2O and then immersed in 1 μg/mL of E-coil-PAK(128-144)ox for 40 minutes at room temperature to allow the formation of the heterodimeric coiled-coil with the receptor binding domain being displayed on the end of the E-coil at the tip of the AFM tip. Alternatively, synthetic E-coil was utilized to generate an Au-coated AFM tip which displays only the heterodimeric coiled-coil construct as a control AFM tip. The functionalized tips were then washed

with distilled H$_2$O and then air dried for subsequent use. The peptides were prepared as previously described with the purity of the peptides being confirmed by HPLC reversed phase chromatography and mass spectroscopy as previously described. Additional peptides utilized in this study includes a synthetic PAO pilin receptor binding domain, PAO(128-144)ox, and the scrambled PAO pilin receptor binding domain, PAO(128-144)ox_Scrambled, the purity of these peptides, and the oxidation state of the disulfide bond was confirmed as previously described. Table 3.1 describes all peptide sequences used in this study.

Table 3.1. Synthetic peptides and peptide sequences employed or referred to in this study.

Peptide	Sequence
PAK(128-144)ox	Ac-K-**C**-T-S-D-Q-D-E-Q-F-I-P-K-G-**C**-S-K-OH
PAO(128-144)$_{OX}$_Scrambled	Ac-N-C-P-D-F-D-P-T-K-K-G-M-Q-A-C-T-S-OH
PAO(128-144)ox	Ac-A-C-K-S-T-Q-D-P-M-F-T-P-K-G-C-D-N-OH
cys-K coil	Ac-C-(K-V-S-A-L-K-E)$_5$-OH
E-coil	Ac-(E-V-S-A-L-E-K)$_5$-OH
E-coil PAK(128-144)ox	H$_5$-(E-V-S-A-L-E-K)$_5$-K-**C**-T-S-D-Q-D-E-Q-F-I-P-K-G-**C**-S-K*

Stainless Steel Surface Characterization

Commercial grade 304 stainless steel specimens with dimensions of 2x2x2cm were annealed at 1160^0 C for 20 minutes in Ar atmosphere followed by air cooling. The steel surface was then polished, using sand papers up to 1200# and then with an aqueous slurry of 0.05 μm colloidal silica. The polished sample surface was etched with a hydrochloride/nitric acid solution for 10 sec, washed ultrasonically with reagent grade acetone (10 min) and ethanol (5 min). The average grain size of the

stainless steel specimens was ~ 30µm, as determined by microscopic examination with polarized light.

In order to determine the adhesive force at the grain boundary, the adhesive force between the AFM tip and a stainless steel surface was measured using an atomic force microscope by two experimental approaches: 1) a direct measurement utilizing a coiled-coil derivatized tip as a reference, and 2) abolishing the interaction by pre-treating the surface with a synthetic receptor binding domain or a scrambled sequence that does not interact with steel. The AFM tip was moved from one grain to another (Fig 3.4) so that the adhesive force at different locations could be measured. The adhesive force at the grain boundary and within grains was then determined. (The adhesive force was determined from the deflection of the tip cantilever possessing a spring constant of 0.06N/m.)

sam5
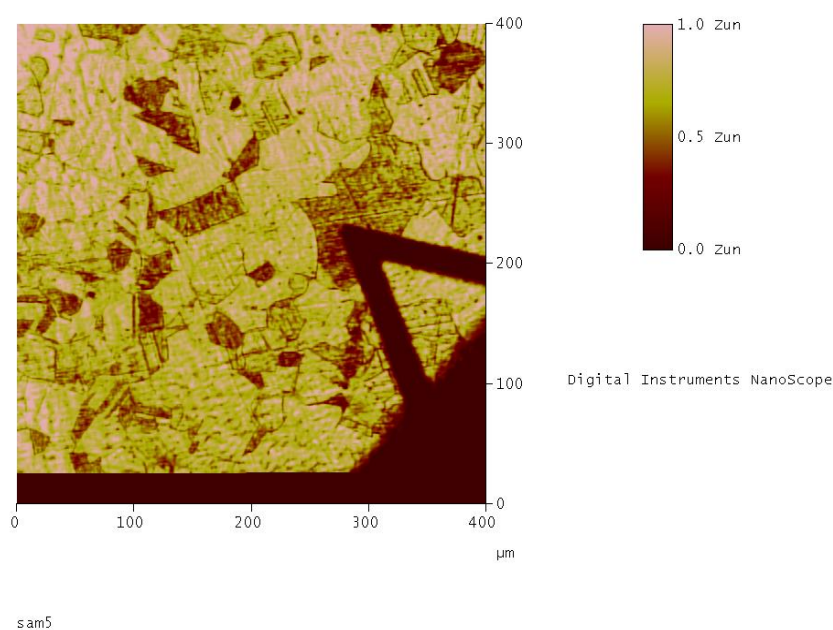
Fig 3.4   Optical image from AFM showing the stainless steel surface (note the obvious grains and grain boundaries) and the AFM probe.

3.3 Interaction of Receptor Binding Domain Derivatized AFM Tips With Steel

The adhesive force between AFM silicon nitride tip and stainless steel surface was determined across 20 grain boundaries (replicated 3 times for each grain). The average adhesive force within a grain was 17.5 ± 1.0 nN while that at a grain boundary was 30.5 ± 1.0 nN. (Figure 3.5) The results indicate that the adhesive force at grain boundaries was ~1.74 fold higher than that within grains. The increased adhesive force at grain boundaries is largely attributed to an increase in electron activity at a grain boundary; this has been evidenced by observed decrease in the electron work function (EWF) at grain boundaries in other metals [89] and confirmed relationship between the EWF and adhesion [90].
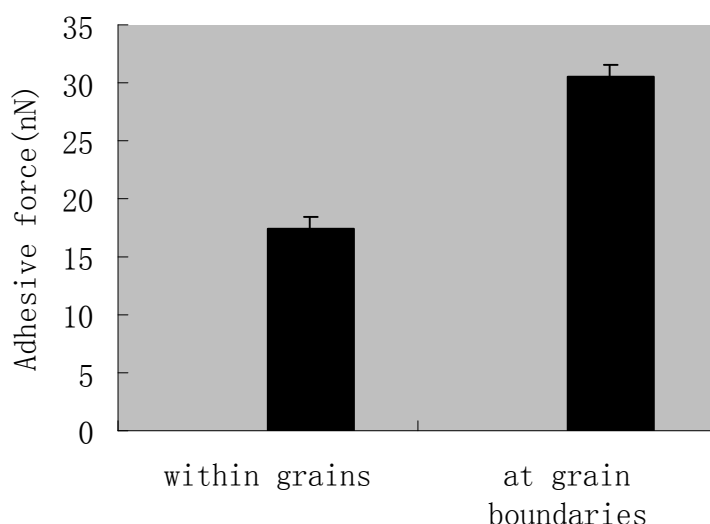
Fig 3.5 Average adhesive force within grains and at grain boundaries using AFM regular silicon nitride tip.

The adhesive force between the derivatized AFM tip and the stainless steel surface was then determined as described above (20 grain boundaries and their respective grains were examined with each observation being replicated 3 times). As anticipated the adhesive force between the receptor binding domain derivatized AFM tip and the steel was observed to be considerably stronger than that observed for the standard Si_3N_4 AFM tip. The mean adhesive force at the grain boundary for the peptide (coiled-coil-PAK(128-144)ox) derivatized tip was 86.8 $\pm$ 13.3 nN while the mean adhesive force within a grain was observed to be 47.6 $\pm$ 10.7 nN. Figure 3.6 illustrates a single adhesive force measurement of a coiled-coil-PAK(128-144)ox derivatized AFM tip with stainless steel surface, the measurement was performed at a grain boundary and several position within grains near the grain boundary.
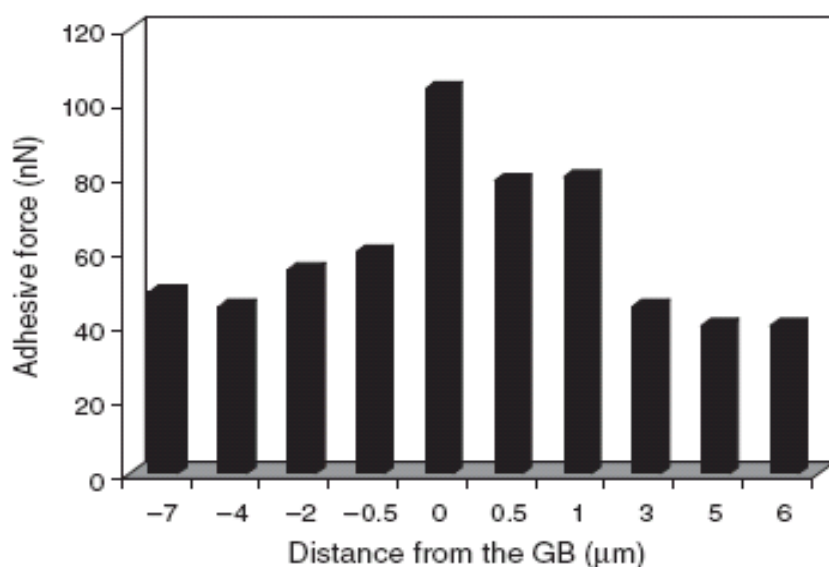
Fig 3.6   Direct adhesive force measurements (in nN) of a AFM tip derivatized with the coiled-coil PAK(128-144)ox construct as a function distance of the AFM tip from a grain boundary (in μm) with the stainless steel surface. The data presented represents a single experiment.

This represents an increase of 2.84 fold and 2.72 fold in the adhesive force between the derivatized AFM tip relative to the standard AFM tip for the grain boundary and within the grain respectively, and with the grain boundary adhesive force being ~1.84 fold greater than that observed within the grains. Derivatized AFM tips were robust and did not exhibit any evidence of performance decay or change until ~ 80 independent measurements were taken. While these observations suggest that the receptor binding domain mediates direct binding to the steel surface, the derivatized AFM tip varies considerably from the standard AFM tip (i.e., 20 nm Au coating, and multiple coiled-coil constructs with displayed receptor binding domains).

To ascertain how much of the additional adhesive force was attributable to the receptor binding domain-steel interaction two independent strategies were utilized: a) The adhesive force of control derivatized AFM tips were determined by employing AFM tips coated with Au and derivatized with an equivalent concentration of the heterodimeric coiled-coil but where there was no receptor binding domain present, and b) Pre-treated the steel surface with either a synthetic receptor binding domain (PAO(128-144)ox which was previously demonstrated to inhibit pilus mediated binding to steel or a peptide that had the same amino acid composition as the receptor binding domain but where the amino acid sequence was altered such that the peptide did not bind to steel (PAO(128-144)ox_Scrambled [83] and then measured the adhesive force of a derivatized AFM tip that displayed a receptor binding domain on the coiled-coil structures. The additional approach utilizing a scrambled

non-functional peptide sequence displayed on the coiled-coil structures was not deemed feasible due to significant difficulties in oxidizing the two cysteine residues in the scrambled sequence to form the disulfide bond found in the native receptor binding domain (extremely low yields of the PAO(128-144)ox_Scrambled peptide were obtained in multiple syntheses) and high probability that free sulfhydryl groups could confound our studies.

Statistical analyses of all assays were preformed with GraphPad Prism Version 4.0. P-values ere determined to be significant at P< 0.05. A non-parametric one-way ANOVA test of the Data (the observed data did not differ significantly form normally distributed data, but some portions of the data were significantly skewed) was employed to determine the statistical significance of the results. Individual binding assays, with six replicates per assay, were repeated three times. Fig 3.7 illustrates the adhesive measurements on stainless steel surface, in which the error bars represents the standard deviation of the mean of adhesive forces.

Adhesive force measurements with coiled-coil derivatized AFM tips(Coiled-coil-PAK(128-144)ox and coiled-coil) indicates that the derivitization of the AFM tip had minimal effect on the adhesive force measurements relative to the standard AFM tip by (Table 3.2 and Figure 3.7.)
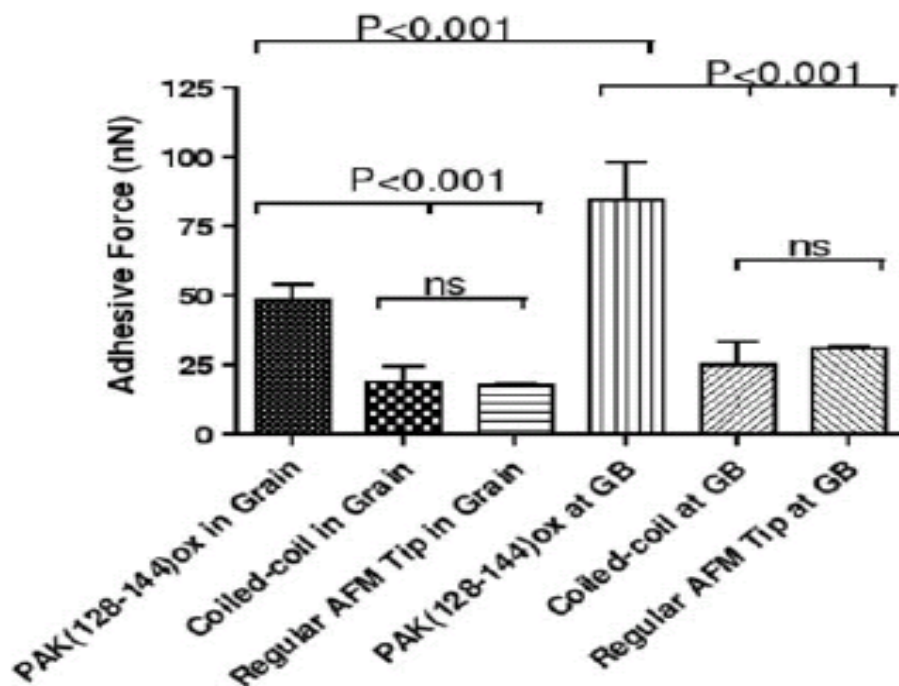
Fig 3.7 Adhesive force measurements of AFM tips derivatized with coiled-coils fused with PAK(128-144)ox and with coiled-coils which lacked the sequence with stainless steel within and at GBs. A one way ANOVA analysis was utilized to determine the probabilities of the data being significantly different.

AFM Tip	Adhesive Force Within Grain (nN)	Adhesive Force at Grain Boundary (nN)	Fold Increase at Grain Boundary
Coiled-coil-PAK(128-144)ox	47.6 $\pm$ 10.7	86.8 $\pm$ 13.3	1.82
Coiled-coil	19.6 $\pm$ 3.6	24.6 $\pm$ 5.7	1.26
Standard AFM tip	17.5 $\pm$ 1	30.5 $\pm$ 1	1.74
Attributable to PAK(128-144)ox	**28.0 $\pm$ 14.3**	**62.2 $\pm$ 19.1**	**2.22**

Table 3.2   Adhesive force measurement using peptide coated AFM tips

The adhesive force attributable to the PAK(128-144)ox receptor binding domain interaction with the steel surface can thus, with this experimental approach, be deduced to be 28.0 $\pm$ 14.3 nN within grains and to be 62.2 $\pm$ 19.1 nN or 2.21 fold higher at a grain boundary (Table 3.2).   It is interesting to note that force required to disrupt the steel- peptide interaction is proportionately higher for grain boundaries that is attributable to the materials properties of grain boundaries as observed for the standard or coiled-coil derivatized AFM tips.

An alternative approach for determining the adhesive force attributable to the PAK(128-144)ox peptide-steel interaction is to pre-treat the steel surface with saturating concentrations of a synthetic peptide that binds to the steel surface, preventing PAK(128-144)ox binding to the steel. This synthetic peptide does not interact with the PAK(128-144)ox peptide or the derivatized AFM tip.   A synthetic

receptor binding domain derived from PAO pilin, PAO(128-144)ox, has previously be

shown to inhibit PAK(128-144)ox interaction with steel (this peptide does not interact

with either the PAK(128-144)ox peptide or with the derivatized AFM tip, data not

shown) while the scrambled peptide, PAO(128-144)ox_Scrambled, does not bind to

steel and does not prevent PAK(128-144)ox binding to steel.   Utilizing this approach,

the adhesive force attributable to the PAK(128-144)ox-steel interaction was deduced

to be 20.2 ± 17.9 nN within grains and was found to be 2.12 fold higher or $42.9 \pm$

25.7 nN at grain boundaries (Table 3.3 and Fig 3.8)

Table 3.3. adhesive force measurement using another group of peptide coated AFM

tips

AFM Tip	Competitor	Adhesive Force Within Grain (nN)	Adhesive Force at Grain Boundary (nN)	Fold Increase at Grain Boundary
Coiled-coil-PAK(128-144)ox	PAO(128-144)ox	39.5 ± 9.4	44.5 ± 11.6	1.13
Coiled-coil-PAK(128-144)ox	PAO(128-144)ox_Scrambled	59.7 ± 8.4	87.5 ± 14.2	1.47
Attributable to PAK(128-144)ox		**20.2 ± 17.9**	**42.9 ± 25.7**	**2.12**
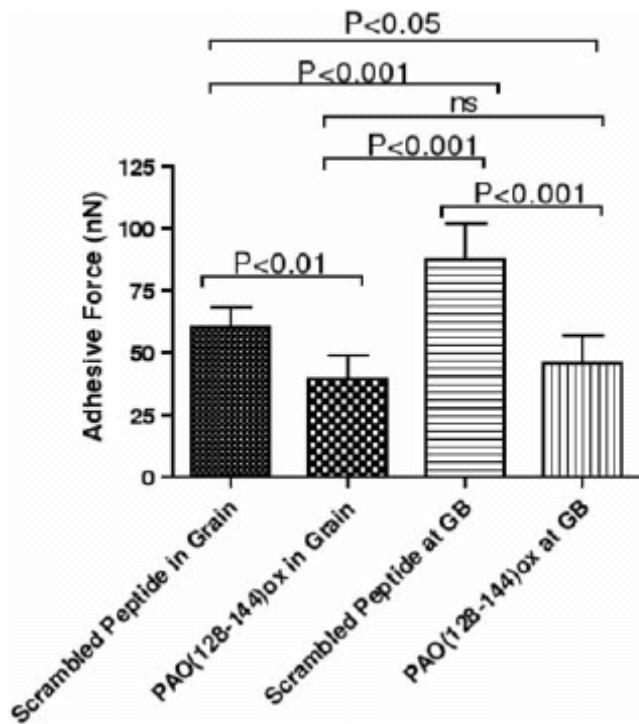
Fig 3.8 Adhesive force measurement of AFM tip derivatiezed with peptide and stainless steel that had been pre-treated with either PAO(128-144)ox peptide to inhibit PAK(128-144)ox binding to the steel or with PAO(128-144)ox_scrambled peptide which does not interact with the steel surface.

These results, obtained by a competitive approach, are in reasonable agreement with the values previously determined by a direct approach. Notably, both methods report that the peptide-steel interaction is ~ 2 fold stronger at grain boundaries. Averaging the results obtained by the two experimental approaches, the adhesive force attributable to the peptide-steel interaction indicates that within the grains the force of interaction is 24.1 nN, which is ~2.2 fold lower than that at grain boundaries with an average value of 52.6nN.

In another control test, the adhesion of an Au coated silicon nitride tip to the steel surface was determined. The average adhesive force between the tip and steel surface is approximately 17nN within grains, which is similar to that measured using the

silicon nitride tip and considerably smaller than that measured using a peptide-coated tip. This further confirms that the larger adhesion between the peptide-coated tip and the steel surface is attributed to the interaction between the coated peptide and the steel.

The observation that the adhesive force between the peptide and the grain boundary, particularly the enhanced interaction relative to what could attributable to the basic
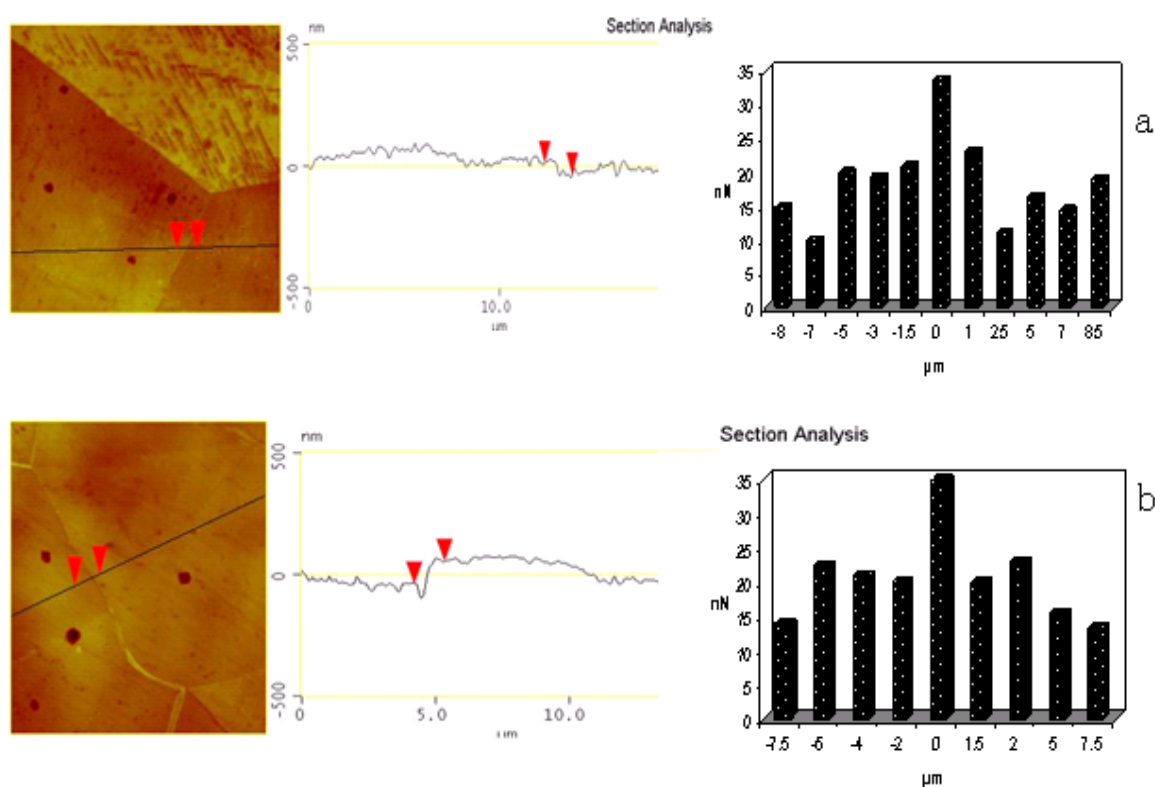
Fig 3.9 The optical image of the etched for 10 s (a), and for 20 s (b) steel surface with the AFM tracing of AFM tip displacement when dragged along the surface from the initial red triangle to the second red triangle, a linear path that crosses the grain boundary. Note that the different time periods of etching resulted in a significant difference in geometry at the grain boundary but did not result in any apparent difference in direct force measurements of the coiled-coil PAK(128-144)ox derivatized AFM from the steel as a function of the etching time.

properties of the steel grain boundary, raised a question as to the basis for the enhanced interaction of the peptide with the grain boundary. Acid etching of the steel surface causes a loss of material at grain boundaries and thus the possibility that the altered geometry of the grain boundary could affect the adhesive force measurements was considered. Steel samples were etched for 10 s or 20 seconds respectively and the degree of loss of material was determined by AFM examination of grain boundaries, and adhesive force measurements with the PAK(128-144)ox derivatized AFM tip. We observed no difference in the adhesive force at the grain boundary of steel surfaces etched for the different periods of time, although the geometric difference in grain boundary was readily determined by AFM (Fig. 3.9(a) and (b).

Thus a differential geometry at the grain boundary on etched surfaces did not contribute significantly to alteration in adhesive forces we observed at the grain boundary. This indicates that the increased strength of the peptide-grain boundary interaction could be mainly affected by the steel grain boundary properties.

3.4   Strength of the Peptide-Steel Interface

One of the biological functions of type IV pili is to power an unusual form of motility, the pilus attaches to solid surfaces through the pilin receptor binding domain, the pilus is then retracted or depolymerized back into the cell to effectively pull the cell towards the surface at a rate of 0.5 μm/s with substantial tension on the pilus [91].

In order to determine if our direct force measurements were consistent with the biological observations, we estimated the force required to disrupt a single peptide-steel interaction. The potential number of coiled-coil-PAK(128-144)ox molecules that were displayed on an AFM tip and which could potentially interact with the surface of a stainless steel specimen was estimated. The average length of coiled-coil is approximately 82.5Å(h). The tip of a gold-coated AFM tip is roughly a spherical cap with a radius of 70 -90 nm(R), bearing in mind that the Au coat is approximately 20 nm thick. Thus, the effective potential contact area may be estimated (Figure 3.10)
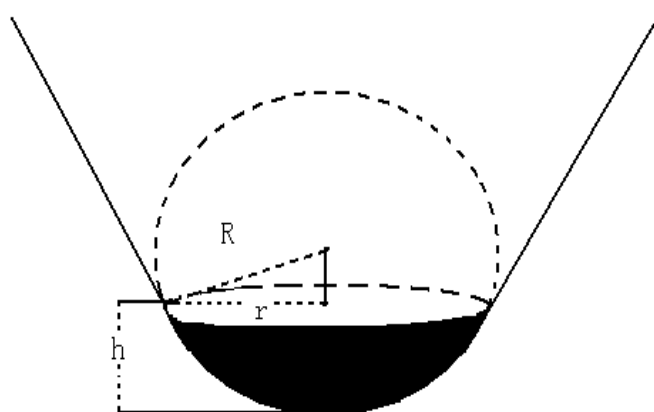
Fig 3.10 Diagram of the AFM tip indicating the portion of the tip that interacts with the stainless steel surface, and the equations for the calculation of the maximum contact area.

as S=πR(2h+r)= 1.3 * 10^6 $Å^2$ for R = 90 nm or 513083 $Å^2$, corresponding to R = 70 nm. The minimal surface area occupied by a vertically attached coiled-coil is represented by a rectangle (as determined by an examination of molecular structures

of a number of two stranded anti-parallel coiled-coils available in the protein data base) of 26 X 21 Å (including a van der waals surface for the molecule and a single layer of water as a hydration layer [this water is physically associated with the peptides and does not dissociate from the peptide when the peptide is air dried]).   Thus the minimal surface area occupied by a vertical coiled-coil is ~ 546 $Å^2$. Thus one can accommodate from 940 molecules/AFM tip (R = 70 nm) to 2,381 molecules/AFM tip (R = 90 nm).   Employing the average value reported by the two experimental methods we estimate that the strength of the PAK (128-144)ox steel interaction is in the range from 10 pN/molecular interaction to 26 pN/molecular interaction within the grain and from 22 pN/molecular interaction to 55 pN/molecular interaction at the grain boundary.   Current molecular modeling of the *P. aeruginosa* pilus suggests that the structure consists of 3-intertwined filaments that display 3 independent binding domains at the tip of the pilus [92], the left-handed three-start helix model is supported by kinetic analysis of pilin nanotube binding to steel [93]. Thus 3 pilin receptor binding domains could enable the pilus to withstand 66 to 165 pN of force when bound to steel.   The estimated force measurements are consistent with existing biological data that indicates a retracting pilus is under ~ 10 pN of stress [91] and less than the 70-120 pN force required to rupture a type IV pilus fiber [94]. .

3.5   Molecular Basis for Peptide-Steel Interaction

Bacterial biofilm formation on aqueous surfaces and their associated conditioning

films has long been recognized [95,96], which is closely related to the substrate's surface free energy, but accurate modeling of bacterial adhesion to surfaces has been challenging due to the complexities of the systems, conditioning films and hydrophobic interactions of cells and surfaces in an aqueous environment [97-99]. The current experimental approach employs conditions where hydrophobic effects are minimized (non-aqueous, "dry" environment with minimal bulk solvent effects on ligand interactions), and the potential involvement of a conditioning film (the steel surfaces were polished, etched and solvent cleaned) have been eliminated. The direct interaction of the peptide with the steel surface was then measured by AFM. A portion of the interfacial interaction between the peptide and steel surface can be directly attributed to material properties of the steel both within grains and at grain boundaries. However, the peptide-steel interaction is dependent on the peptide's sequence rather than it's molecular composition, and the interaction displays a significant preference for grain boundaries that exceeds what is predicted based on the difference in surface free energy or materials adhesive force increase at the grain boundary (~2 fold increase in adhesive force for the peptide at the grain boundary as compared to a ~1.7 fold increase observed with standard or ~1.3 fold increase observed with coiled-coil derivatized AFM tips). The pilin receptor binding domain is a self-folding domain which in aqueous solution at room temperature contains two discrete β-turns [100] and two families of conformers due to the existence of both a *cis* and a *trans* conformation of the proline in the sequence. The solution structure of the PAK pilin receptor binding domain is similar to that observed in the crystal

structure of PAK pilin in a low solvent content crystal [101] but the molecular

structure of the air dried pilin receptor binding domain is unclear. The molecular

basis for the interaction of the peptide and steel is uncertain at this time, but likely

results from the stabilization or sharing of surface electrons from the metal in addition

to the expected van der Waals interactions (which are generally fairly weak). The

higher adhesive force at GB could be largely attributed to increased electron activity

at GB corresponding to lower EWF [89] (Electron work function-the minimum

energy required to move electrons from inside a metal to its surface). The more active

the electrons at a surface, the more reactive is the surface [102]. As demonstrated

previously [103],   the defects such as dislocations at GB excite electrons and render

them more active in participating reactions occurring on surfaces [104]. It should be

mentioned that high affinity protein-metal interactions have not been frequently

observed, although proteins that bind very effectively to metal surfaces have been

documented [105], and the pilin receptor binding domain may represent a novel

protein architecture that has evolved primarily for this function. It is interesting to

note that other type IV bacterial pili have recently been observed to function as

nano-wires to transfer electrons to or from the bacterial cell surface [106,107].

3.6   Conclusion

The *P. aeruginosa* pilin receptor binding domain is a self folding domain that

interacts directly and with high affinity to stainless steel surfaces. The synthetic

peptide displaying a ~2 fold stronger binding interaction with grain boundaries in

stainless steel is estimated to have a molecular interaction strength of 26-55 pN/molecular interaction. The interaction of the peptide with steel is dependent upon the peptide's 3^D molecular shape, and the peptide can be conjugated or fused to other molecules while retaining it's steel binding activity.   Bacteria have evolved a highly effective ligand to mediate binding to metal surfaces, with a preferential affinity for grain boundaries which appears to account for initial of biofilms on metal grain boundaries.   The pilin receptor binding domains thus provides a robust probe for assessing biofilm formation potential on surfaces and for identifying the location of grain boundaries.

The pilin receptor binding domains may have considerable potential in fabricating a variety of nanodevices where biological material is specifically coupled to metal surfaces. Nature appears to have illuminated an eminently feasible method of generating biometallic interfaces, the peptide can be readily coupled to other molecules and then used to readily attach biological molecules to metal surfaces in a highly specific orientation.

Chapter 4

Surface nanocrystallization of stainless steel for reduced bio-film's adherence

4.1   Introduction

Bacterial adherence to the surface of a metal significantly influences the formation of a biofilm on the material and is largely affected by its surface free energy.[109,110]. Surface nanocrystallization of metallic material surface has been demonstrated to be an effective approach for modifying the surface energy of metals [111]. The surface energy is directly related to surface activity, which can be characterized by the Electron Work Function (EWF) [112]. In general, the EWF is   expressed as:

$$\varphi = E0 - Ef$$

 E0 is the energy of electron at infinity and Ef is the Fermi energy. The value of φ is approximately the depth of the potential well or the work required to move a electron from the highest electron state of a metal to infinity.[113,114] The EWF can be determined by direct or indirect techniques. The direct techniques are based on the electron emission from a metal. EWF has been found to have strong relationship with adhesion [115]. EWF is thus a

characteristic parameter that reflects interactions between metals and foreign substances, including organisms. If a surface is active, the interaction between the material and the surrounding medium would be strong, resulting in a large adhesive force. Recent studies demonstrated that nano-crystallization strongly influenced the adhesion between two materials, since the high density grain boundaries association with the nano-sized grains changes the surface properties of materials. [116] One effective approach for the fabrication of nanocrystalline metallic surfaces is a combination of sandblasting and annealing (recovery) treatments. [117] Practical metallic materials are usually polycrystalline, whose surface activity and adhesive force are strongly affected by the density of grain boundaries. [118] Using small sand particles to impinge on the metal surface causes high density dislocations, which introduces nano-scale dislocation cells into a surface layer. [119] During the recovery heat treatment, the dislocation cells turn into nano-sized grains with sharp grain boundaries. Surface nanocrytallization has been demonstrated to be particularly beneficial to passive materials such as stainless steel for improved surface stability and resistance to corrosion.[120] Cr in the stainless steel results in the formation of a Cr_2O_3 film that blocks electron interaction with the surrounding environment. The diffusion of Cr is faster in a nano-crystallized stainless steel due to the increased number of grain boundaries that facilitates Cr diffusion, [121] which is promoted at elevated temperatures. The more Cr diffuse to the nanocrystalline surface, the stronger the passive film[122]. As a result, the rapidly formed oxide film on nanocrystalline stainless steel surface will more effectively block electron interaction with the surrounding medium. One may anticipate that the interaction of a nano-crystalline stainless steel surface with bacteria will be lower than that of

a micro-crystalline structured stainless steel surface. The objective of this work is to investigate how the surface nanocrystallization combined with thermal oxidation influences the biofilms' adherence.

It has been reported that the *Pseudomonas aeruginosa* receptor binding domain, a self-folding domain of 17 amino acid residues derived for the PilA structural protein, could bind to the steel very tightly. *P. aeruginosa* utilizes type IV pili to bind to stainless steel surfaces and initiate biofilm formation. [123] A synthetic receptor binding domain has been shown to inhibit homologous and heterologous *P. aeruginosa* binding to steel surfaces [123] in a sequence specific manner, with very high affinity for the steel surface. The synthetic peptide was therefore used in this study to investigate the effects of nanocrystallization of stainless steel 304 and thermal oxidation on the adhesion of biofilm to its surface.

4.2   Specimen Preparation

Nano-structured stainless steel surfaces were fabricated via a sandblasting and annealing process. Commercial grade 304 stainless steel specimens with dimensions of 2x2x2cm were annealed at 1160^0 C for 20 minutes in Ar atmosphere followed by air cooling. The steel surface was then polished, using sand papers up to 1200# and then with an aqueous slurry of 0.05 μm colloidal silica. The polished sample surface was etched with a hydrochloride/nitric acid solution for 10 sec, washed ultrasonically with reagent grade acetone (10 min) and ethanol (5 min). The average grain size of the stainless steel specimens was ~ 30µm, as determined using a microscope with polarized light.

The 304 stainless steel specimens were then blasted vertically by silicon carbide

particles carried by an air flow. The silicon carbide particles had an average diameter of approximately 500um and the air flow pressure was 230 kPa. After sandblasting, eight sandblasted specimens and two specimens without sandblasting were slightly polished and etched using a 50% (v/v) HCl and HNO_3 solution for 20 seconds following annealing [124] under different conditions. The sandblasted stainless steel specimens were divided into two groups: (1) 4 sandblasted specimens annealed in Ar for 1 hour at 350°C, 300°C, 250°C, 200°C, respectively; (2) 4 specimens annealed in air for 1 hour at 350°C, 300°C, 250°C, 200°C, respectively. For comparison, two specimens without sandblasting (with an average grain size of 30 µm) were annealed in Ar and air respectively at 200°C for 1 hour. The surfaces were examined using an atomic force microscope. Fig 4.1 shows several nano-crystallized stainless steel surfaces, from which the average grain sizes of the specimens can be determined. The average grain size of specimens can be determined by AFM imaging system. For specimens annealed at 350°C, 300°C, 250°C, 200 °C (both in Ar and air), the average grain sizes are 112.35 nm, 108.45 nm, 96.58 nm, and 32.5 nm, respectively, and the average grain size of the micro-crystalline surface is around 40um.
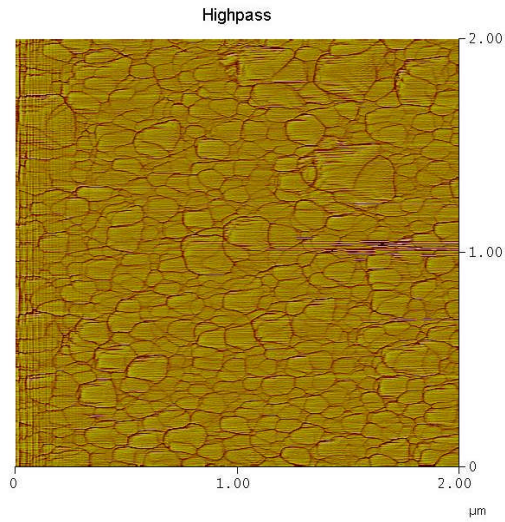
A
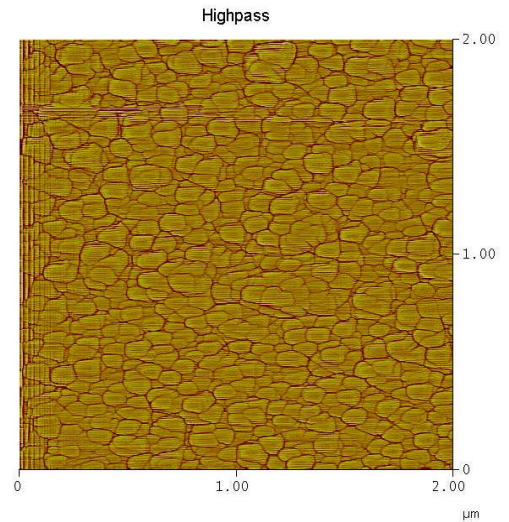
B
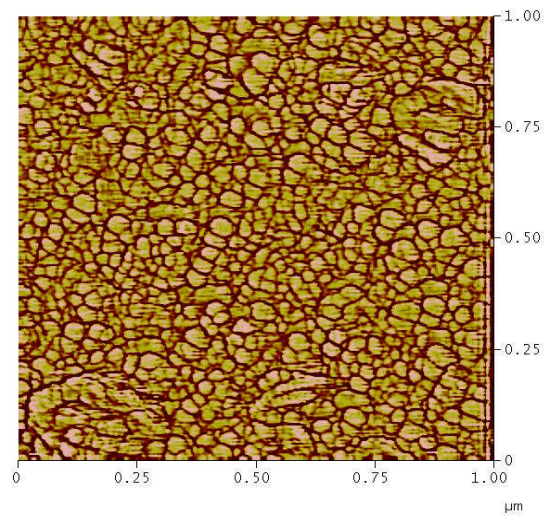
C
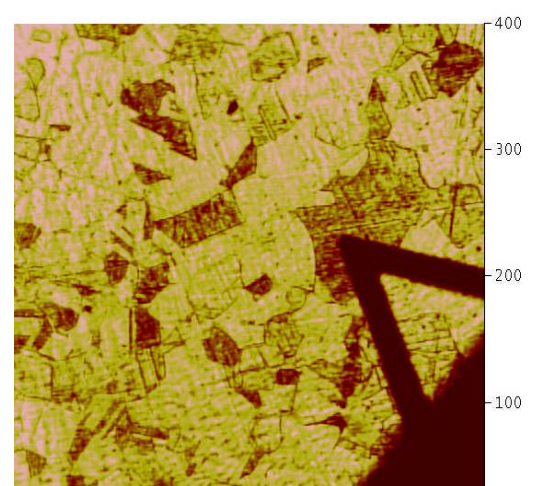
D

Fig 4.1 Fig.4.1A illustrates a nano-crystalline surface annealed at 300°C in air with its average grain size equal to 108.45nm. Fig 4.1B shows nano-crystalline surface with its average grain size equal to 96.58nm, which was annealed at 250 °C. Fig 4.1C shows a nanocrystallized surface with its average grain size equal to 32.5nm when the annealed temperature was 200°C. Fig 4.1D illustrates a microcrystalline surface with its average grain size around 40um.

4.3 Interaction of Receptor Binding Domain Derivatized AFM Tips With Steel

In order to measure the adhesive force between a biofilm and a stainless steel surface, AFM with a peptide-coated tip was employed. [125] A standard AFM silicon nitride tip was coated with Au (20 nm thick) by sputter coating; the Au-coated tip was immersed in 25 μM K-coil peptide synthesized with an additional N-terminal cysteine residue in PBS pH 7.2 for 40 min at room temperature such that the K-coil was coupled to the Au coating through the free sulfhydryl of the cysteine residue. The derivatized AFM tip was then washed with distilled H_2O and then immersed in 5 mM cysteine in PBS pH 7.2 for 40 minutes at room temperature, washed with distilled H_2O and then immersed in 1 μg/mL of E-coil-PAK(128-144)ox for 40 minutes at room temperature to allow the formation of the heterodimeric coiled-coil with the receptor binding domain being displayed on the end of the E-coil at the tip of the AFM tip. The functionalized tips were then washed with distilled H_2O and then air dried for subsequent use. The peptides were prepared as previously described [123]. Additional peptides utilized in this study include a synthetic PAO pilin receptor binding domain, PAO(128-144)ox, and the scrambled PAO pilin receptor binding domain, PAO(128-144)ox_Scrambled. The purity of these peptides and the oxidation state of the disulfide bond was confirmed as previously described [123]. Table 1 describes all peptide sequences used in this study.

The AFM was used in the "contact mode" to determine the adhesive force between the AFM tip and a target surface. When the AFM tip is pulled away form a surface, the

deflection of the cantilever reflects the adhesive force. The deflection of the cantilever is detected by a laser beam, from which the related force can be quantitatively determined if the spring constant of the cantilever is known. The spring constant of the cantilever of the AFM utilized in the present studies is 0.06 N/m. Adhesion of the peptide to each specimen was determined by averaging 20 measurements per specimen.

The adhesive force between a peptide coated AFM tip and a nano-crystallized stainless steel surface and that between the AFM tip and a microcrystalline surface were determined, respetively.   As shown in Fig.4.2a, there is an obvious difference in adhesion between the nano-crystalline surface and the microcrystalline one. Compared to the adhesion of peptide derivatized AFM tip to microcrystalline surface annealed in air at 200 °C for 1 hour (the result shows average adhesive forces of approximately 32 nN and 35 nN for annealing in air and Ar, respectively), the nano-crystalline specimen annealed in air at 200 °C displayed an adhesive force of 21 nN. Thus, the surface nanocrystallization and thermal oxidation can markedly influence the adhesion of the peptide to the stainless steel surface. Steel binding assays were performed to assess the ability of *Pseudomonas aeruginosa* to bind to nanocrystalline and microcrystalline stainless steel surfaces. Nanocrystalline and microcrystalline stainless surfaces were washed in 20 mL 95% ethanol for 10 minutes with gentle agitation and rinsed with distilled water.   Immediately before use, all samples were washed for 1 minute in 20 mL of acetone with gentle agitation and rinsed with distilled water. The samples were fixed to sterile glass slides using double-sided tape and placed in a sterile polystyrene Petri dish. Overnight cultures of *P. aeruginosa* PAK were sub-innoculated into 20mL of pre-warmed Luria-Bertani broth (LB). Cultures were standardized to an OD_{600} of

1.0 and 3 mL were centrifuged at 10 000 xg for 3 minutes at 4 C. Bacterial pellets were washed twice with sterile phosphate buffered saline (PBS) (10 mM sodium phosphate buffer pH 7.4 containing 150 mM NaCl), resuspended into 1.5 mL of PBS, and 1 mL was used to inoculate 50 mL of PBS. The bacterial solution was then gently poured into the Petri dish until the steel samples were completely immersed and were incubated at room temperature for one hour with gentle agitation. The samples were washed six times with 50 mL PBS and were stained in 30 mL of 1M Acridine Orange stain for 2 minutes, briefly rinsed with 95% ethanol, and washed with distilled water. Samples were observed using a Leitz Laborlux K microscope equipped with a 40X Neoflour lens and epifluorescent illumination. Images were captured on Fujichrome Provia 400F 36 mm film using a MSP4 camera system. The number of bound $P.$ $aeruginosa$ per 40X field of view was counted. One hundred and ten fields of view per sample were enumerated. The change in adhesive force of the peptide to microcrystalline steel was illustrated by a significant (P<0.001) decreased adherence of whole cells of $P.$ $aeruginosa$ strain PAK from 12.0 ± 5.4 bacteria bound per 40X field to 5.2 $\pm$ 3.18 bacteria bound per 40X field, a decrease in binding of ~56% (Fig 4.2b). However, bacterial adherence to the nanocrystalline steel was not significantly (P>0.05) altered by changing the atmosphere (air or Ar) in which the recovery treatment was carried out. This could be a reflection of the high susceptibility of the nanocrystalline steel surface to oxygen, resulting in rapid development of an oxide film on surface. It should be indicated that the Ar environment was established by letting an Ar flow go through a tube furnace during the entire heat recovery treatment. Air might not be completely removed from the furnace. A thinner oxide layer could still form on the samples that experienced the heat treatment in

such an Ar environment.
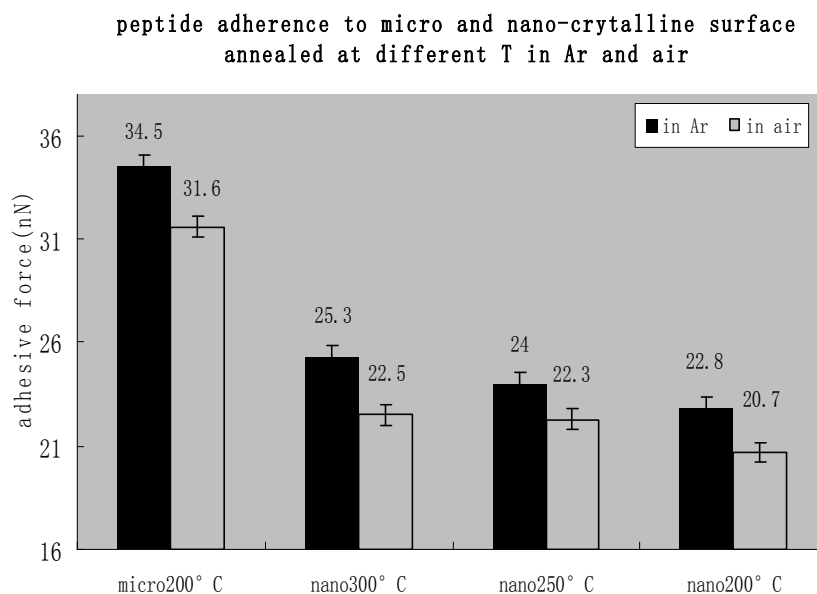
Fig 4.2a. Peptide adherence to microcrystalline and nanocrystalline surfaces annealed at different temperatures in Ar and air, respectively. The adhesion of peptide to the nanocrystalline surface is markedly lower than that to the microcrystalline stainless steel surface.
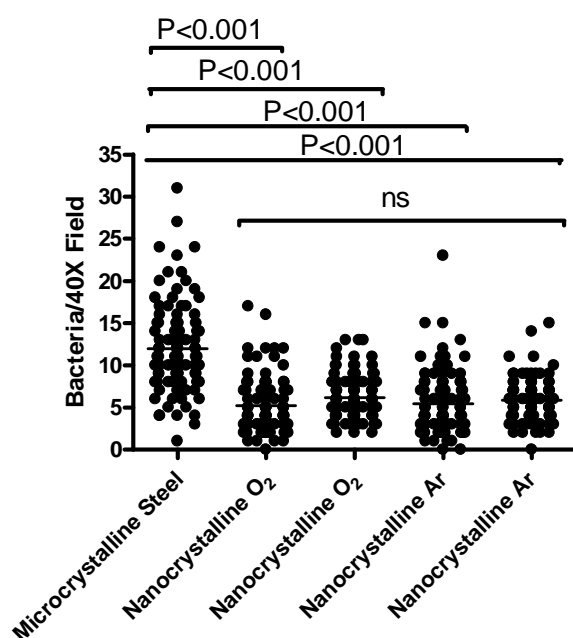
Fig 4.2b. Binding of *Pseudomonas aeruginosa* strain PAK cells to microcrystalline steel annealed in air and to the nanocrystalline steel annealed in air and Ar environment, respectively.

4.4 Electron work functions of nanocrystalline and microcrystaline specimens

Electron work functions of the specimens were measured using a Kelvin Probe [127]. This is a non-invasive, non-contact vibrating capacitor technique, which measures to mV resolution the voltage between a vibrating micro-electrode and a conducting or semiconducting sample. Applications include the fundamental study of corrosion, surface passivation, fabrication of low and high work function surfaces for ion and electron emission, fundamental surface adsorption studies, semiconductor oxide quality, etc.

A vibrating tip (amplitude of vibration can be digitally changes from a few microns to 1-2 mm) moves in a plane-parallel fashion with respect to the sample. The mean tip-to-sample spacing is usually in the 0.3 - 1.0 mm range, although measurement can be made with larger tips with an off set of 2-5 mm. The tip actuator is voice-coil driven, powered from a computer controller digital oscillator with a 0.2 - 0.3 Hz frequency resolution. Electric potential (potential energy per unit of change associated with a static electric field, and typically measured in volt) offset can be determined due to the high sensitivity of Kelvin probe.

The Kelvin Probe provides the relative work function between the tip and sample. (Electron work function of Au is 5.1)   A tip made of Au was used to scan an area of 100 * 100 um to determine the electron activity at each sample surface. EWF is the minimum energy required to move electrons from inside a metal to its surface. The higher the EWF, the less active the electron activity, hence the weaker the interaction

between this metal and its surrounding medium. The EWF of each specimen was determined 5 times, based on which the mean EWF was calculated. Fig 4.3 illustrates the EWFs of different stainless steel specimen surfaces. As shown, the EWF of a nanocrystalline surface is considerably higher than that of a microcrytalline surface. The EWF of the nanocrystalline surface annealed at 200 °C in air is 5.05eV, which is 0.55 eV higher than that of the microcrystalline surface annealed at 200 °C in air. In addition, for the same grain size, the EWF of stainless steel specimens annealed in air is relatively higher than the specimens annealed in Ar but the difference is not large possibly due to the high susceptibility of the nanocrystalline stainless steel surface to oxygen when the air could not be completely removed during the heat treatment.
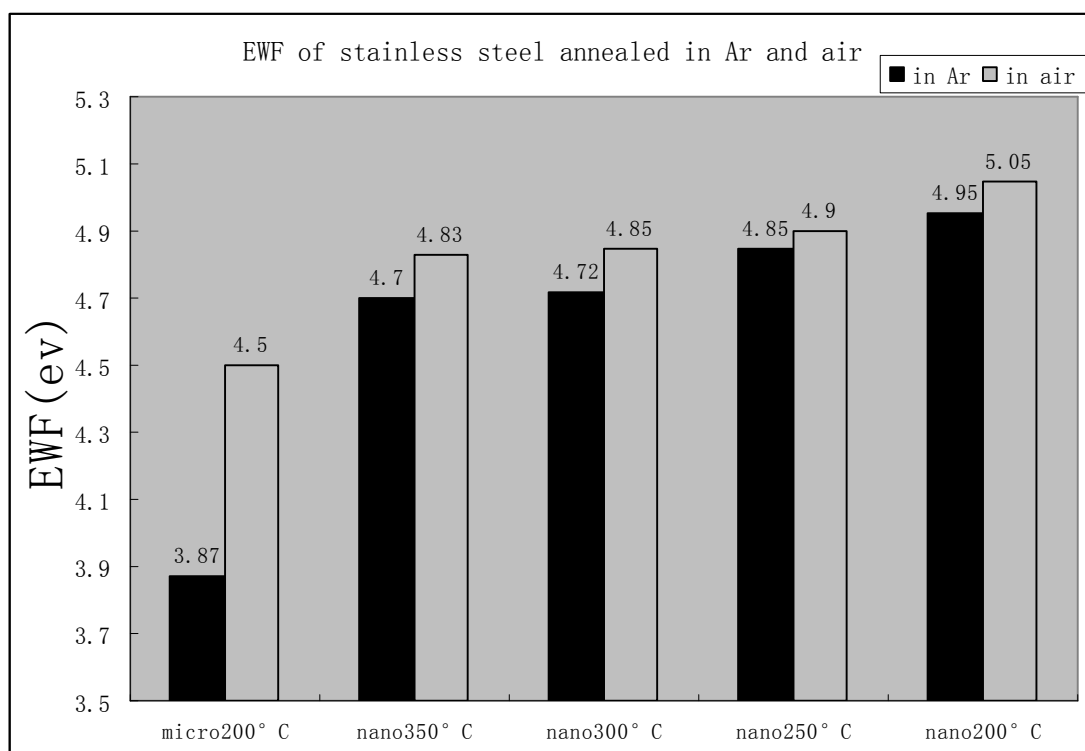
Fig 4.3. EWF of the specimens annealed in air is higher than that of specimens annealed in Ar at different temperatures. The microcrystalline surface annealed in Ar has lowest EWF, while the nanocrystalline surface annealed in air at 200°C has the highest EWF

The oxide film on the nanocrystalline surface is more protective and blocks electrons more effectively than that on the microcrystalline surface, because gain boundaries of high density promoted faster Cr diffusion faster, which makes the surface more stable as demonstrated in an earlier study. [128]

4.5 Scratch and Nano-indentation tests

In order to investigate how the nanocrystallization and oxidation treatment influence properties of the oxide film on stainless steel, scratch and nano-indentation tests were performed using a universal micro-tribometer (UMT) and a nano-mechanical probe, respectively.

Scratch test

Figure 4.4 below illustrates the UMT system used for scratch test.

Fig 4.4 Universal micro-tribometer for scratch tests

Fig 4.5 is a schematic illustration of the scratch test performed on the oxide film on a stainless steel specimen surface. During the scratch test, the surface was scratched under a normal load, which was increased linearly. The scratch probe was made of tungsten carbide.

During scratching, the tip scratched the surface under an applied load that was increased at a certain velocity. At the same time, changes in the contact electrical resistance (ECR) between the tip and specimen surface with respect to the load were recorded.
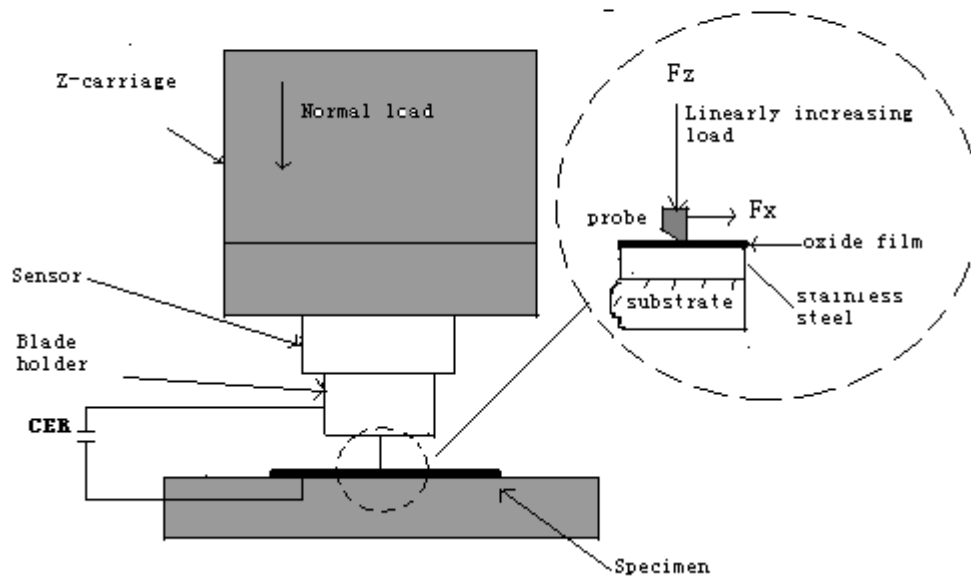
Fig 4.5 Schematic of the scratch test evaluating the scratch resistance of the oxide film on a stainless steel specimen.

The stainless steel surface has a nonconductive thin passive film(Cr_2O_3), as the applied load is increased to a certain level at which the film is broken, the surface electric contact resistance (ECR) drops. The corresponding critical force reflects the resistance of the oxide film to scratching as well as the film-substrate bond strength. Figure 4.6 illustrates a normal load ~ ECR curve obtained during a scratch test. We tested nanocrystalline and microcrystalline stainless steel specimens annealed at 200 °C in Ar and air, respectively,. For the microcrystalline steel annealed in Ar, its film started to fail at a normal load around 0.45N, and the film was completely damaged at 0.7N. For microcrystalline steel annealed in air, its

oxide film started to fail at 0.5N, and was completely damaged at 1.45N. The nanocrystalline steel has an enhanced oxide film. As measured, the oxide film on nanocrystalline stainless steel annealed in Ar started to fail and was fully damaged at loads of approximately 1.0N and 2.0N, respectively, while those for the nanocrystalline steel annealed in air were 1.0N and 3.0N, respectively. The table below illustrates CER changes of the specimens in scratch tests. The scratch tests clearly demonstrate that the oxide film on the nanocrystalline stainless steel is more protective and has a stronger bond to the substrate, compared with that on the microcrystalline stainless steel.
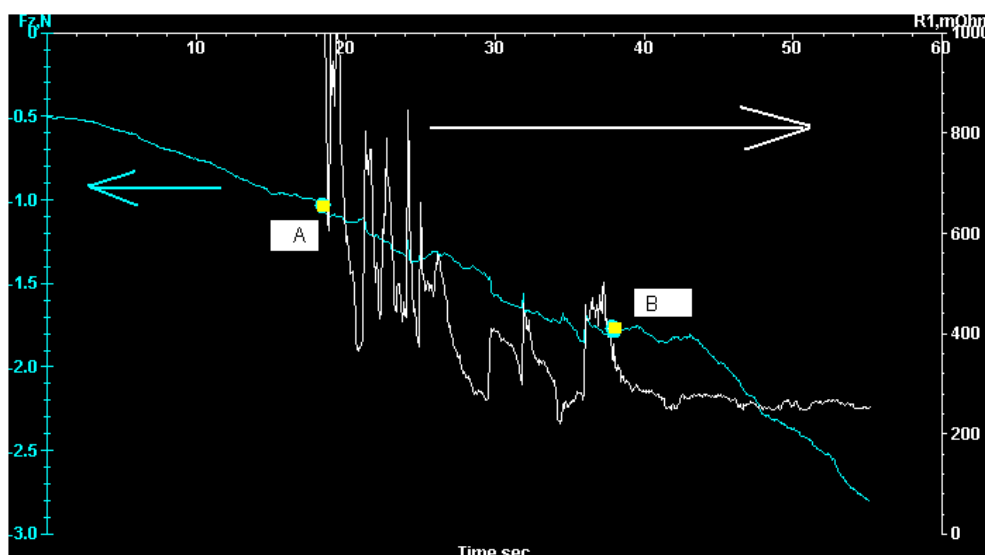
Specimens	Load at failure initiative	Load at complete failure
Microstructure surface annealed in Ar at 200° C	0.45N	0.70N
Microstructure surface annealed in air at 200° C	0.50N	1.45N
Nanostructure surface annealed in Ar at 200° C	1.00N	1.80N
Nanostructure surface annealed in air at 200° C	1.00N	3.20N

Fig 4.6. A scratch test with *in situ* monitoring changes in the contact electrical resistance (CER). The figure shows CER signals when a nanocrystalline surface was scratched under an increasing normal load (the normal load is compressive and thus represented using a negative value). As shown, the electrical resistance curve begins to decline at normal load of 1 N, and becomes relatively stable at approximately 1.8 N. The table below illustrates scratch test results for specimens that annealed at different temperatures both in Ar and air.

Nano-indention test

Mechanical properties of the oxide films were directly evaluated using a nano-indenter. In principle, under a given load the smaller the penetration depth, the harder is the material. The recovered displacement reflects the elastic behavior of the oxide film. Figure 4.7 is a schematic illustration of the nano-indentation test on material.
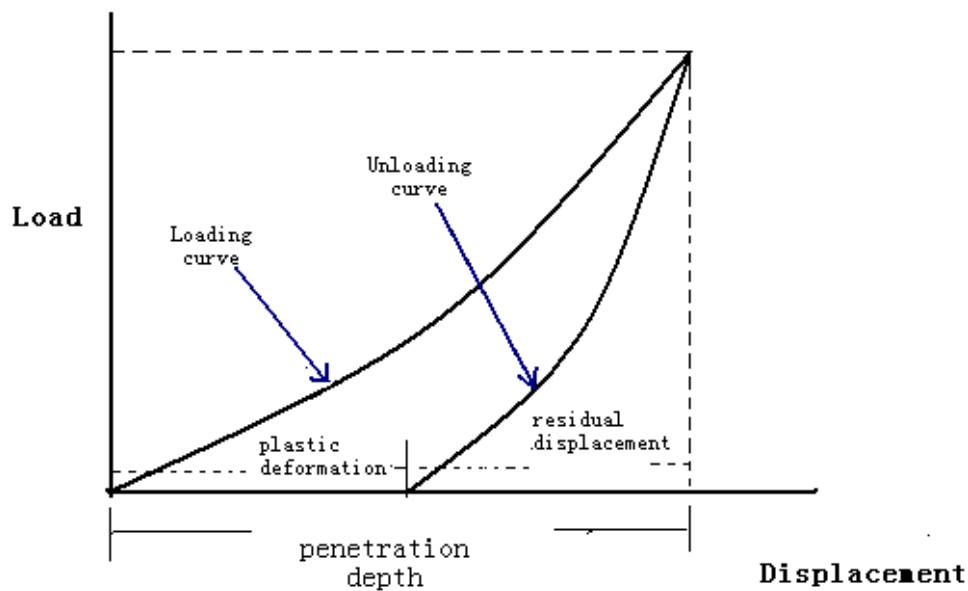
Fig 4.7 Schematic illustration of a nano-indentation test curve which represents hardness and elasticity of a material.

Figure 4.8 illustrates force-displacement curves of nanocrystalline and microcrystalline specimens. As shown, the oxide film on the nano-crystalline steel surface is considerably harder (with a smaller displacement) and more elastic (with little residual displacement) than that on the microcrystalline surface.
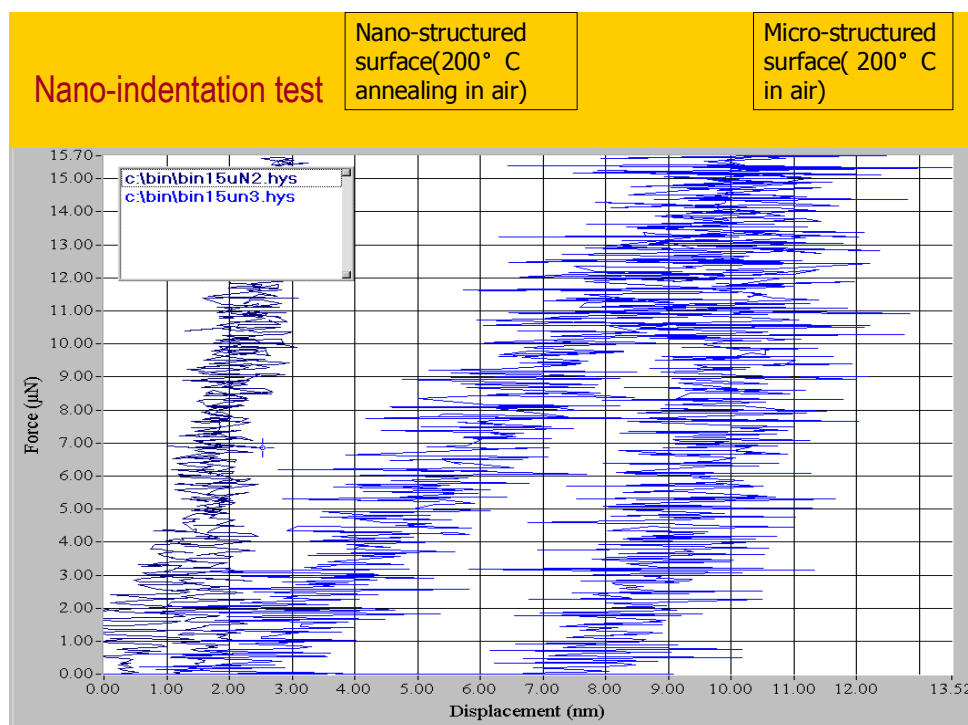
Fig 4.8 Nano-indentation tests on oxide film of microcrystalline surface and nanocrytalline surface annealed in air at 200°

4.6 Conclusions

This study demonstrates that the combined surface nanocrystallization and thermal oxidation provide an effective way to generate a more protective oxide film on stainless steel surfaces, which has greater bond to the substrate, higher hardness, and a higher degree of inertness so as to prevent electrons reacting with the environment. As a result, the interaction between the peptide derivatized AFM tip and the stainless steel surface decreases. Since the synthetic peptides have properties similar to those of biofilms, the nanocrystallization and thermal oxidation treatment would help to suppress the formation of biofilms on metallic materials, thus providing a surface technique to minimize the formation of bacterial biofilms on implant surfaces for improved orthodontic and orthopedic applications.

Chapter 5

Quantitative evaluation about the influence of grain size of nanograined stainless steel on the surface activity and bacterial binding

5.1 Objective

As demonstrated, surface nanocrystallization provides an effective way to generate a more protective passive film on stainless steel surfaces, which shows a higher degree of inertness so as to prevent the formation of biofilm. In order to evaluate quantitatively how the surface activity and bacterial binding change with the grain size in nano grained stainless steel, these properties were investigated through quantitative determination of EWF, the standard surface adhesive force (the adhesion measured by a regular silicon nitride AFM tip), and peptide adhesion testing using a previously de novo designed heterodimeric coiled-coil system with an embedded PAK(128-144)ox peptide, which has been shown to mimic the nativeT4P binding site in the bacterial pathogen *P. aeruginosa* in order to approximate the adhesive force

between the bacterial cells and the stainless steel surface. Bacterial binding assays were also performed on microcrystalline and nanograined surfaces to determine bacterial colonization trends on the steel surface with viable bacteria.

5.2 Adhesion measurement

Several surface nano-crystallized steel specimens are fabricated via sandblasting and annealing process under different annealing temperature. (Fig 5.1)
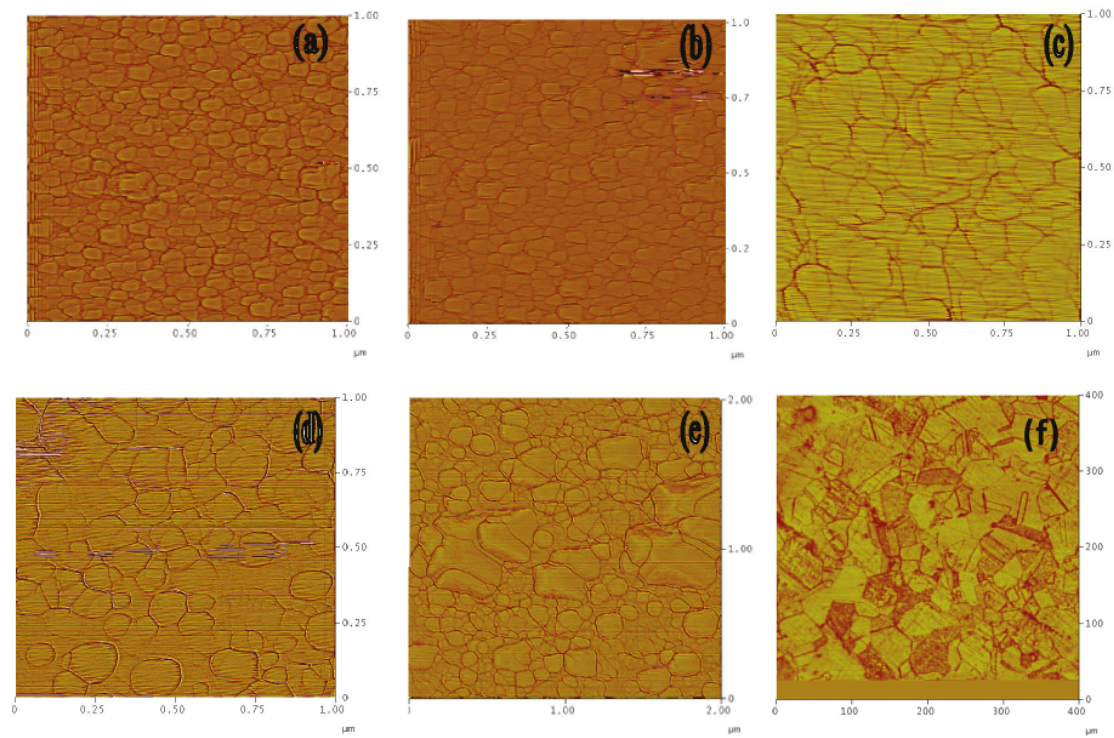
Figure 5.1. Sandblasted surfaces annealed at different temperatures for different average grain sizes: (a) 31±1.8, (b) 42±4.5, (c) 505 ±.5, (d) 85±6.4, and (e) 105±8.7 nm. (f) The original or microcrystalline stainless steel (annealed without sandblasting) had its average grain size equal to 35 ±6 μm.

Adhesive force measurements were performed at these specimen surfaces using either a standard AFM tip or a peptide coated AFM tip. As shown in Figure 5.2, the adhesive force decreased with the grain size and the attained experimental values are

23.0 (2.2, 21.6±1.9, 18.0 ±1.6, 17.4 ± 1.7, and 16.0 ± 1.7 nN for samples having average grain sizes of 105, 85, 50, 42, and 31 nm, respectively. This decrease in adhesion implies that there is a decrease in the strength of bacterial biofilm binding as the grain size decreases in nanocrystalline stainless steel because the peptide-coated tip has the same amino acid sequence as the PilA binding site on the T4P of *P. aeruginosa* cells. The original or microcrystalline stainless steel sample had an adhesive force of 26.1 ± 2.4 nN. Thus nanocrystallization had a significant effect on peptide adhesion, where the smallest grain size had the lowest adhesive force as measured using the coiled-coil peptide tip. The sandblasted-without-annealing sample (denoted as S.B.) showed the highest overall adhesive force of 27.0 ±2.5 nN. This is attributed to the fact that sandblasting generates only a nanocellular structure or a dislocation network that differs from a nanocrystalline structure as the former contains interior dislocations and diffuse boundaries between cells and the latter has nearly defect-free nanocrystals with sharp grain boundaries.
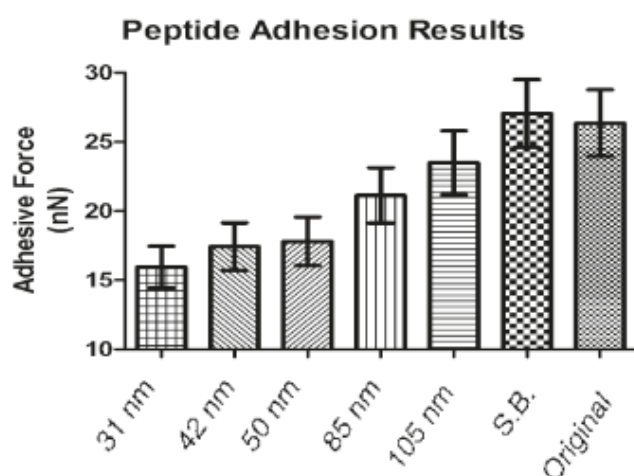
Figure 5.2. Adhesive force of the peptide-coated coiled-coil tip with

thePAK(128-144)ox residue designed tomimic the native T4P binding of P. aeruginosa cells. Here the peptide adhesion decreaseswith grain size for the annealed samples,which indirectly illustrates a trend toward decreased bacterial binding with grain size.

Adhesive force testing was also performed using the standard silicon nitride tip; results for nanocrystallized samples are reported in Figure 5.3. The average adhesive force was 16.0 ±1.6, 16.2 ± 1.5, 13.0 ± 1.2, 10.1 ±1.1, and 10.0 ± 1.0 nN for samples having average sizes of 105, 85, 50, 42, and 31 nm, respectively. The adhesive forces of the original stainless steel sample (as received and annealed) and the sandblasted sample (no annealing) were significantly higher than those of the sandblasted and annealed samples, with values equal to 18.8 ± 1.2 and 20.2 ±1.6 nN, respectively. The adhesive or attractive force of the steel surfaces for the standard tip is lower than that for the peptide coated tip, but general trends in the variation in adhesive force with grain size are similar.
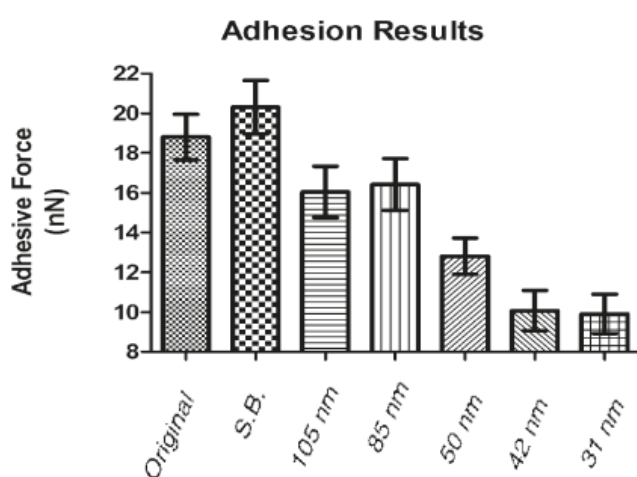
Figure 5.3. Adhesive force of the stainless steel samples using a regular AFM tip. The adhesive force (nN) was obtained by multiple testing, with error bars representing the standard deviation of the test data.

5.3 Bacterial binding assay and EWF

Bacterial binding assays were also performed on these specimens. As shown in Figure 5.4, the nanocrystallized samples had markedly smaller numbers of bound bacterial cells, compared to those of unannealed (S.B.) and microcrystalline (original) stainless steel samples. A general trend in increased bacterial binding with increased grain size is shown for the nano-grained samples. The scattering data of the S.B. sample resulted from its higher surface inhomogeneity caused by sandblasting.
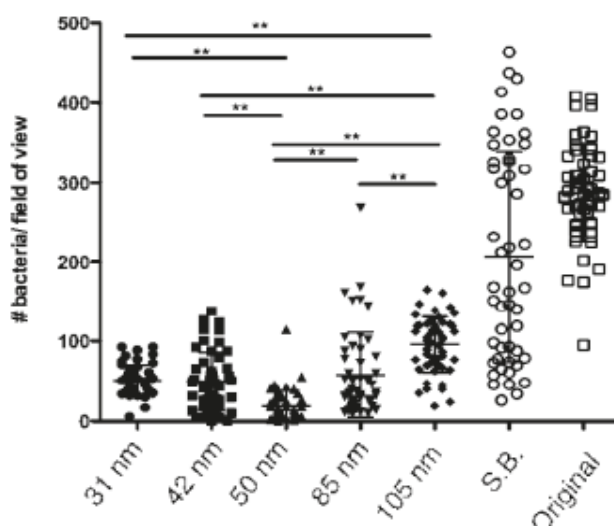
Figure 5.4. Bacterial binding of P. aeruginosa cells to the surface of the stainless steel samples, as enumerated under a 40x objective lens with epifluorescent illumination. The bars overhead illustrate ostatistical differences in data of $p < 0.01$.

Electron work functions of the samples were measured to correlate the observed adhesion behavior and bacterial binding to the activity of surface electrons, which is related to surface inertness to bacterial binding and biofilm formation. Results of the EWF measurement are presented in Figure 5.5. The general increase in the EWF as the grain size decreases for the annealed samples indicates an increase in surface stability. Also, similar to previous results, the microcrystalline stainless steel sample

and the unannealed S.B. sample had smaller EWFs, which indicates that the electrons

in the surfaces were more readily accessible or more likely to interact with the

surrounding medium.
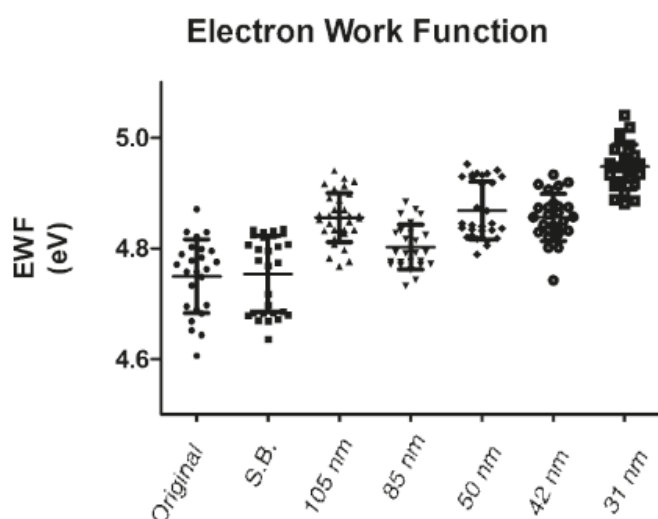
Figure 5.5, EWF of the stainless steel samples, measured in electron volts. Increased electron activity is characterized by a lower EWF value. The unannealed sandblasted sample has the lowest EWF, and the annealed 200 _C sample has the highest EWF

The key factor responsible for the reduced adhesion, bacterial binding, and higher

EWF of nanocrystallized surfaces was the formation of a more protective passive film

on nanocrystalline surfaces, which formed faster and likely contained more Cr   that

enhanced the passivation capability. Nanocrystallization also influences the interfacial

bonding between the substrate and passive film, thus affecting its resistance to

mechanical and electrochemical attack. The passive film on a nanocrystalline

substrate may develop inward-growing oxide pegs at high-density grain boundaries,

resulting in stronger interfacial bonding between the substrate surface and exterior

passive film compared to that of microcrystalline and sandblasted surfaces, where the

grain boundary density is lower or effective inward-growing pegs are unlikely to form.

The apparent decreases in adhesion, peptide adhesion, and bacterial binding with a decrease in grain size and an increase in the EWF for nanograin steel are consistent and expected. Although the electron activity is known to increase at grain boundaries, in nanocrystalline stainless steel overall chromium diffusion is considerably promoted because of its high-density grain boundaries along which atomic diffusion is accelerated. when chromium reacts with oxygen, it forms a protective layer or passive film on a surface that acts as a relatively inert barrier to the surrounding environment. As the grain size decreases, corresponding to an increase in the grain boundary density, the promoted atomic diffusion helps to reduce the formation of vacancies or pores, forming a more compact passive film with a higher Cr concentration, which would more effectively block the interaction between surface electrons and the surrounding medium or increase the surface inertness or stability. This study provides quantitative information regarding how specific grain boundary density or changes in grain size on the nanometer level could affect the stability of the surface. The sandblasted but unannealed sample, which superficially appeared to be nanograined under AFM, did not correspond to this described trend because it had a significant difference in adhesion, bacterial binding, and EWF as compared to its annealed counterparts. This sample had a much higher adhesive force measured using both the standard and peptide-coated AFM tip, the number of P. aeruginosa bacteria per field of view was much greater on average, and the EWF was significantly lower, all of

which are implications of the potential for increased biofilm formation. As mentioned earlier, without annealing, a sandblasted surface had a nanocellular structure consisting of dislocation cells and dislocations also existed inside the cells, which increased the electron activity and rendered surface more active, as demonstrated by its lower EWF shown in Figure 4. It was also noticed that the grain size varied with the annealing temperature in a roughly linear fashion. This demonstrates that with the chosen method of sample preparation stainless steel surfaces could be modified using this cost-effective process with low-temperature annealing or recovery in order to increase the surface stability for reduced biofilm formation. This inexpensive surface-modification technique could effectively be used to suppress the formation of bacterial biofilms not only in medicine but also in food production and others sectors involving biocorrosion and bacterial contamination.

5.4. Conclusions

The electron activity, characterized by the EWF, was lowered as the grain size decreased in nanocrystallized sample surfaces, corresponding to a decrease in the surface adhesive force. Because the derived coiled-coil PAK(128-144)ox peptide contains the same amino acid sequence as and is known to duplicate the binding affinity of the bacterial binding site in P. aeruginosa, a common bacterium compromising biofilms, the decrease in the peptide adhesive force suggests a decrease in the binding force of bacteria to the stainless steel surface. Consequently, the increased inertness of nanocrystallized surfaces led to a decrease in attracting bacteria as observed in the bacterial binding assays. The increase in the surface inertness of

nanocrystallized stainless steel surfaces to bacterial binding is attributed to its highdensity grain boundaries, which accelerate atomic diffusion and modify the Cr content in the passive film, leading to a decrease in the activity of surface electrons interacting with the surrounding medium.

Chapter 6

Surface nanocrystallization of silver incorporated 304 stainless steel for reduced *Pseudomonas aeruginosa* biofilm formation and enhanced corrosion resistance

6.1 Introduction

It is well known that silver is an effective anti-bacteria element, which has found a variety of applications because its toxicity to human cells is considerably lower than that to bacteria. It is logical to expect that coating a medical implant or adding Ag into its surface layer may directly kill bacteria, thus preventing bacterial infection. Previous studies[151-154] have demonstrated that adding Ag to biomaterials can reduce bacterial infection. For instance, an antibacterial silver rich layer can be generated on implant's surface by physical coating techniques as well as ion implantation process. However, recent research indicates that implant steel with incorporated Ag, though showing higher antibacterial ability, has low corrosion resistance, resulting in other problems. In this study, an attempt was made to enhance the corrosion resistance of the silver incorporated 304 stainless steel was enhanced by

surface nanocrystallization.

It was demonstrated earlier [156,157] that the surface nanocrystallization is an effective approach to enhance the corrosion resistance of passive metals, such as stainless steel. In nanocrystalline stainless steel, the high-density grain boundaries considerably accelerate diffusion of Cr atoms, which largely enhances the self-repairing capability of its passive film. As demonstrated, surface nanocrystallization is also an effective approach to reduce the adherence of biofilm[158] due to the formation of a more protective passive film that effectively blocks electron interaction with the surrounding medium, including organisms. Chromium (Cr) is a main ingredient in stainless steel. Cr will react with oxygen and form a Cr_2O_3 passive thin film (a ceramic material which is inert) at steel surface. Enhancing the diffusion of Cr to steel surface is beneficial to form the passive film with promoted passivation capability and higher inertness.

Surface nanocrystallization may compensate the loss of corrosion resistance of stainless steel when anti-bacteria agents such as Ag atoms are incorporated into its surface layer (which may act as microelectrodes to stimulate corrosion reactions) due to faster Cr diffusion that helps to restore the local corrosion resistance when impurities (anti-bacteria agents) exist. It is expected that diffusing Ag atoms into a nanocrystalline stainless steel surface or coating an Ag film on a nanocrystalline stainless steel, the high corrosion resistance of stainless steel could be retained. If this can be confirmed, adding anti-bacteria agents such as Ag into a nanocrystallized surface layer of implants or coating it with Ag would provide an effective and feasible

approach to suppress bacterial growth on medical implants and thus consequent bacterial infection.

6.2 Experimental approach

Nanostructured stainless steel surfaces incorporated with Ag were fabricated via punching and annealing process. Commercial grade 304stainless steel specimens with dimensions of 2 cm × 2 cm ×2 cm were annealed at 750 ◦C for 45 min in Ar atmosphere followed by air cooling. The steel surface was then polished, using sand papers up to 1200# and then with an aqueous slurry of 0.05 μm colloidal silica. The polished sample surface was etched with a hydrochloride/nitric acid solution for 10 s, washed ultrasonically with reagent grade acetone (10 min) and ethanol (5 min). The average grain size of the stainless steel specimens was ~ 40 μm, as determined using a microscope with polarized light.

Nanocrystalline stainless steel surfaces incorporated with Ag were fabricated. Ag powders (0.7~ 1um in diameter) were deposited on the substrate of the stainless steel specimens, which were then punched for 1 hour using a punch drill with a head of 5mm in diameter, and respectively annealed at 200 ◦C , 250 ◦C, 300 ◦C in Ar for 1 hour. Fig 6.1 illustrates several Ag-containing nanocrystallized steel surfaces with different grain sizes.
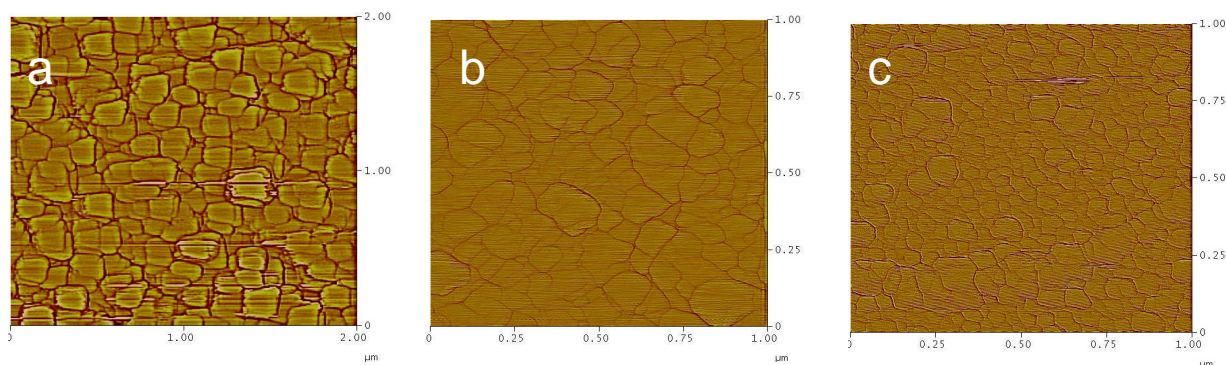
Fig 6.1. .(a) nanocrystalline surface with average grain size of 135nm annealed at 300 °C. (b) nanocrystalline surface with average grain size of 91nm annealed at 250 °C. (c) nanocrystalline surface with average grain size of 40nm annealed at 200 °C in Ar.

For comparison, microcrystalline surfaces with Ag were fabricated via Ag powder depositionin combination with annealing treatment. Ag powders were deposit on the stainless steel surface using a high voltage(50kV) powder coating gun following an annealing process at 200 ∘C in Ar for 1 hour. After annealing process, Ag-steel samples were slightly polished using sand paper with1200# grit in order to flatten the surface and eliminate the oxidation. Ag layers can be observed under optical microscope and the concentration of Ag were measured using EDX. Several steel samples with 10% and 50% Ag coverage were fabricated for either nanocrystalline or microcrystalline surfaces.

6.3 Corrosion test

Corrosion test were performed in a simulated body fluid solution (1.2%NaCl, 0.02%KCl, 0.02%MgCl2, 0.012%KH2PO4, 0.02%MgSO4, 0.028%CaCl2) on either Ag-added nanocrystalline surfaces or Ag-added microcrystalline surfaces.

In order to investigate the *Pseudomonas aeruginosa* bacterial binding activities on steel sample specimens, steel binding assays were performed. Surfaces were

washed with 50mL 95% EtOH for 15 minutes with gentle agitation and rinsed with distilled water.   Immediately before use, all samples were washed for 1 minute in 20mL acetone with gentle agitation and rinsed with distilled water.   The samples were placed into individual wells of a sterile polystyrene Costar 6-well cell culture plate (Corning Incorporated).   Overnight cultures of *P. aeruginosa* PAK pilT mutant were sub-inoculated into 20 mL of pre-warmed Luria-Bertani broth (LB) containing 50 g/mL of tetracycline.   Cultures were incubated until an OD_{600} of ~0.2 was reached.   Cultures centrifuged at 10 000g for 3 minutes.   Bacterial pellets were washed twice with once with sterile phosphate buffered saline (PBS) (10 mM sodium phosphate buffer, pH 7.4 containing 150 mM NaCl) and were resuspended to a final OD_{600} of 0.6.   Seven millilitres of 1X PBS were placed into each well to cover each sample and 0.5mL of resuspended bacteria were added to the PBS.   Samples were incubated for 1 hour at room temperature with gentle agitation.   The samples were washed six times with 10mL of distilled water and were stained in 10mL of 1M acridine orange stain for 3 minutes.   Samples were briefly rinsed with distilled water and were observed using a Leitz Laborlux K microscope equipped with a 40X Neoflour lens and epifluorescent illumination.   40 images per sample were captured using a Canon EOS Rebel XS digital camera and the number of bound *P. aeruginosa* per 40x field of view was enumerated.

The corrosion tests showed that the nanocrystalline surfaces incorporated with Ag have higher corrosion resistance than that of microcrystalline surface, especially for the 10% Ag coverage samples in a simulated body fluid. Fig 6.2(a) illustrates the

polarization curves with 10% Ag coverage. The curve of nanocrystalline surface with 10% Ag shows lower current density and higher corrosion potential than the microcrystalline surface with 10% Ag.

(a)

(b)
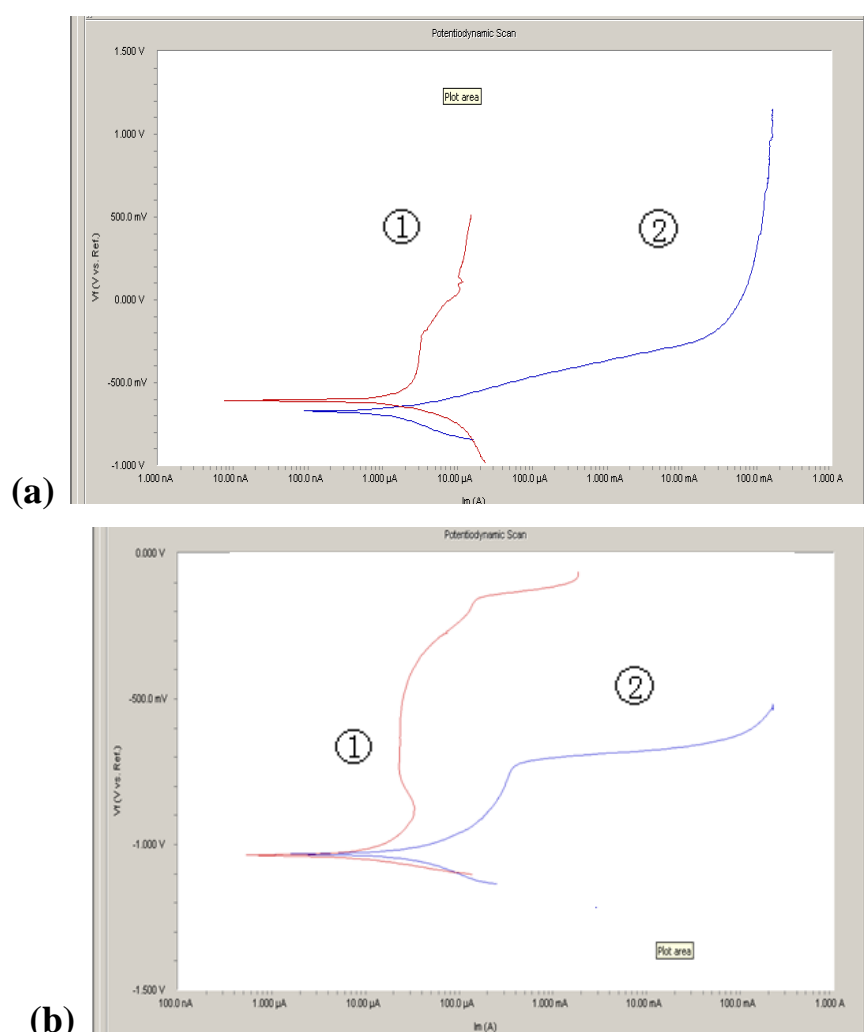
Figure 6.2(a) Polarization curves of (1) a nanocrystalline surface with ~10% Ag coverage, and (2) a microcrystalline surface with ~10% Ag coverage. 6.2(b) (1) a nanocrystalline surface with ~50% Ag coverage, and (2) a microcrystalline surface with ~50% Ag coverage.

The situation was similar when the surfaes were coverd with 50% Ag as shown in

Fig 6.2(b). The corrosion current and corrosion rate of these two specimens were also calculated. The results showed that microcrystalline surface incorporated with 10% and 50% Ag had the higher orrosion current and corrosion rate than the nanocrystalline surface incorporated with Ag (Figure 6.3)

(a)

(b)
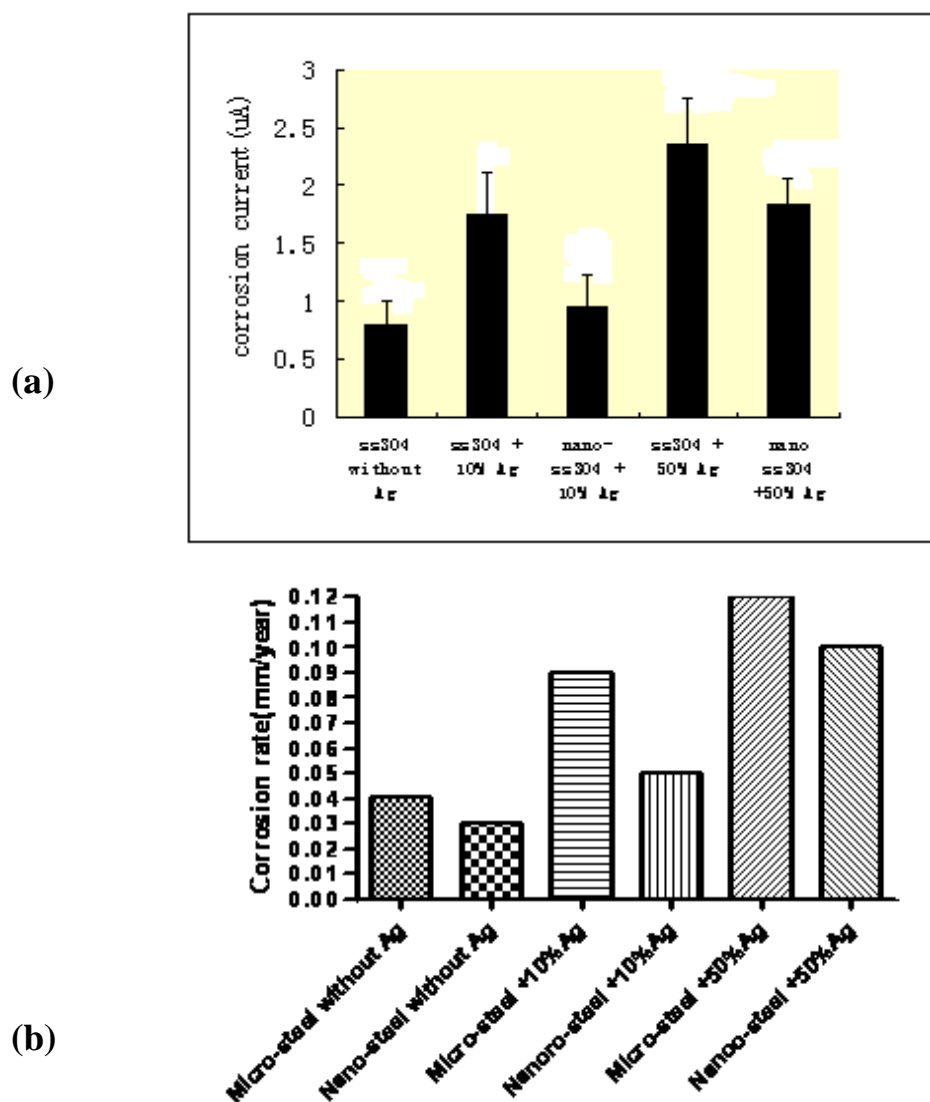
Figure 6.3 illustrates the corrosion current (a) and corrosion rate (b) of micro-steel without Ag, micro-steel with 10% Ag coverage, nanocrystalline steel with 10% Ag coverage, micro-steel with 50% Ag coverage, and nanocrystalline steel with 50% Ag coverage.

6.4 Bacterial binding assay tests and adhesion tests

Bacterial binding assay tests and adhesion tests using AFM are also performed on these specimens. Fig 6.4a illustrates that the nanocrystallized (punched) steel attracted fewer bacteria than the microcrystalline (regular) stainless steel. After Ag was incorporated into the nanocrystalline surface, the bacteria binding was further reduced. The combination of Ag incorporation and nanocrystallization can reduce the *P. aeruginosa* bacterial binding activities, and the latter minimizes the galvanic effect brought by the added nobel Ag. Surface nanocrystallization also helps to reduce surface adherence for bacterial biofilms. As shown in fig 6.4(a), there are less dead bacteria binding on the Ag incorporated steel surface. The nobel silver diminishes the surface reactivity and thus the surface adherence; its ions suppress the colonization of microorganisms by inhibiting DNA and RNA replication, disrupting the cell membrane, and interfering with cell respiration [159,160]. Ag+ ions are detrimental to living bacteria; bacteria could sense a certain signal from the harmful Ag ions and avoid to interact with the Ag-incorporated steel surface. As a result, fewer dead bacteria bind on the Ag-incorporated steel surface. In this study adhesion tests were performed on the sample surfaces using AFM. 50 adhesive force measurements were performed on each sample specimens using AFM silicon nitride tip. The tests demonstrated that the microcrystalline surface is more active and shows the highest adhesive force with an average value of 20 nN. In comparison, Ag- incorporated steel surface has the lowest adherence with average adhesive force, 8.5 nN. The nanocrystalline surface showed a lower average adhesive force of 11.4 nN and the nanocrystallized one with Ag showed

even lower adhesive force. Lowering the adhesive force by Ag could be explained. Ag has a lower surface electron activity reflected by its electron work function compared to that of stainless steel. This helps to reduce the surface activity and thus adhesion. It should be pointed out that the measured adhesion reflect general electron behavior. Both of the added antibacterial capability and reduced surface activity made contributes to the reduction of number bacteria on the Ag incorporated nanocrystallized stainless steel surface.   Fig 6.4b illustrated the adhesive force measurements at substrate of microcrystalline steel (regular), nanocrytallized steel (punched), and Ag-incorporated nanocrystallized (Ag punched) steel surface, respectively.

(a)   **(b)**
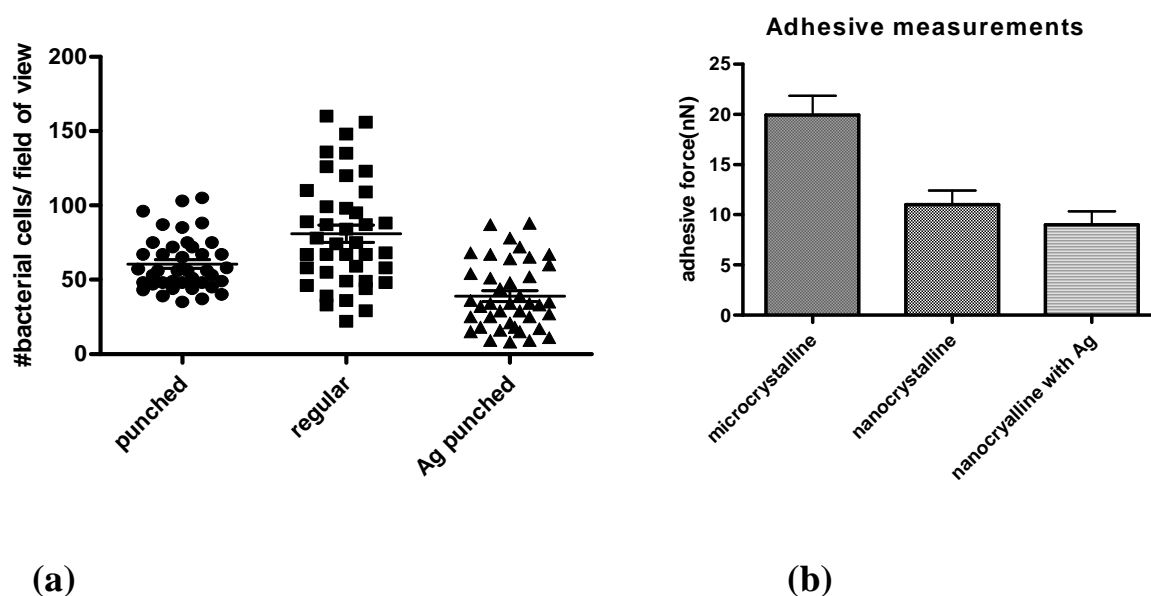
Fig 6.4 (a), *Bacterial binding results of P. Aeruginosa cells to the surface of the stainless steel samples, as enumerated under 40X objective lens with epiflourescent illumination. b), Adhesive force measurement between AFM silicon nitride tip and surface of microcrystalline steel, nanocrystallized steel, Ag-incorporated (10%) nanocrystallized stainless steel, respectively.*

6.5 Conclusion

In this study, we demonstrated an effective approach to reduce bacteria binding to stainless steel by incorporating Ag, an antibacterial agent, into the steel surface while minimize resultant decrease in corrosion resistance by surface nanocrystallization treatment. It demonstrated that nanocrystallization did not only reduce the bacterial binding activities, but also increased the corrosion resistance of Ag-incorporated stainless steel surfaces through enhancing Cr diffusion, which led to faster passivation and a more compacted passive film with more Cr. Although the study was conduced using 304 stainless steel as a sample material, the conclusion drawn from this study should be applicable to other metallic and passive materials.

Chapter 7

GENERAL CONCLUSIONS

Bacterial biofilms gives rise to many medical implant related infections. Biofilm related infections have become a significant obstacle in surgical medical intervention. Efforts have been made to suppress the biofilm formation on medical implants through various approaches including antibiotics treatment, antimicrobial material coating on medical implants, and nanotechnology applications. In this study, the adhesive forces between biofilm and microcrystalline and nanocrystalline surfaces of 304 stainless steel were investigated. Based on extensive experimental studies, the following main conclusions are drawn:

- Bacteria have a high affinity to metallic materials. The adherence of bacteria to stainless steel surface is particularly higher at grain boundary than inside grains.

- A synthetic peptide having some properties similar to those of *P. aeruginosa* biofilm was used as a substitute of bacterial biofilms for this study. The adhesive force attributable to the PAK(128-144)ox receptor binding domain interaction with the steel surface is 21.4nN within grains and 52.6nN at grain boundary. Thus the peptide displays a ~2 fold stronger binding interaction

with grain boundaries in stainless steel than that with grains. The synthetic peptide is estimated to have a molecular interaction strength of average 26-55 pN/molecular interaction to stainless steel surface.

- Surface nanocrystallization is an effective approach to reduce the adherence of biofilm to stainless steel surface. The adhesive force between the peptide and a nanocrystallized stainless steel surface is markedly lower than that of a microcrystalline surface. Although bacteria have larger adhesive force at grain boundaries in microcrystalline stainless steel, the surface nano-crystallized stainless steel with high-density grain boundaries resulted in a more protective passive film that more effectively blocks electron interaction with the surrounding medium, leading to reduced adhesive force for biofilms.

- The resistance of stainless steel to biofilm formation can be further improved to a certain degree by a thermal oxidation process, especially for nanocrystalline stainless steel surface.
- It demonstrated that nanocrystallization can not only mitigate the bacterial binding activities, but also enhance the corrosion resistance of Ag-incorporated stainless steel surfaces.

BIBLIOGRAPHY

1) Allison ,DG,McBain,AJ and Gilberta,P,microbial biofilms:problems of control.In;Community structure,,and cooperation in Biofilms (Eds.Allison,DG,Gilberta,P,Lappin-scott,H and Wilson,M),society for General Microbiology Press,Reading,UK,pp.309-327

2) Costerton,J.W.Overview of microbial biofilms,J.Indus.Microbiol.1995.

3) Costerton,J.W,z.Lewandowski,D.E.Caldwell,D.R.Korber,and H.M.Lappin-scott.Microbial biofilms,1995 P.711-745

4) Costerton,J.W,"Introduction to Biofilm,"International Journal of Antimicrobial Agents,1999.11:217-221.

5) Costerton,J.W,P.S.Stewart,and E.P.Greenberg,"Bacterial Biofilms:A Common Cause of Persistent Infections"1999

6) Michael Givskov,A new approach to the control of bacterial infections.2004

7) Locci R, peters G,Microbial colonization of prosthetic devices.Scanning electron microscopy of intravenous catheters invaded by yeasts.1981

8) Locci R,Peters G, Adherence and growth of coagulase-negative staphylococci on surfaces of intravenous catheters,1982

9) Allison,DG,McBain,AJ and Gilbert,"Microbial biofilm;problems of control In:Community Structure and Cooperation in Biofilms"(Eds.Allison,DG,Gilbert,P,Lappin-scott,H and Wilson,M),Society for General Microbiology Press,Reading,Uk,pp,309-327,2000.

10) Costerton,JW,"Purification and characterization of adhesive exopolysaccharides form Pseudomonas putida and Pseudomonas fluorescens.Canadian Journal of Microbiology 33,1080-1090.1987

11) Hoyle,BD,Wong,CK and Costerton,JW(1992) Disparate efficacy of tobramycin on Ca(2+),Mg(2+),and HEPES-treated Pseudomonas aeruginosa biofilms.Canadian Journal of Microbiology,1992.

12) Huang,CT,Yu,FP,McFeters,GA and Stewart, Non-uniform spatial patterns of respiratory activity within biofilms during disinfection.Applied and Environmental Microbiology.1995.

13) Giwercman,B,Jensen,ET,Hoiby,N,Kharazmi, A and Costerton,JW, "induction of lactamase production in Pseudomonas aerugiosa biofilms.Antimicrobial Agents and Chemotherapy.1991.

14) Lambert,PA, Giwercman,B and Herby,"Chemotherapy of Pseudomonas aeruginosa in cystic fibrosis.Inc Bacterial Biofilms and their Control in Medicine and Industry".1993

15) Suci,PA, Mittelman,MW,Yu,Fu and Geesey,GG, "investigation of ciprofloxacin penetration into Pseudomonas Aeruginosa biofilms.Antimicrobial Agents and Chemotherapy.1994.

16) Stewart,PS,"Theoretical aspects of antibiotic diffusion into microbial biofilms."Antimicrobial Agents and Chemotherapy.1996. "Analysis of biofilm transport limitation in an artificial biofilm system,Journal of Applied Microbiology ,1998.

17) Brown,MRW, Collier,PJ and Gilbert,"Influence of growth-rate on the susceptibility to antimicrobial agents:Modification of the cell envelope and batch and continuous culture".Antimicrobial Agents and Cemotherapy.1990.

18) Wentland,EJ,Stewart,PS,Huang,CT and McFeters,GA," Spatial variations in growth rate within Klebsiella Pneumoniae colonies and biofilm.Biotechnology Progress.1996.

19) Gilbert,P and Allison,DG,"Biofilms and their resistance towards antimicrobial agents.Inc Dental Plaque Revisited:Oral Biofilms in Nature and Disease.1999

20) O'Toole,GA and R.Kolter."The initiation of biofilm formation in Pseudomonas fluorescens WCS365 proceeds via multiple,convergent signaling pathways:a genetic analysis.1998.

21) Davey ME and O'toole GA,"Microbial biofilms:from ecology to molecular gentics." Department of Microbiology,Dartmouth Medical School,Hanover.New Hampshire.2000.

22) Stoodley,P,J.D,Boyle ,and H.M. lappin-scott,"Influence of Hydrodynamics and Nutrients on Biofilm structure,"1999.

23) Dalton,H,M,and P.E.March.".Molecular genetics of bacterial attachment and befouling ."Curr.Opin.Biotechnol.9:252-255.1998

24) Flowers,RH,Schwenzer,KJ,Kopel,RF,Fisch,MJ,Tucker,SI and Farr,BM,"Efficacy of an attachable subcutaneous cuff for the prevention of intravascular catheter-related infection.Journal of the American Medical Association.1989.

25) Karchmer AW,Gibbons GW,"Infections of prosthetic heart valves and Vascular grafts."In:Bisno AL,Waldvogel FA eds.Infections associated with indwelling devices 2nd ed.1994.

26) Tunney et al,"Defining the Relationship:An Examination of Infectious Agents Associated with Chronic Diseases."1999.

27) Whipple,GC ."Changes that take place in the bacterial contents of waters during transportation."1901.

28) Allison,DG."biofilm-associated exopolysaccharides."Microbiology Europe.1993.

29) Boyle,et,"Biofilms and survival of opportunistic pathogens in recycled water."Waste Management and Resarch.1991.

30) Fletcher,M and Pringle ,JH."The effect of surface free energy and medium surface tension on bacterial attachment ot solic surfaces."1983

31) Waler,et."Microscopy methods to investigate structure of potable water biofilms."2001

32) Costerton,et."Phenomena of bacterial adhesion."1985.

33) King,CH,et,"Survival of coliforms and bacterial pathogens within protozoa during chlorination."1988.

34) Nichols,W."Biofilm permeability to antibacterial agents."1994

35) Jass,J and Lappin-scott,H."The efficacy of antibiotics enhanced by electrical currents against P.aeruginosa biofilms."1996.

36) Cho.A.et."New anti-MRSA cephalosporins with a basic aminopyridine at the c-7 position.2001.

37) Kihlerg,J.et.”Mapping the PapG-adhesin receptor site of uropathogenic E.coli by inhibition of hemagglutination using synthetic analogures of galabiose.”1989.

38) Busscher,HJ,et.”Preliminary observations on influence of dairy products on biofilm removal form silicone rubber voice prostheses in vitro.”2000.

39) Marrie,Tj and Costerton,JW.”Morphology of bacterial attachment to cardiac pacemaker leads and power packs”Journal of Clinical Microbiology.1984.

40) Gristina,AG, and Costerton,JW,”Bacterial adherence to biomaterials and tissue.The significance of its role in clinical sepsis.American Journal of Joint and Bone Surgery.1985.

41) Gristina,AG,Hobgood,CD,Webb,LX and Myrvik,QN.”Adhesive colonization of biomatials and antibiotic resistance.Biomaterials.1987

42) Gristina,AG,Jennings,RA,Naylor,PT,Myrivik,QN and Webb,LX “Comparative in vitro antibiotic-resistance of surface-colonizing coagulase-negative staphylococci.Antimicrobial Agents and Chemotherapy.1989.

43) Bisno,AL and Waldvogel,FA,In:”Infections associated with indwelling medical devices.”2000.

44) Johnson,DP and Bannister,GC.”The outcome of infected arthroplasty of the Knee.”Journal of Bone and Joint surgery.1986.

45) Steckelberg,Jm and Osmon,DR.”Prosthetic joint infections.In:Infections Associated with Indwelling Medical Devices.2000.

46) Bayston,R,”A orocess for prevention of device related infection:results of challenge in vitro and duration of antimicrobial activity.In:The life and Death of Biofilm.1995.

47) Ceri,,H,Olson,ME,Stremick,C,Read,RR,Morck,D and Buret.A.”The Calgary biofilm device:new technology gor rapid determination of antibiotic susceptibilies of bacterial bioflms”1999.

48) Dreghorn,CR and Hamblen,DL.”Revision arthroplasty”:a highprice to pay British Medical Journal.1989.

49) hanssen and Osmon.DR.”The use of prophylactic antimicrobial agents during and after hip arthroplasty.”Clinical Orthopaedics.1999.

50)   Schmitt,SK,Knapp,C,Hall,GS,Longworth,DL,McMahon,JI and Washington,JA."Impact of chlorhexidine-silver sulfadiazine-impregnated central

51Stickler,DJ and winters,C."Biofilms and urethral catheters.In:Bacterial biofilms and their control in medicine and industry."1994.

52)Hughes,G,et,"Biofilms,bacteriophage interactions and bacteriophage therapy."2001.

53)Hentzer,M."Inhibition of quorum sensing in P.aeruginosa biofilm bacteria by Hlogenated furanone compound ."2002.

54)Hood, S.K., Zottola, E.A. (1997) Adherence to stainless steel by foodborne microorganisms during growth in model food systems. *Internat J Food Microbiol* **37**: 145– 153.

55)Tredget, E.E., Shankowsky, H.A., Joffe, A.M., Inkson, T.I., Volpel, K., Paranchych, W. , *et al.* (1992) Epidemiology of infections with *Pseudomonas aeruginosa* in burn patients: the role of hydrotherapy. *Clin Infect Dis* **15**: 941– 949.

56)Watnick, P., Kolter, R. (2000) Biofilm, city of microbes. *J Bacteriol* **182**: 2675– 2679.

57)Beachey, E.H. (1981) Bacterial adherence: adhesion–receptor interactions mediating the attachment of bacteria to mucosal surfaces. *J Infect Dis* **143**: 325– 345.

(58)Kumon, H., Watanabe, T., Vincent, P., Nickel, J.C. (1997) Fully hydrated images of *Pseudomonas aeruginosa* biofilm on the surface of catheter material. *Can J Urol* **4**: 416– 421.

59)McNeil, S.A., Nordstrom-Lerner, L., Malani, P.N., Zervos, M., Kauffman, C.A. (2001) Outbreak of sternal surgical site infections due to *Pseudomonas aeruginosa* traced to a scrub nurse with onychomycosis. *Clin Infect Dis* **33**: 317– 323.

60)Traverso, C.E., De Feo, F., Messas-Kaplan, A., Denis, P., Levartovsky, S., Sellem, E. , *et al.* (2005) Long term effect on IOP of a stainless steel glaucoma drainage implant (Ex-PRESS) in combined surgery with phacoemulsification. *Br J Ophthalmol* **89**: 425– 429.

61)Leake, E.S., Gristina, A.G., Wright, M.J. (1982) Use of chemotaxis chambers for studying *in vitro* bacterial colonization of biomaterials. *J Clin Microbiol* **15**: 320–

323.

62)Tredget, E.E., Shankowsky, H.A., Joffe, A.M., Inkson, T.I., Volpel, K., Paranchych, W. , *et al.* (1992) Epidemiology of infections with *Pseudomonas aeruginosa* in burn patients: the role of hydrotherapy. *Clin Infect Dis* **15**: 941– 949.

63)A.S. Edelstainand and R.C Cammarata. Nanomaterials: Synthesis properties and Application. Institute of Physica, Bristol. 1996.

64)H.Gleither. Nanostrutural materials: basic concepts,microstructure and properties. Nanosicience and Technolgy: Novel structures and Phenomena.

65)Y. Lu and S. C. Chen .Micro and nano-fabrication of biodegradable polymers for drug delivery. Biomimetic Systems and Nanotechnology in Drug Delivery   2004, Pages 1621-1633

66) Diaz.C.Nano/microscale order affects the early stages of biofilm formation on metal surfaces. PubMed. 11206-10. 2007

67) C.Politis. Preparation of amorphous tilxcux by mechanical alloying. Journal of Applied pHysics, 1147-1151, 1986.

68) R.Z. Valiev. Approach to nanostructured solids through the studies of submicron grained polycrystals. Nanostructured Materials. 1995

69) R. Birringer. Encyclopedia of materials science, volume 11. Pergamon, Oxford, 1998.

70) M.Kohler. Nanotechnology: An introduction to nanostrucring techniques. Wiley-VCH, 2004.

71) U.Erb, K.T. Aust. Nanostructured materials processing, properties and potential application, pages 179-215.

72) G. Bining, C.F. Quate, and Ch. Gerber. Phys. Rev. Lett. 56. 930, 1986.

73) B. Bushan. Handbook of Micro/Nano Tribology. CRC press, Boca Raton, 2 edition, 1999.

74) 3. Shao, Z., J. Mou, D. M. Czajkowsky, J. Yang, and J.-Y. Yuan. 1996. Biological atomic force microscopy: what is achieved and what is needed. *Advances in Physics.* 45:1-86.

75) Bustamante, C., and D. Keller. 1995. Scanning Force Microscopy In Biology. *Physics Today.* 48:32-38.

76) Hansma, H. G., and J. Hoh. 1994. Biomolecular imaging with the atomic force microscope. *Annual Review of Biophysics and Biomolecular Structure.* 23:115-139.

77) HG Hansma, I Revenko, K Kim and DE Laney, Atomic force microscopy of long and short double-stranded, single- stranded and triple-stranded Nucleic acid.Nucleic acids Research, Vol 24, Issue 4 713-720, 1996

8) Jianxun Mou, Daniel M. Czajkowsky, Yiyi Zhang and Zhifeng Shao，High-resolution atomic-force microscopy of DNA: the pitch of the double helix，1995.

79) J. Larmer, S.W.Schneider. Imaging excised apical plasma memebraine patches of MDCK cells in physiological conditions with atomic force microscopy. Pflugers archive. Volume 434,p254-260, 1997.

80) Ilya Reviakine, Wilma Bergsma-Schutter and Alain Brisson, Growth of Protein 2-D Crystals on Supported Planar Lipid Bilayers Imaged*in Situ*by AFM, 2002

81) Campoccia, D., L. Montanaro, and C.R. Aricola, *Biomaterials* 27, 2331 (2006).

82) Ciltner, C.L., van Schaik, Erin J., Audette, G.F., Kao, D., Hodges, R.S., Hassett, D.J., Irvin, R.T.,
Mol Microbiol 59, 1083 (2006).

83) Giltner, C.L., van Schaik, E.J., Audette, G.F., Kao, D., Hodges, R.S., Hassett, D.J., Irvin, R.T. *Mol Microbiol,* 60, 813 (2006).

84) Chao, H., Houston, M.E., Jr., Grothe, S., Kay, C.M., O'Connor-McCourt, M.,

Irvin, R.T., Hodges, R.S., *Biochemistry* 35, 12175 (1996).

85) Chao, H., Bautista, D.L., Litowski, J., Irvin, R.T., Hodges, R.S. *J Chromatogr B Biomed Sci Appl,*

715: 307 (1998).

86) Tripet, B., Yu, L., Bautista, D.L., Wong, W.Y., Irvin, R.T., Hodges, R.S., *Protein Eng.,* 9, 1029 (1996).

87) De Crescenzo, G., Litowski, J.R., Hodges, R.S., O'Connor-McCourt, M.D., *Biochemistry* 42, 1754   (2003).

88) Litowski, J.R., Hodges, R.S., *J Pept Res* 58: 477 (2001).

89) Li, W., Li, D.Y. , *Surf. Rev. and Lett*. 11, 173 (2004).

90) Li, Y., Li, D.Y., *Journal of Applied Physics* 95, 7961 (2004).

91) Skerker, J.M., Berg, H.C., *Proc Natl Acad Sci U S A* 98, 6901 (2001).

92) Craig, L., Pique, M.E., Tainer, J.A., *Nat Rev Microbiol* 2, 363 (2004).

93) Irvin, R.T., Doig, P., Lee, K.K., Sastry, P.A., Paranchych, W., Todd, T., Hodges, R.S., *Infect Immun*

57, 3720 (1989).

94) Touhami, A., Jericho, M.H., Boyd, J.M., and Beveridge, T.J., *J Bacteriol* 188, 370 (2006).

95) Zobell, C.E., Allen, E.C., *J Bacteriol* 29, 239 (1935).

96) Zobell, C.E., *J Bacteriol* 46, 39 (1943).

97) Li, B., Logan, B., *Colloids Surf B Biointerfaces* 3, 81 (2004).

98) Morra, M., C, C., *J Biomater Sci Polym Ed.* 9, 55 (1997).

99) Pereni, C.I., Zhao, Q., Liu, Y., Abel, E., *Colloids Surf B Biointerfaces* 48: 143 (2006).

100) Campbell, A.P., Wong, W.Y., Houston, M., Jr., Schweizer, F., Cachia, P.J., Irvin, R.T., Hindsgaul, O.,   Hodges, R.S., Sykes, B.D., *J Mol Biol* 267, 382 (1997).

101) Hazes, B., Sastry, P.A., Hayakawa, K., Read, R.J., Irvin, R.T., *J Mol Biol* 299, 1005 (2000).

102) Li, Yanping, Li, D. Y., *J. of   Appl. Phys*. 12, 7961 (2004).

103)   Li, W., Li, D.Y., *Mater. Sci. & Tech.*, 18, 1057 (2002).

104)   Li, W., Li, D.Y., *Appl. Surf. Sci*   240, 388 (2005).

105)   Suci, P.A., Geesey, G.G., *Colloids Surf B Biointerfaces* 22, 159 (2001).

106)   Gorby, Y., Yanina, S., McLean, J., Rosso, K., Moyles, M., Dohnalkova, A., Beveridge, T., Chang, I.S., Kim, B., Kim, K., Culley, D., Reed, S., Romine, M., Saffarini, D., Hill, E., Shi, L., Elias, D., Kennedy, D., Pinchuk, G., Watanabe, K., Ishii, S., Logan, B., Nealson, K., Fredrickson, J., *PNAS* 103: 11358 (2006).

107)   Reguera, G., McCarthy, K.D., Mehta, T., Nicoll, J.S., Tuominen, M.T., Lovley, D.R., *Nature* 435: 1098 (2005).

108) Allison, DG, Mcbain, Aj and Gilberta, P, microbial biofilms: problems of control. In; Community structure, and cooperation in Biofilm, society for General Microbiology Press, Reading, UK, 2000, pp.309-327

109) Bagge, D, Hjelm,, Huber, and Gram,L, Shewanella prtrefaciens adhesion and bioflm formation on food processing surfaces.Appl Environ Microbial，2001, 67:2139-2151

110) Fletcher, M, and marshall, K.C, Bubble contact angle method for evaluating substratum interfacial characteristics and its relevance to bacterial attachment. Appl Environ Microbiol, 1982, 44:184-192.

Fletcher,M "How do bacterial attach to solid surface" Microbiological Science, 1987, 5:133-136

111)X.N. Du. B. Q. Wang. Formation of nanocrystalline surface of a cu-Zn alloy under electropulsing surface treatment. J.Met. 2007, 22, 1947-1953.

112) Li, W, and Li.D.Y.. Effect of grain size on the electron work function of Cu and Al. Surf. Rev and lett. 2004, 11, 173-178

113) G. Meyer and N.M. Amer. Novel optical approach to atomic force microscopy. Applied Physics Letter, 1988, 53(12): 1045-1047.

114) W.A. Harrison. Electronic structure and properties of solids: the physics of the chemical bond. Freeman, San Francisco, 1980.

115) Y.P. Li and D.Y. Li. Experimental studies on relationships between the electron work function, adhesion, and friction for 3d transition metals. Apply Physics, 2004, 95:7961-7965.

116) G. Liu a, J lu. Surface nanocrystallization of 316L stainless steel induced by ultrasonic shot peening. Materials science and Engineering, 2000, 286, 91-95.

117) Linchun Wang and D.Y.Li. mechanical, electrochemical and tribological properties of nanocrystalline surface of brass produced by sandblasting and annealing. Surface and coating Tech, 2003, 167, 188-196..

118) Chawick, G, and Smith, D. Grain boundary structure and properties. London: Academic Press.1987.

119) D.Y.Li, L. Wang and W.Li. Effects of grain size from micros scale to nanoscales on the yield strain of brass under compressive and tensile stressed using a velvin probing technique .Materials science and Engineering . 2004, 384,355-360.

120) Simming, U, Photoelectrochemical studies passive films . Electrochim. Acta. 1986, 31, 415-429,

121) Z.Liu, Y.He . Surface nano-crystallization of 310S stainless steel and its effect on oxidation behavior . J. Material engineering and performance.. 1997, 7, 1059-9495.

122) D.Y. Li, Electron work function at grain boundary and the corrosion behavior of nanocrystalline

metallic materials, Mat. Res. Soc. Symp. , 2006, 887, 0887-Q05-03.

123)   Giltner,C.L, Van Schaik, E.J, Audette, G.F, Kao and Irvin, R.T.. The pseudomonas aeruginosa type Iv pilin receptor binding domain functions as and adhesion for both biotic and abiotic surfaces. Mol Microbiol, 2006, 60, 813

124)   Lee Yuh-Lang, Effects of heat annealing on the film characteristic and gas sensing properties of substituted and unsubstituted copper phthalocyanine films. Applied surface science , 2001, 172,191-199.

125)   Bin Yu, D.Y.Li, Randall T.Irvin. A novel biometallic interface: high Affinity Tip-Associated Binding by pilin-derived protein nanotubes. Journal of Bionanoscience. 2007, 1, 73-83.

126)   Andrew Guzzetta. Reverse phase HPLC basics for LC/Ms. IonSource Tutorial. 2001

127) M.Nonnencacher. M.P.O'Boyle, and H.K. Wickramasinghe. Kelvin probe force microscopy. Appl. Phys. Lett. 1991, 58. 2921.

128) Zhu, X.M, Zhang, Y.S. Investigation of the electrochemical corrosion behaviour and passive film for Fe-Mn, Fe-Mn-Al, and Fe-Mn-Al-Cr alloys in aqueous solutions. Corrosion, 1998, 54,. 3-12.

129)Yu, B.; Giltner, C. L.; van Schaik, E. J.; Bautista, D. L.; Hodges, R. S.; Audette, G. F.; Li, D. Y.; Irvin, R. T. J. Bionanosci. 2007, 1, 73–83.

130) Yu, B.; Davis, E. M.; Hodges, R. S.; Irvin, R. T.; Li, D. Y. Nanotechnology 2008, 19, 335101

131) Wang, X. Y.; Li, D. Y. Wear 2003, 255, 836–845

132) Mao, X. Y.; Li, D. Y.; Fang, F.; Tan, R. S.; Jiang, J. Q. Philos. Mag. Lett. 2010, 90, 349–360

133) D.Y. Li, Electron Work Function at grain boundary and the corrosion behavior of nanocrystalline metallic materials, *Mater. Soc. Symp.* **887** (2006) 0887-Q05-03.1

134) Busscher, H. J.; Weerkamp, A. H.; Van der Mei, H. C.; Van Pelt, A. W. J.; De Jong, H. P.; Arends, J. Appl. Environ. Microbiol. 1984, 48, 980–983.

135) Fang, H. H. P.; Chan, K. Y.; Xu, L. C. J. Microbiol. Methods 2000, 40, 89–97.

136) Guan, X. S.; Dong, Z. F.; Li, D. Y. Nanotechnology 2005, 16, 2963–2971.

137) Ashcroft, N. W.; Mermin, N. D. Solid State Physics; Saunders: Philadelphia; 1976

138) Belly, R. T., and G. C. Kydd. Silver resistance in microorganisms. Dev. Ind. Microbiol. 1982.**23:**567-577.

139) Bragg, P. D., and D. J. Rainnie. The effect of silver ions on the respiratory chain of *Escherichia coli*. Can. J. Microbiol.1974. **20:**883-889

140) Richards, R. M. E., H. A. Odelola, and B. Anderson. . Effect of silver on whole cells and spheroplasts of a silver resistant *Pseudomonas aeruginosa*. Microbios. 1984.**39:**151-158

141) Liau, S. Y., D. C. Read, W. J. Pugh, J. R. Furr, and A. D. Russell. Interaction of silver nitrate with readily identifiable groups: relationship to the antibacterial action of silver ions. Lett. Appl. Microbiol. 1997.   **25:**279-283.

142) Furr, J. R., A. D. Russell, T. D. Turner, and A. Andrews.. Antibacterial activity of Actisorb Plus, Actisorb and silver nitrate. J. Hosp. Infect. 1994.**27:**201-208

143) Fuhrmann, G. F., and A. Rothstein. 1968. The mechanism of the partial inhibition of fermentation in yeast by nickel ions. Biochim. Biophys. Acta **163:**331-338.

144) Miller, L. P., and S. E. A. McCallan. 1957. Toxic action of metal ions to fungus spores. Agric. Food Chem. **5:**116-122.

145) Brown, T., and D. Smith. 1976. The effects of silver nitrate on the growth and ultrastructure of the yeast *Cryptococcus albidus*. Microbios Lett. **3:**155-162

146) Richards, R. M. E., H. A. Odelola, and B. Anderson. 1984. Effect of silver on whole cells and spheroplasts of a silver resistant *Pseudomonas aeruginosa*. Microbios **39:**151-158.

147) Yakabe, Y., T. Sano, H. Ushio, and T. Yasunaga. 1980. Kinetic studies of the interaction between silver ion and deoxyribonucleic acid. Chem. Lett. **4:**373-376.

148) Izatt, R. M., J. J. Christensen, and J. H. Rytting. 1971. Sites and thermodynamic quantities associated with proton and metal ion interaction with ribonucleic acid, deoxyribonucleic acid, and their constituent bases, nucleosides, and nucleotides. Chem. Rev. **71:**439-481

149) Berger, T. J., J. A. Spadaro, R. Bierman, S. E. Chapin, and R. O. Becker. 1976. Antifungal properties of electrically generated metallic ions. Antimicrob. Agents Chemother. **10:**856-860

150) Berger, T. J., J. A. Spadaro, S. E. Chapin, and R. O. Becker. 1976. Electrically generated silver ions: quantitative effects on bacterial and mammalian cells. Antimicrob. Agents Chemother. **9:**357-358

151] Feng Zhang, G.K. Wolf, Xianghui Wang and Xianghuai Liu, Bactericidal and corrosive properties of silver implanted TiN thin films coated on AISI317 stainless steel Surf. Coat. Technol. 148, p. 65. 2001

152) Feng Zhang and Xianghuai Liu *et al.*, A study on antibacterial properties of Ag$^+$-implanted pyrolytic carbon *Surf. Coat. Technol.* 103–104, p. 146, 1998..

153)   Xianghui Wang and Feng Zhang *et al.*, A study on biocompatibility and bactericidal properties of pyrolytic carbon by silver ion implantation *Surf. Coat. Technol.* 128–129 ,p. 36, 2000.

154)   K. Meinert and G.K. wolf, *Surf.* Zinc/manganese multilayer coatings for corrosion protection   *Coat. Technol.* **98**, p. 1148, 1998.

155)   Hallab, NJ, Jacobs, JJ, & Katz, JL. In Ratner, BD, Hoffman, AS, Schoen, FJ, & Lemons, JE (Eds.).. Orthopedic applications. *Biomaterials Science, An Introduction to Materials in Medicine* (pp.526-55). San Diego, CA: Elsevier Academic Press,2004

156)   X.Y. Wang and D.Y. Li, Mechanical and electrochemical behavior of nanocrystalline surface of 304 stainless steel, *Electrochem. Acta*, 47 (2002) 3939-3947.

157)   Tiansheng Wang, Jinku Yu, Bingfeng Dong, surface nanocrystallization induced by shot peening and its effect on corrosion reistance of 1Cr18Ni9Ti stainless steel. *Journal of Surface and coatings technology*, Vol. 200, pp 4777-4781, 2006.

158) Bin Yu, et al, Surface nanocrystallization of stainless steel for reduced bio-film' adherence, Nanotechnology, 19 (2008) 335101

159)Gabriel MM, Mayo MS, May LL, Ahearn DG. *In vitro* evaluation of the efficacy of a silver-coated catheter. Curr Microbiol. 1996;33:1-5.

160) Cooper R, Kingsley A, White R. *Wound Infection and Microbiology.* : Medical Communications (UK) Ltd for Johnson & Johnson Medical, 2003